8-2009

Experimental Studies of Exotic Negative Ions

Shaun Gerald Ard
University of Tennessee - Knoxville

To the Graduate Council:

I am submitting herewith a dissertation written by Shaun Gerald Ard entitled "Experimental Studies of Exotic Negative Ions." I have examined the final electronic copy of this dissertation for form and content and recommend that it be accepted in partial fulfillment of the requirements for the degree of Doctor of Philosophy, with a major in Physics.

Robert N. Compton, Major Professor

We have read this dissertation and recommend its acceptance:

Janice Musfeldt, Pengcheng Dai, Robert Grzywacz

Accepted for the Council:

Carolyn R. Hodges

Vice Provost and Dean of the Graduate School

(Original signatures are on file with official student records.)

To the Graduate Council,

I am submitting herewith a dissertation written by Shaun Gerald Ard entitled "Experimental Studies of Exotic Negative Ions." I have examined the final electronic copy of this dissertation for form and content and recommend that it be accepted in partial fulfillment of the requirements for the degree of Doctor of Philosophy, with a major in Physics.

Robert N. Compton, Major Professor

We have read this dissertation
and recommend its acceptance:

Janice Musfeldt

Pengcheng Dai

Robert Grzywacz

Accepted for the Council:

Caroline R. Hodges
Vice Provost and Dean of the Graduate School

(Original signatures are on file with official student record)

Experimental Studies of Exotic Negative Ions

A Dissertation
Presented for the
Doctor of Philosophy
Degree
The University of Tennessee, Knoxville

Shaun Gerald Ard
August 2009

Dedication

To my loving wife Kelly, whose everlasting patience and support has made this whole endeavor possible.

Acknowledgements

First and foremost, I would like to thank my advisor, Dr. Robert Compton, for the significant role he has played in my development as a scientist in these last five years. Dr. Compton's never ending curiosity and love of physics has proven to be quite contagious. I would like to thank all of the former and current members of the Compton research group. The numerous discussions about each other's research, as well as current events, have greatly added to my understanding and perspective of the world as a whole. I would also like to offer my appreciation to my entire family for helping shape me into who I am today. Their unwavering love and support have been invaluable.

Abstract

Although negative ions have been studied extensively for quite some time, their study continues to offer insight into developing and refining quantum chemical modeling techniques. Negative ion states remain difficult to treat ab initio due to the significant electron-electron correlation, thus putting a premium on experimental results to guide the way. Experimental techniques such as Electrospray Ionization (ESI) and Rydberg Electron Transfer (RET) have made study of some exotic negative ions in the gas phase possible for the first time. Multiply Charged Anions (MCAs) of several families of molecules were studied using Collision Induced Dissociation (CID) and Infrared Multi Photon Dissociation (IRMPD) to consider the relative stabilities toward electron detachment and ionic fragmentation, as well as the influence of the Coulomb Barrier in these systems. The Coulomb Barrier is a potential barrier adding stability to MCAs due to the Coulombic repulsion between the excess charges. This study has shown for the first time that the magnitude of this barrier towards ionic fragmentation fits the simple electrostatic model of e2/r, as was found by Wang et al. for electron detachment.

Dipole-bound anions are another rare species of negative ions in which the excess electron is loosely bound to a polar molecule through its dipole moment. The electron affinity of these anions (as determined from RET formation and Field detachment measurements) has been shown to be primarily a function of dipole moment, yet this work has highlighted the significant influence of rotations on these anionic states. Observations of neutrals formed from detachment of these anions (black body

photodetachment and rotational autodetachment), has shown significant coupling to the moment of inertia of the molecule. In the first study of dipole bound anions of HCN, it has been shown that these rotational effects essentially truncate this anionic system such that only two rotational levels remain bound. Formation of the ground state and first rotationally excited state of the dipole bound anion has been observed in the RET spectra and field detachment measurements for the first time.

Table of Contents

List of Tables

List of Figures

Chapter 1

Introduction

In the gas phase, negative ions, or anions, are atoms or molecules that have a net negative charge resulting from supporting a number of electrons in excess of their respective number of protons. Negative ions are also found prominently in solutions or in the solid state (crystals, etc.). Since the discovery of gas phase negative ions by Thompson[1] in 1907, much has been learned about the formation of these ions and the increasing role they have been observed to play in numerous fields of science and technology. It has been shown that ~80% of known naturally occurring elements support bound negative ion states[2] (i.e. having a positive electron affinity (*EA*) as defined as the energy required to remove the outermost electron) with notable exceptions such as N, Mg, Be, Hg, and Zn. Stable negative ions typically involve the excess electron occupying an empty or partially filled orbital of the neutral atom or molecule. Rare gasses, which possess fully occupied *p* and/or *s* orbital shells are not expected to form bound negative ion states, though some evidence suggest Xe may have a bound anionic state[3]. In addition to atomic negative ions, many molecules have been shown or calculated to support a bound negative ion state (Fig 1.1). Many reviews on negative ions, such as Massey's expansive review summarizing most of what was known about negative ions up to 1979[4,5], detail much of the current knowledge about the electron affinity[6] and structure[7,8,9] of these atomic and molecular states. Although the book by

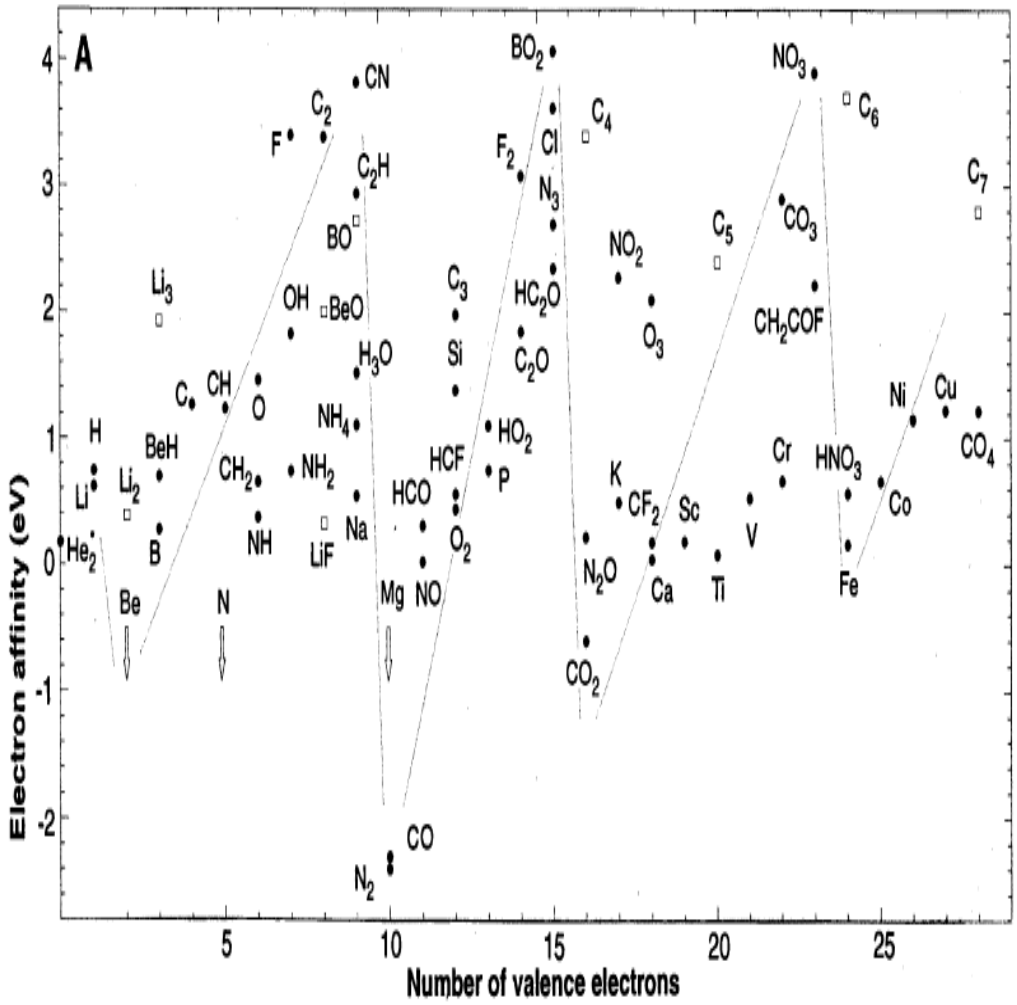

Figure 1.1 Experimentally measured (closed circles) and calculated (open squares) electron affinities for numerous atoms and molecules with respect to the number of valence electrons[9].

Massey is quite complete in its treatment of conventional negative ions, recent discoveries of exotic negative ion states, such as multiply-charged negative ions and dipole-bound negative ions, continue to offer systems in which we can further develop our fundamental understanding of negative ions.

The importance of negative ions reaches far beyond the fields of atomic and molecular physics. Negative ions play a crucial role in such diverse fields as astronomy, atmospheric sciences, chemistry, biology, and possibly even psychology. It has been found that H^- is a significant source of the observed absorbance in the red and infrared wavelength regions of solar radiation[10,11, 12, 13] signifying its importance in stellar mechanics. C_6H^- has been observed in the interstellar medium[14], and it has been speculated that anions of other organic chains may play a significant role in the so-called Diffuse Interstellar Bands (DIBs), absorption features observed in the spectra of stars seen through significant column densities of interstellar material[15]. Furthermore, the associative attachment process, $H^- + H \rightarrow H_2 + e^-$, is the dominant mechanism leading to the formation of hydrogen molecules in interstellar gas clouds. Negative ions have been show to be intimately involved with gas phase chemical reactions in the atmosphere. For example, it has been shown that in the lower region (the D region) of the Earth's ionosphere negative ions such as O^- and O_2^- help determine the number of free electrons, which highly influences radio communication and other aeronomical phenomena[16].

Anions are found abundantly in solution, and as such play a crucial role in chemistry and biology. The basicity of a solution is directly related to the number of hydroxide (OH^-) anions, thus anions are important as catalysts for many chemical reactions. An atoms propensity to attract electrons, or its electro-negativity, is important in understanding the bonding of atoms in molecules. Anions in solution have been show to have a great effect on large scale properties of the solution, such as the freezing point or conductivity. Considering the prevalence of anions in solution and the many effects associated with them, it is clear that anions play an important role in biology. In fact anions are involved with intracellular signaling, cell life and cell death. Biologically relevant anions, chloride for example, regulate ion channels involved with transport across cellular membranes such as the Voltage Dependant Anion Channel (VDAC) [17]. Specific ion channels involving the chloride anion are involved in a wide range of biological functions, including epithelial fluid secretion, cell-volume regulation, neuroexcitation, smooth-muscle contraction and acidification of intracellular organelles[18], thus are of considerable importance for pharmaceutical applications. Studies have shown that negative ions may even improve ones mood[19], though much of the evidence in that regard is anecdotal and unproven definitively.

Perhaps the most important aspect of negative ions is that they offer a system with which to experimentally study predictions of quantum chemistry. Quantum chemistry involves applying quantum theory toward complete modeling of isolated molecules and ions. The hydrogen atom is the only system that can be solved exactly, as it is referred to

as a two-body problem: a single electron and a single nuclear center. For atoms with a larger number of electrons, and molecules with numerous electrons and nuclear centers, complex analytical methods must be employed. These calculations quickly increase in difficulty as the system increases in size, limiting *ab initio* techniques (techniques based on first principles) to small or simple molecular systems. Of considerable focus in the field is simplification of these massive calculations through the development of approximations such as Density Functional Theory (DFT). This approximation method generally involves neglecting the interaction between every pair of electrons, and instead treating it as an interaction between an electron and the average of the other electrons. Negative ions are an ideal system with which to study the efficacy of various calculational methods. The charge carried by the molecule allows for its study in the gas phase by isolation and detection through mass spectrometry. Measurements of electron affinity, vibrational modes, and rotational levels can then be directly compared to calculations with the goal of improving models and calculational methods. Additionally, the study of rare or exotic negative ion states offer systems with which to address one of the primary difficulties in this field, the treatment of electron correlation. As mentioned previously, the inclusion of every electron-electron interaction greatly increases the difficulty the calculation. Negative ions typically portray greater sensitivity to electron correlation due to effective screening of the nuclear charge by the inner shell electrons. The exotic negative ion systems studied herein, dipole bound and multiply charged anions, allow us to probe electron correlation effects as well as address other widely used approximations of quantum chemistry. Dipole bound anions are systems in which the

excess electron is very weakly bound as the result of the dipole moment of a highly polar molecule. This weakly bound electron is very sensitive to dispersion forces resulting from the valence electrons of the molecule. Furthermore, experiments to be discussed will address the application of the Born-Oppenheimer approximation to dipole bound anions. The Born Oppenhiemer approximation is fundamental to many quantum chemical calculations, as it contends the nuclear and electron wave functions can be treated separately, resulting in a significantly smaller number of coupled equations, and thus simpler calculations. This assumption is based on the thought that the electron moves so fast relative to the nuclear centers, due to the large mass discrepancy between the two, that the electron observes the molecule as stationary, regardless of the molecules vibrational or rotational state. This contention seems to break down for dipole-bound anions, however, as they are shown to be very sensitive to the rotational state of the molecule, and will be discussed in some detail in this thesis. Multiply Charged Anions (MCAs) offer another system in which electron correlation becomes paramount due to the excess of electrons involved. In fact, the long range Coulomb interaction between the excess charges allows for stabilization of the anion towards dissociation as seen in the Jackson's treatment[20] of a point charge in the presence of a charged, insulated, conducting sphere. The experimental study of MCAs probes the role of the Coulombic interaction in these systems, giving some insight to the transition state of these anions towards their dissociation, notoriously difficult to model. Experimental studies of negative ions, in particular exotic negative ions such as dipole bound and multiply

charged anions, are vital in improving our understanding of the world at the molecular level and importantly, the ability to model it efficiently and effectively.

Chapter 2

Experimental Studies of Dipole-Bound Negative Ions

Introduction

Dipole-Bound negative ions can be described as an exotic negative ion state in which the excess electron is essentially bound as a result of the dipole moment of a highly polar molecule. Theoretical consideration of these anionic states began in 1947 by Fermi and Teller[21], interestingly while treating the stopping of negatively charged mesons in matter. Their work predicts that an electron can bind to a theoretical "point" dipole with a critical charge separation of .639 a_o (Bohr radius, a_o=5.29 x10^{-11} m). This theoretical conclusion was supported by Wightman[22] a short time later, in a similar but independently derived treatment. Theoretical consideration continued, oddly unaware of the results of Fermi, Teller, and Wightman, by considering the minimum dipole moment required to bind an electron to a stationary finite dipole, with a consensus reached of D_{min}=.639 a_o or 1.625 Debye (D) [23, 24, 25, 26]. Efforts continued by attempting to determine the electron affinity (*EA*) of this dipole bound negative ion state as a function of the molecules dipole moment[27, 28], however in retrospect this appeared short sighted as geometrical aspects of the molecule, dispersion forces, and importantly rotational affects considerably impact the binding energy of an electron to the dipole field of a polar molecule. Soon thereafter, Garrett[29] showed that D_{min} required to bind an electron is dependant on the moment of inertia and length of the dipole, and furthermore D_{min} will

increase with increasing rotational quantum number. Crawford and Garret[30, 31, 32] went on to show that any real, rotating molecule must be in a very low rotational state, with D_{min}~2-2.5 D. The importance of rotational considerations in understanding dipole bound states cannot be understated, and thus is the focus of much of the research herein.

The initial experimental observation of a dipole bound anion was by Stockdale, Compton, and Klots[33] upon production of the acetonitrile (CH_3CN) anion though collisions of neutral acetonitrile with rare gas Rydberg atoms excited to highly excited Rydberg states by electron impact. Acetonitrile did not bind slow electrons, and calculations suggested no bound valence state was available. At the time it was thought that the electron was in a very diffuse orbit, similar to that of the excited Rydberg state necessary for its creation. Attempts at recreating this observation by using a laser to excite an alkali atom to a specific n, ℓ state (n being the principle quantum number and ℓ being the orbital angular momentum quantum number) for collisions with acetonitrile were unsuccessful in producing the dipole bound anion. This null result was not an indictment of the original experiment, as we now know it was due to the very narrow range of excited Rydberg states capable of forming the dipole bound anion. Outside of this range of principal quantum number the formation rate for the dipole state drops off rapidly, and thus the distribution of excited Rydberg states formed by electron impact in the original experiment must have had sufficient overlap with the required range. The first unambiguous observation of a dipole-bound negative ion state was by Bowen et. al. in study of negative ions of the water dimmer ($(H_2O)_2$)[34]. Study of these rarely observed

states has continued as they have been produced using electron attachment under high pressure nozzle jet expansion conditions[35], photo dissociation of neutral atomic iodine/acetone and atomic iodine/acetonitrile clusters[36], dissociative electron attachment to clusters such as (CH_3CN) [37], as well as resonance charge transfer from highly excited Rydberg states (RET) employed in the experiments to be discussed herein. These states have also been indirectly probed by Brauman[38] and Lineberger[39], who have reported very narrow resonance features in the photodetachment thresholds for valence to dipole-bound anion transitions corresponding to rotationally excited shape and Feshbach resonances for many dipole-bound radical anions.

A great deal has been learned thus far about the formation and electron affinity of this weakly bound state for numerous polar molecules, as discussed in reviews by Compton and Hammer[40] and Desfrancois et. al. [41], primarily employing Rydberg Electron Transfer (RET) to produce and study these states. As mentioned before, dipole bound anions formed in this manner are shown to exhibit a sharp maximum over a narrow range of excited Rydberg states referred to by their effective principle quantum number n* (where $n^*=n-\delta_\ell$ accounting for the ℓ dependant quantum defect δ_ℓ). The excited state producing the largest relative ion signal (n^*_{max}) is independent of the Rydberg atom employed, typically a rare gas or alkali atom. Empirically[42] it was determined that the relationship between the electron affinity and n^*_{max} was

$$EA=23(\text{eV})/n^{*2.8}_{max} \qquad [1]$$

This simple relationship is useful, yet it does not fully consider the manner in which the anion was formed. Desfrancois[43] went on to form a theoretical framework for relating the *EA* of the dipole bound state to the n^*_{max} observed for its formation. Briefly, the interaction of the excited Rydberg atom and polar molecule is described in terms of a curve-crossing model. Covalent potential curves corresponding to the Rydberg atom excited to a specific n, ℓ state and the neutral polar molecule, cross an ionic Coulombic diabatic curve corresponding to the ionized Rydberg atom and the newly formed dipole bound anion. At each avoided crossing the system can jump from one curve to the other with an adiabatic probability. Desfrancois was able to create a computational program to calculate this adiabatic probability, and thus formation rate, for various n, ℓ states predicting the RET spectra for a given *EA*. This program was used extensively in the analysis of the experimental data herein for comparison to observed RET spectra and determination of the *EA* of the produced dipole bound states.

Another, more direct, method employed to determine the *EA* of these states is through electric field detachment. Desfrancois et al[44] was able to model the rate of field detachment of a dipole bound state for a given electric field in a manner similar to that of atomic field ionization. The electric potential observed by an excited electron of a Rydberg atom (defined as a atom with a single electron outside of a closed electronic shell such that it is effectively modeled as atomic hydrogen) in an applied electric field is

$$V(r) = -e/r - Fr \qquad [2]$$

This one-dimensional (the direction of the applied field) equation with F being the strength of the applied field, r the distance to the atomic center, and e electrons charge, results in the effective ionization potential of the atom being lowered by $2(eF)^{1/2}$. Applying this approach to a dipole bound anion, the field observed by the electron is

$$V(r) = -\mu/r^2 - Fr \quad [3]$$

where μ is the molecular dipole moment. The effective binding of this electron is now lowered by $3(\mu F^2/4)^{1/3}$. Including the possibility of tunneling, Desfrancois was able to arrive at an equation for the fraction of anions left undetached (f) for a given electric field as

$$f = \exp^{-wT} \text{ (atomic units)} \quad [4]$$

Here T is the time spent in the electric field. For the experiments herein the electric field is produced in the source region of a time of flight mass spectrometer, thus

$$T=(2md/F)^{1/2} \quad [5]$$

Where d is the acceleration distance, and m is the mass of the anion. w is given by

$$w = N^2F/4\gamma^2 \, (\exp -2\,\gamma^3/3F) \quad [6]$$

with N the normalization constant for the dipole bound anion radial wave function, and

$$\gamma = (2\,EA)^{1/2} \quad [7]$$

with EA the electron affinity of the dipole bound anion. This theoretical frame work allows one to calculate the electric field dependence of the dipole bound anion signal. Comparisons with the experimentally measured field dependence then allows for accurate determination of the binding energy of this weakly bound state.

These techniques of Rydberg electron transfer (RET) and electric field detachment have been applied to produce and study numerous dipole bound anions. Hammer et. al. [45] and Desfrancois et.al. [46] employed these techniques to measure the dipole-bound electron affinities for numerous polar molecules of various molecular classes. With few exceptions, all of the molecules displayed the sharp peak in ion formation relative to n*, indicative of dipole-bound anion formation, allowing for application of the curve-crossing model to determine the *EA* of the observed state (Fig 2.1). This *EA* was further supported by electric field detachment of the anions formed displaying a sharp decrease in ion signal with increasing electric field, with the *EA* determined from Eq. [4] in excellent agreement with those determined from the RET spectra (Fig. 2.2). The electron affinities range from ~ 0.5 meV for low (~ 2.5 Debye) dipole moment molecules, to ~20 meV for moderate (~ 4 Debye) dipole moment molecules, and to ~ 50 meV for high (~ 5.4 Debye) [47] dipole moment molecules (Table 2.1). While the *EA* is shown to be primarily influenced by the dipole moment of the neutral molecule, other factors such as dispersion forces from electrons in valence states, as well as atomic, geometrical, and rotational characteristics of the molecule have a significant influence as well (Fig. 2.3). The experiments discussed herein attempt to build upon the vast knowledge accumulated on these ionic states in consideration of these factors. The techniques of Rydberg electron transfer and electric field detachment are employed as these techniques have been shown to provide excellent sensitivity to subtle features of these anionic states. For example, multiple conformations of a polar molecule with varying dipole moments have been shown to produce dipole bound anions with

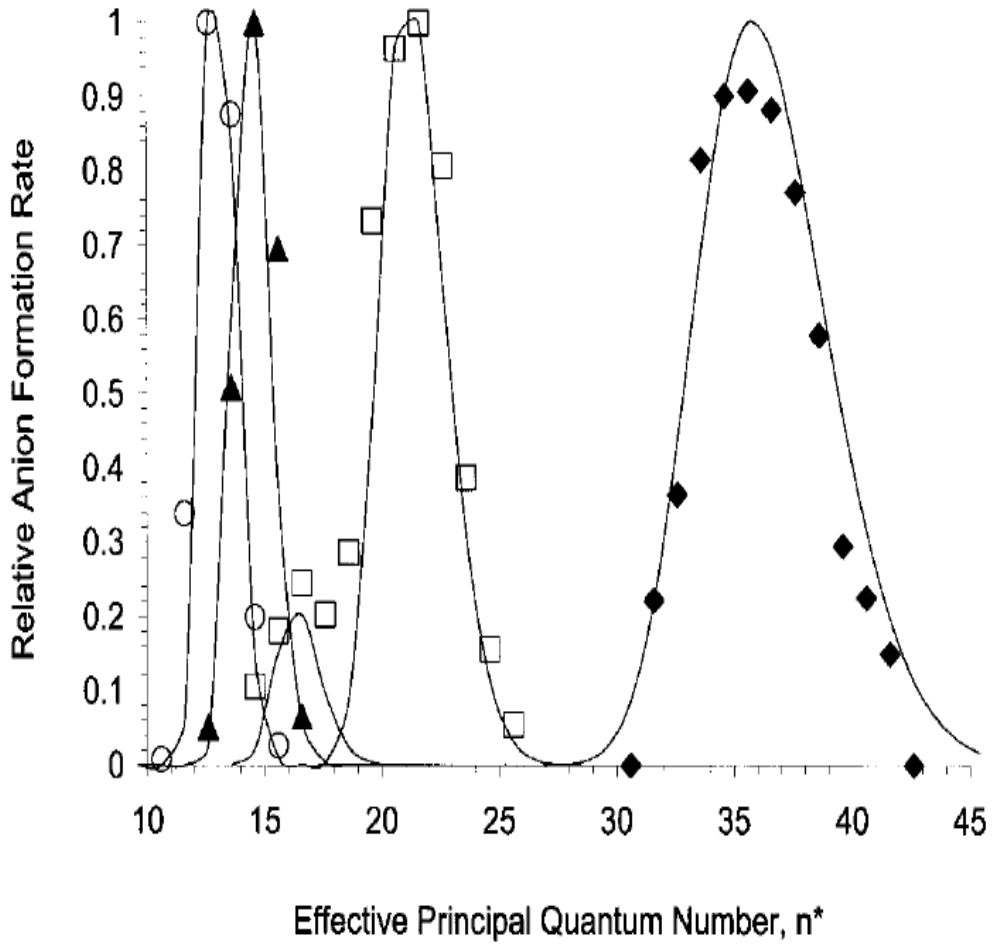

Figure 2.1. Representative examples of relative anion formation over n* for tetramethylenesulfoxide (circles), 2,2-dimethylpropanenitrile (triangles), 3-methylcyclohexanone (squares), and propanal (diamonds). The smooth lines through the data points are a fit to the curve crossing model of Desfrancois allowing for determination of the EA of the state[45].

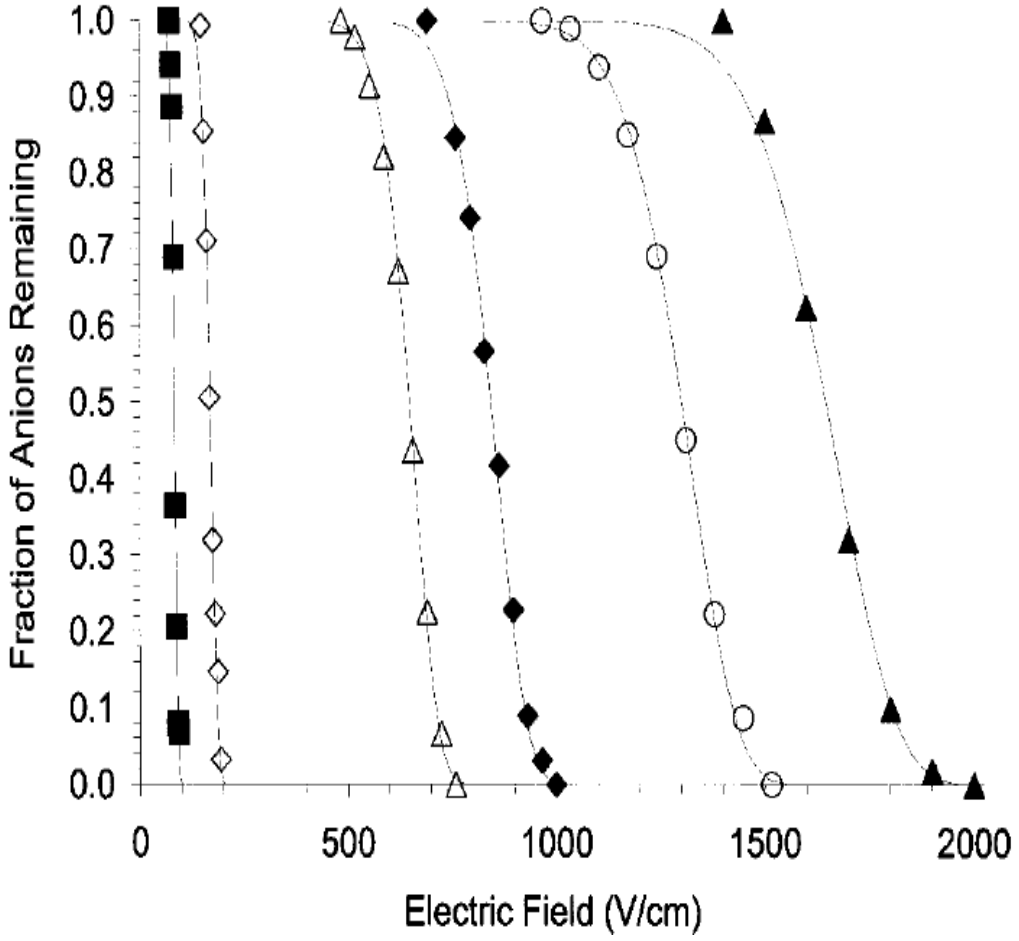

Figure 2.2. Representative examples of relative ion formation for increasing electric field for acetaldehyde (squares), propanal (open diamonds), acetone (open triangles), 3-methylcyclopentanone (diamonds), 3-methylcyclohexanone (open circles), and 2-methylcyclohexanone (triangles). The solid curve through the data point is determined by fitting Eq. [4] to the data, determining the *EA* of the state.

Table 2.1. Dipole moment, molecular polarizabilities, and electron affinities for numerous previously studied dipole bound anions[45].

		Dipole moment (D)			Polarizability (10^{-24} cm^3)				Electron affinity (meV)		
Molecule	Formula	EXP	MP2 PVDZ	MP2 PVTZ	EXP	EMP	MP2 PVDZ	n^*_{max}	RET EMP	RET CALC	FD
Acetaldehyde	CH_3CHO	2.75	2.81	2.80	4.6	4.5	4.50	42.8	0.6	0.6	0.6
Propanal (*cis*)	CH_3CH_2CHO	2.52	2.68	2.68		6.33	6.24	35.8	1.0	1.0	1.0
Propanal (*gauche*)		2.86	2.91	2.91			6.29				
Acetone	CH_3COCH_3	2.88	2.99	2.98	6.4	6.33	6.28	25.7	2.6	2.6	2.5
Cyclobutanone	C_4H_6O	2.89	2.93	2.92	7.7		7.51	30.2	1.7	1.7	1.6
2-Methylpropanal (*gauche*)	$(CH_3)_2CHCHO$	2.69	2.76	⋯	⋯	8.17	8.04	31.5	1.5	1.6	1.1
2-Methylpropanal (*trans*)		2.86	2.91	2.92			8.09				
Butanal (*cis/gauche*)	$CH_3CH_2CH_2CHO$	2.72	2.57	⋯	8.2	8.17	8.15	34.0	1.2	1.2	1.3
Butanal (*cis/trans*)			2.97	⋯			8.15	29.1	1.8	1.8	
2-Butanone	$CH_3CH_2COCH_3$	2.78	2.83	⋯	8.1	8.17	8.03	29.0	1.8	1.8	1.8
Cyclopentanone	C_5H_8O	2.88	3.13	⋯	9.3		9.08	24.9	2.8	2.8	2.8
Pivalaldehyde	$(CH_3)_3CCHO$	2.66	2.74	⋯	10	10.01	9.84	33.7	1.2	1.2	1.0
2-Ethylbutanal	$(CH_3CH_2)_2CHCHO$	⋯	2.62	⋯	⋯	11.83	11.56	31.2	1.5	1.5	1.2
2-Methylcyclopentanone (*axial*)	$C_6H_{10}O$	⋯	2.99	⋯	⋯	11.12	10.81	26.7	2.3	2.4	2.2
2-Methylcyclopentanone (*equatorial*)			2.97	⋯			10.87				
3-Methylcyclopentanone (*axial*)	$C_6H_{10}O$	3.14	3.17	⋯	⋯	11.12	10.82	24.5	3.0	3.0	3.0
3-Methylcyclopentanone (*equatorial*)			3.17	⋯			10.96				
Cyclohexanone	$C_6H_{10}O$	2.87	3.29	⋯	11.5	11.12	10.83	19.4	5.7	5.7	5.9
2-Methylcyclohexanone (*axial*)	$C_7H_{12}O$	⋯	3.21	⋯	⋯	12.97	12.56	21.7	4.2	4.2	4.7
2-Methylcyclohexanone (*equatorial*)			3.09	⋯			12.51				
3-Methylcyclohexanone (*axial*)	$C_7H_{12}O$	⋯	3.24	⋯	⋯	12.97	12.53	16.7	8.7	10.2	8.8
3-Methylcyclohexanone (*equatorial*)			3.26	⋯			12.13	21.3	4.4	4.4	4.1
4-Methylcyclohexanone (*axial*)	$C_7H_{12}O$	3.26	3.35	⋯	⋯	12.97	12.57	18.9	6.1	6.0	6.7
4-Methylcyclohexanone (*equitorial*)			3.31	⋯			12.71				
Acetonitrile	CH_3CN	3.92	3.92	3.94	4.44	4.42	4.36	12.7	18.7	19.3	⋯
Propanenitrile	CH_3CH_2CN	4.05	4.03	4.03	6.47	6.27	6.19	13.7	15.1	15.8	⋯
2-Methylpropanenitrile	$(CH_3)_2CHCN$	4.29	4.04	⋯	8.05	8.11	8.01	15.0	11.7	11.6	⋯
Butanenitrile #1	$CH_3(CH_2)_2CN$	4.07	4.15	⋯	8.4	8.11	8.06	13.4	16.1	17.0	⋯
Butanenitrile #2			3.99	⋯			7.94				⋯
2,2-Dimethylpropanenitrile	$(CH_3)_3CCN$	3.95	4.02	⋯	9.59	9.95	9.80	14.6	12.6	13.2	⋯
2-Methylbutanenitrile #1	$CH_3CH_2CHCH_3CN$	⋯	4.15	⋯	⋯	9.95	9.81	14.5	12.9	13.5	⋯
2-Methylbutanenitrile #2			3.99	⋯			9.88				
3-Methylbutanenitrile #1	$(CH_3)_2CHCH_2CN$	⋯	4.04	⋯	⋯	9.95	9.82	15.0	11.7	11.7	⋯
3-Methylbutanenitrile #2			3.98	⋯			9.71				⋯
Pentanenitrile #1	$CH_3(CH_2)_3CN$	4.12	4.26	⋯	10.4	9.95	9.92	14.6	12.6	12.6	⋯
Pentanenitrile #2			3.95	⋯			9.80				⋯
Dimethyl sulfoxide	CH_3SOCH_3	3.96	4.38	4.14	⋯	⋯	8.10	14.1	13.9	13.9	⋯
Methyl ethyl sulfoxide	$CH_3SOCH_2CH_3$	⋯	4.24	4.01	⋯	⋯	9.93	14.7	12.4	12.5	⋯
Tetramethylene sulfoxide	C_4H_8OS	⋯	4.52	⋯	⋯	⋯	10.77	13.0	17.5	17.5	⋯

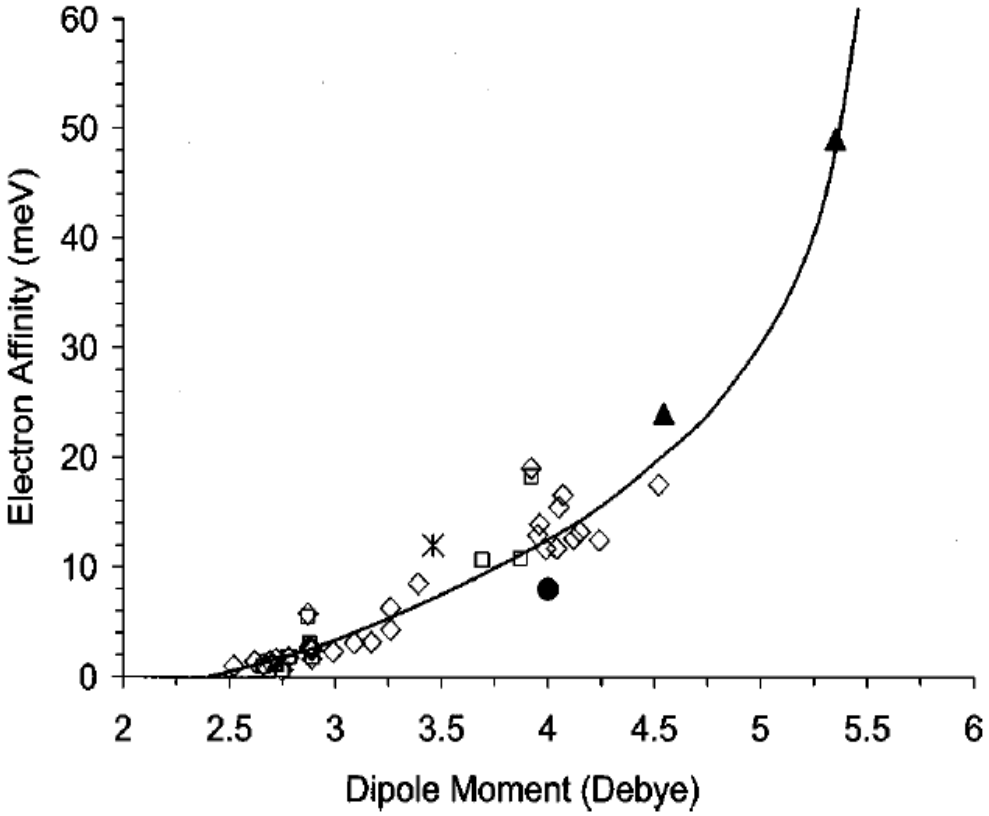

Figure 2.3. Electron affinities of a number of dipole-bound anions. The various shapes indicate the source of the measurements: squares ~(Ref. 39), diamonds ~(Ref. 45), asterisk ~(Ref. 52), circle ~(Ref. 46), and triangles (Ref. 47).

differing *EA*s and RET spectra, such as for the case of butanal (Fig. 2.4). Furthermore, studies of dipole bound anions of acetone and deuterated acetone[48], have been able to ascribe a small (~2%) decrease in *EA* to the slight (~.5%) reduction in the average dipole moment of acetone upon deuteration (Fig. 2.5), highlighting the impressive precision of these techniques. While the vast majority of dipole bound anions studied thus far have shown excellent agreement with the current theoretical understanding of these states, there is still much to be learned. The techniques of Rydberg electron attachment and electric field detachment have proven the ability to produce and study dipole bound anions, as well the sensitivity to probe subtle features of these anionic states. The experiments discussed in this chapter will focus on specific molecular systems, where application of these techniques will allow us to probe the effects of bound valence states and rotational characteristics of the molecule on the formation and lifetime of dipole bound anions.

Experimental Setup

The experimental apparatus and procedure to produce dipole bound anions employed is similar to that employed by Hammer et. al.[45] (Fig. 2.6) and detailed therein. A resistively heated alkali oven is used to heat a small glass ampoule (1 gram) of atomic Rubidium (Sigma Aldrich) to ~170ºC producing a fairly dense vapor (~100 Pa) of rubidium atoms. A small hole in the oven then directs a beam of Rubidium vapor directly into the interaction region, located approximately 30 cm away. The

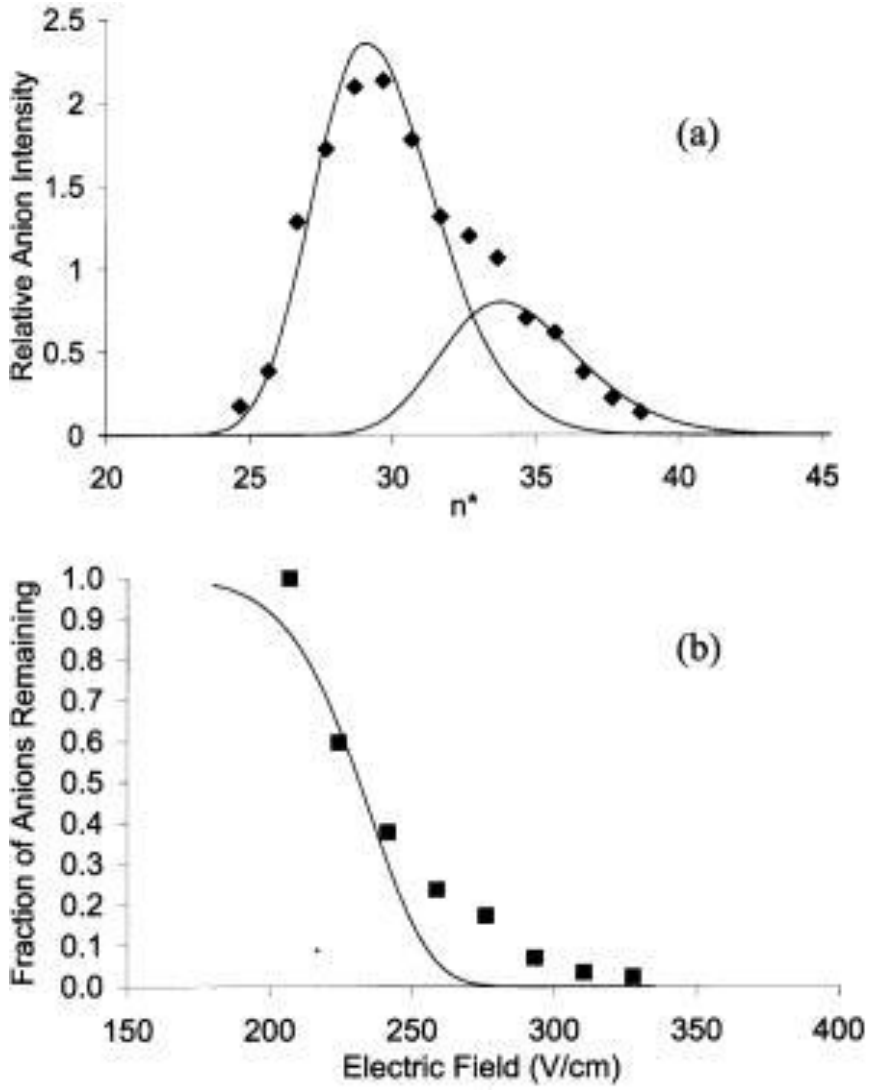

Figure 2.4. Experimental (data points) and theoretical (solid curve) RET spectra and field detachment profile for butanal. Deviations from the model indicate the presence of 2 conformers of this molecule producing two separate dipole states[45].

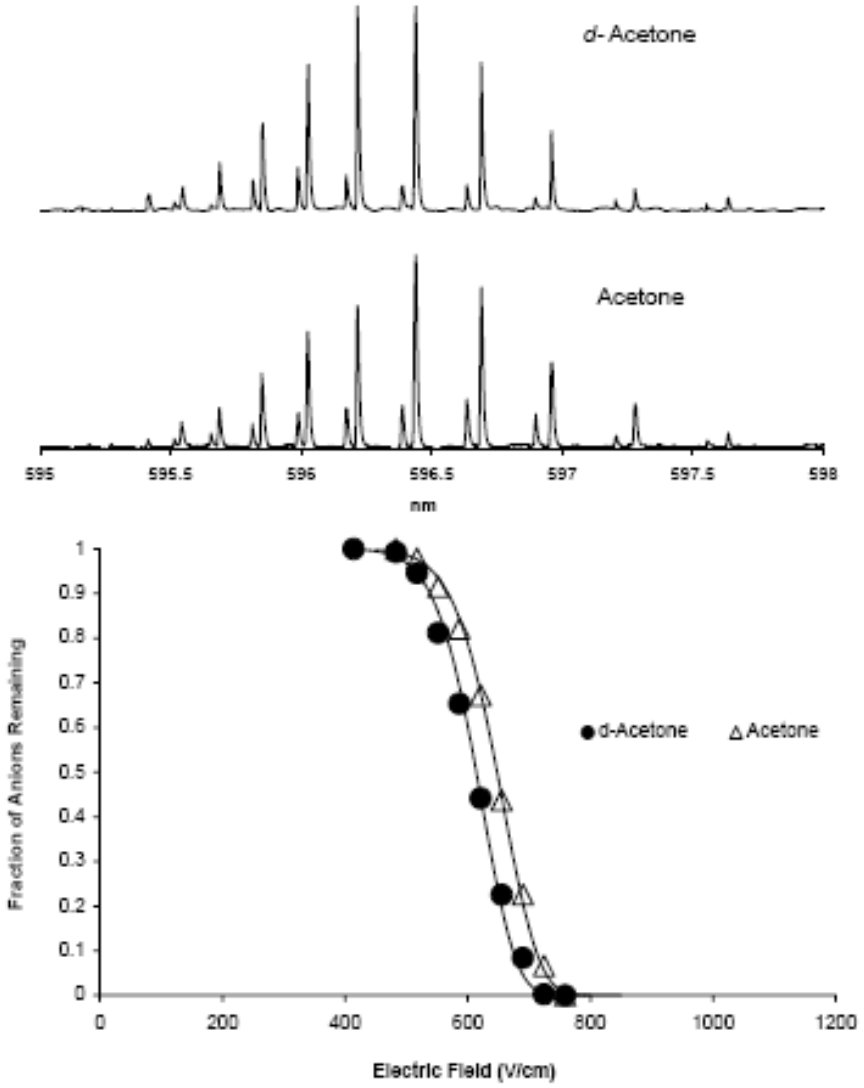

Figure 2.5. RET spectra and field detachment profiles for acetone (triangles) and deuterated acetone (circles) showing a small reduction in electron affinity of the dipole bound state accompanying the small reduction of dipole moment for acetone upon deuteration[48]

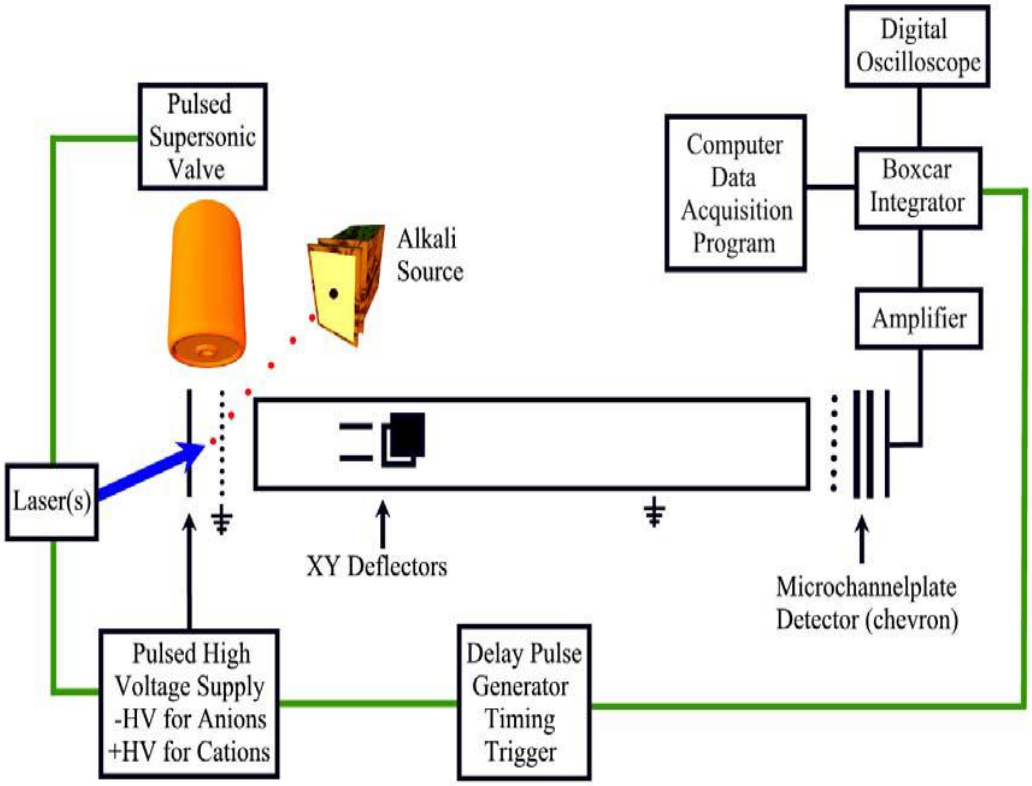

Figure 2.6. Experimental apparatus currently employed, as well as previously by Hammer et. al. 45 for the production and study of dipole bound anions.

rubidium was then excited to various n_s and n_d levels by a resonant two photon process using a Nd:YAG (Continuum Powerlite) pumped tunable pulsed dye laser (Quanta Ray DCR-II). A pulsed supersonic valve (RM Jordan) aligned mutually orthogonal to the incident rubidium vapor, as well as the time-of flight mass spectrometer used for detection, introduces the polar molecule of interest, often seeded with argon gas to promote ro-vibrational cooling[49] of the polar molecule. This is an important aspect of the apparatus, as the weakly bound nature of these states requires the molecule to be in its ground vibrational state as well as a in a low rotational state. The cooled polar molecules then undergo a resonance charge exchange with the excited rubidium atom, forming the dipole bound anion of interest. After a 1 μsec delay, the ions are then pulsed down a one meter time-of-flight mass spectrometer, with horizontal and vertical deflectors used to maximize ion signal. The flight tube of the mass spectrometer (biased at 200 V) was 2cm from the interaction region, with a grounded grid located 1 cm from the interaction region and the flight tube. The ions produced were then detected using microchannel plates (Burle Photonics) configured in a "z-stack" (i.e., three multi-channel plates oriented with a Z configuration of the detector channels to minimize ion back flow), allowing for greater sensitivity in detection of small signals. The signal was amplified (Ortec 474) and gated (SRS SR250) over the ion signal, with the averaged output sent through a data acquisition card to an acquisition program written in Labview. The un-gated raw data was visualized with an oscilloscope (HP Infinium) for empirical maximization of signal by tuning parameters of the pulsed valve or time-of-flight for efficient ion detection. The dye laser is then tuned over the wavelength range (typically between 595nm and 650nm) for 2 photon resonant excitation of various n_s and n_d levels of rubidium ($10 \leq n_s \leq 40$ & $8 \leq n_d \leq 39$) with the

relative ion formation for each resonance level recorded by the Labview program, allowing for determination of the n dependence of the dipole bound ion formation (i.e. the RET spectra).

An important aspect of the time-of-flight setup is an approximately 10 cm region held at ground potential prior to the detector that is free of electrodes, which we have determined allows for the detection of the neutrals resulting from detachment of these weakly bound ions while in flight. This open area provides some focusing of the ions as well as a region for future work on photo-dissociation or photodetatchment of these dipole bound states. The most important feature of this region is the decelerating affect it has on the ions, as shown using the SIMION[50] modeling program (Fig. 2.7). The dipole bound anions may detach as they travel down the flight tube as a result of blackbody photodetachment and/or rotational autodetachment. The neutrals that have been produced will then proceed without this deceleration, allowing for a shorter time-of-flight enabling them to be distinguished from the ion signal. The overall time-of-flight as well as the separation in time of the neutrals and ions were measured exactly as predicted from the model.

The draw out voltage used to pulse the ions down the time-of-flight tube was varied between 200 and 3000V. As previously discussed, the weakly bound dipole state transitions from a 2+1 ionization (2 photons to excite 1 to ionize) to a field ionization of the 2 photon resonant state resulting in increased Rb^+ signal. This allows us to accurately

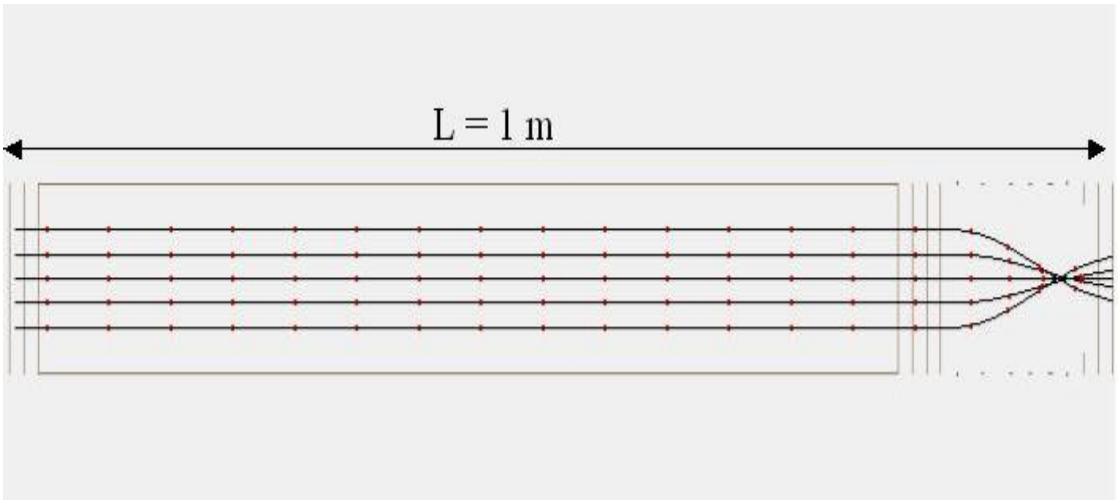

Figure 2.7. A scale model of the time-of-flight mass spectrometer used in this experiment (SIMION)50. The distance traveled by the ions in 2 μsec intervals is shown by the dots along the trajectory. The neutrals created while in the flight tube are assumed to travel at the same velocity as when they are created, allowing for excellent modeling of observed time-of-flight.

calibrate the electric fields employed based on the n level of this transition for varied electric fields (Fig. 2.8). The relative dipole bound anion signal detected for increasing electric fields is then used to determine the electron affinity of the molecule using the previously discussed theoretical framework established by Defrancoius et. al.[44] by employing Eqs. [4-7]. It should be noted that this technique can only be applied to very weakly bound ionic states as the electric fields available in this apparatus (< 2700 V/cm) are insufficient to detach anions that are too strongly bound ($EA \geq 5.5$meV).

Rydberg Electron Transfer to Nitroethane, Nitromethane, and their Dimers

Initial experiments employing this apparatus involved Rydberg electron transfer to nitroethane ($C_2H_5NO_2$), nitromethane (CH_3NO_2) and their respective dimers (Figs 2.9,2.10). This study was performed in collaboration with Dr. Kip Bowen in consideration of negative ions of nitroethane and its clusters[51]. The nitroethane and nitromethane molecules both support bound valence negative ion states, yet have dipole moments of sufficient strength to form a dipole bound anion (3.46, 3.23D respectively). The RET of nitromethane has been previously published[52, 53] and was commensurate with that measured in this experiment (Fig 2.11). The RET spectra for both molecules was very similar, displaying peaks in ion formation characteristic of attachment to a dipole bound state. The width of the peaks, as well as the continuing attachment for increasing n* is indicative of the influence of the valence state. Nitromethane has been shown to attach slow electrons[54] thus the ion formation at large n* for these molecules might be attributed to direct attachment in to the valence state, stabilized by the Rydberg core. The

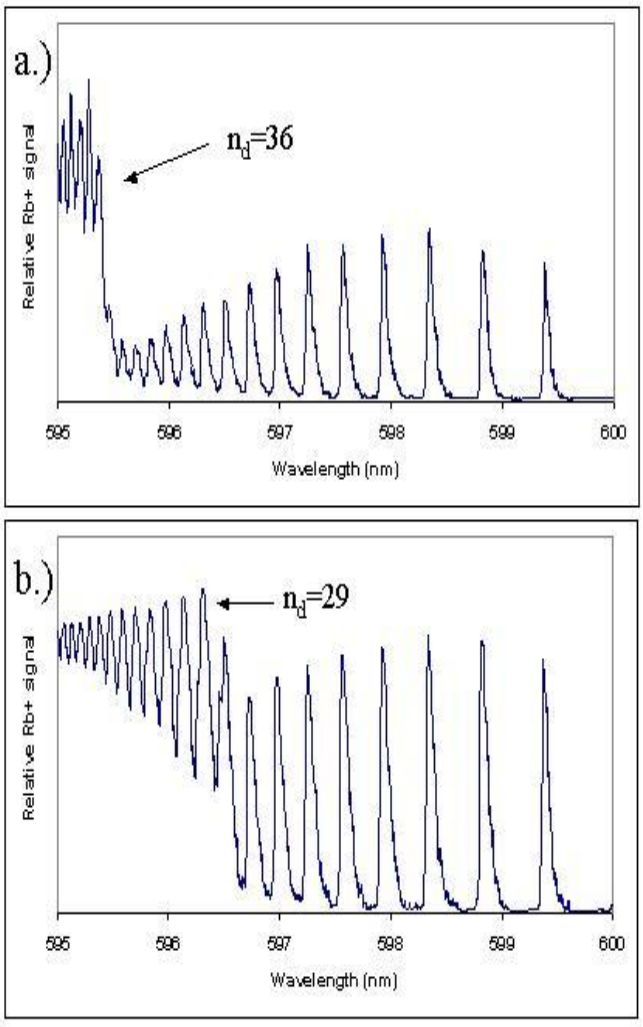

Figure 2.8. Relative ion signal of Rb+ resulting from (2+1) resonant photo ionization and field detachment of the 2 photon resonant state. For a draw out voltage of 250 V (a.) an electric field of ~225 V/cm field ionizes rydberg states with principle quantum number n≥36, whereas a draw out voltage of 750 (b.) produces an electric field of ~675 V/cm ionizing states with n≥29.

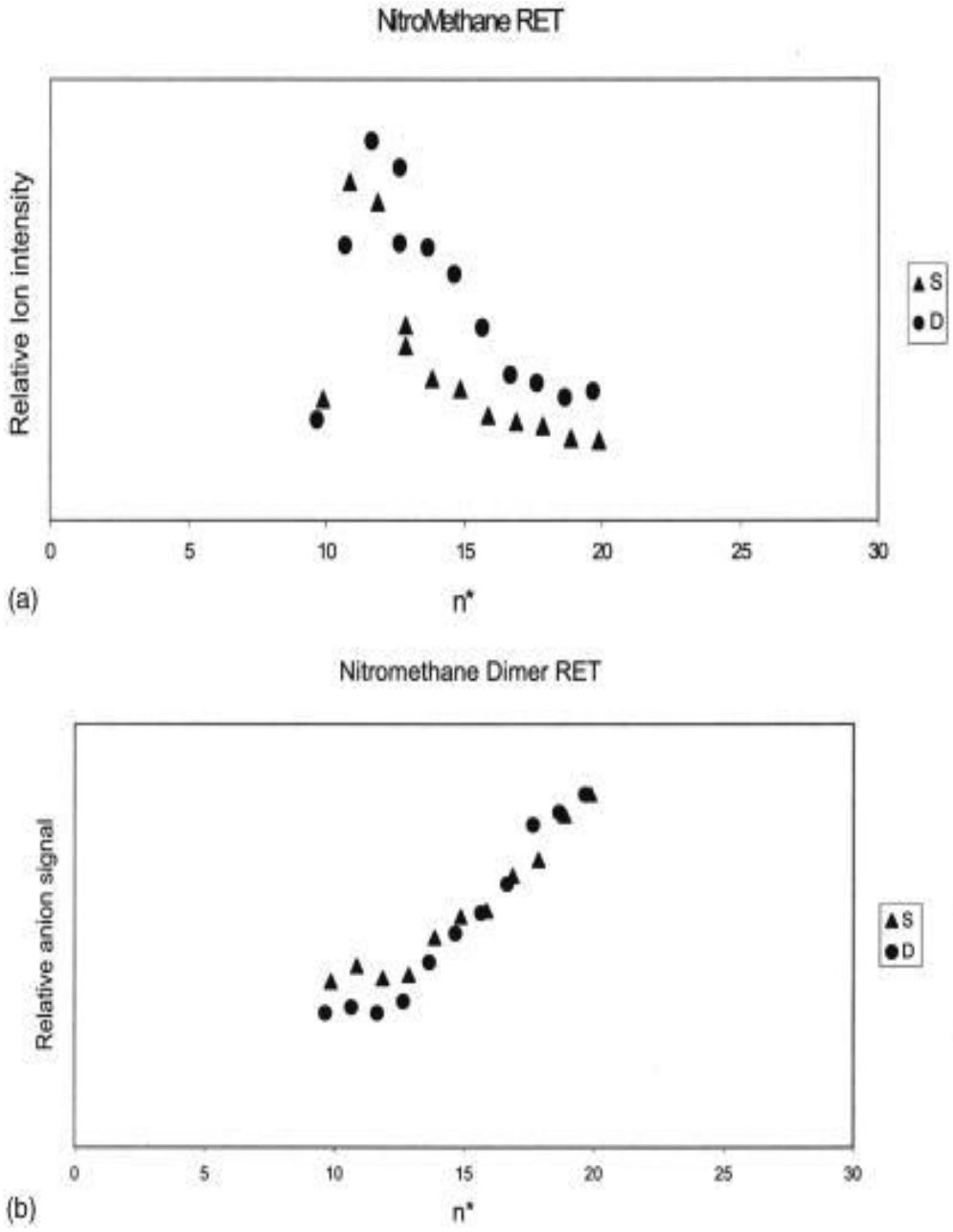

Figure 2.9. Relative anion formation resulting from RET from n_s (triangles) and n_d (circles) for nitromethane (a) and its dimmer (b.).

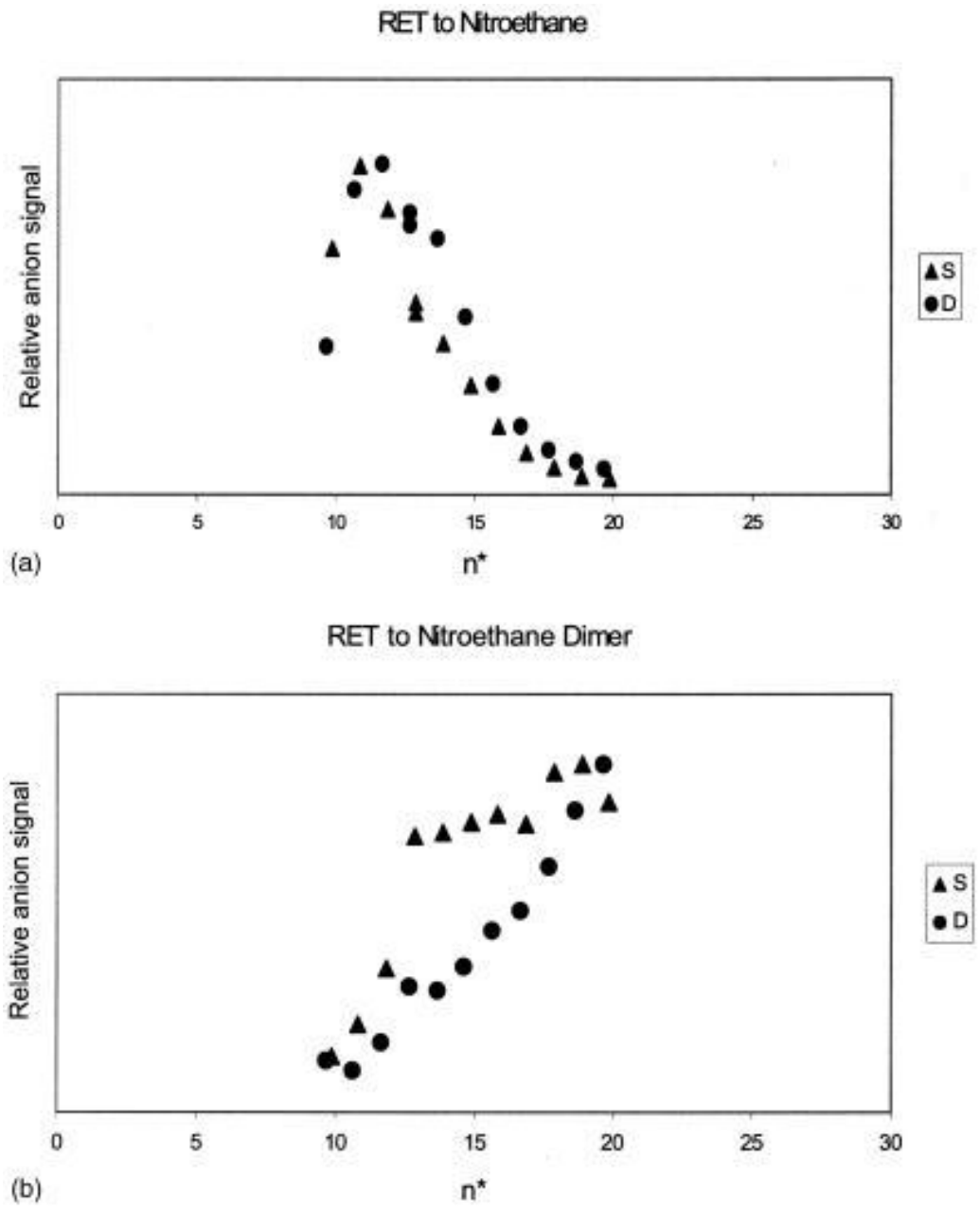

Figure 2.10. Relative anion formation resulting from RET from n_s (triangles) and n_d (circles) for nitroethane (a) and its dimmer (b.).

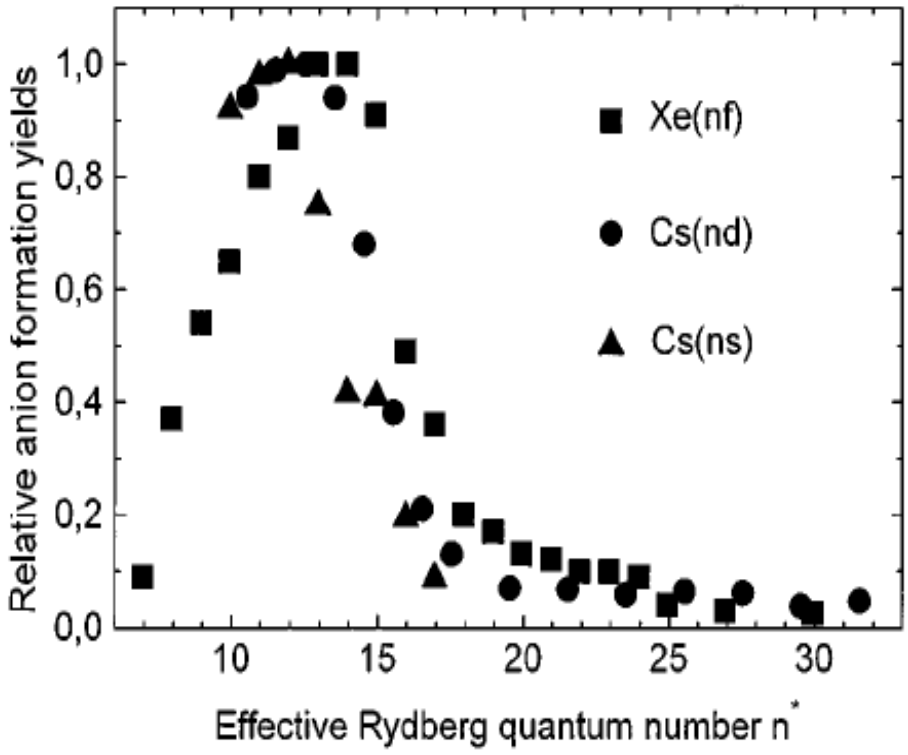

Figure 2.11. Previously published reports of the relative anion formation resulting from RET from n_s states of Cs (triangles), nd states of Cs (circles), and n_f states of Xe for nitromethane53.

peaks in ion formation corresponding to attachment to the dipole states are significantly wider than that observed for molecules without a bound valence state ($\Delta n^*/n^* \approx 1/2$ as opposed the typically observed $\Delta n^*/n^* \approx 1/5$) primarily towards higher n*. This could be indicative of coupling between the dipole bound and valence states. It has been postulated that the dipole bound state may act as a "doorway" state towards the formation of a valence bound anion. In the absence of the lower-lying valence state, anions formed in higher rotational states, which were present in the initially formed dipole bound anions, will autodetach before they can be detected. However, rapid dipole-valence anion coupling could act to stabilize the system through intermolecular charge transfer. RET to the dimers of these molecules primarily shows attachment into the valence state, as evidenced by the increasing ion formation rates for increasing n*.

Although these experiments were conducted to compliment the photoelectron spectroscopy results of Dr. Bowen, they pose several interesting questions with regards to our understanding of the dipole bound state. The RET spectra of both nitromethane and nitroethane show significant ℓ dependence (Figs. 2.9-2.11). Ions formed from n_s states (ℓ=0) displayed a lower n^*_{max} as well as a sharper peak than those formed from n_d (ℓ=2) states. The previously published reports on nitromethane also show this observation, with the dipole bound anions formed from n_f (ℓ=3) rydberg states continuing the trend of higher n^*_{max} for RET from higher ℓ states, but this feature was not commented upon. This ℓ dependence on the RET spectra has not been observed or discussed previously for any of the dipole bound anions studied thus far. Understanding the basis for the observed

ℓ dependence may garner insight into the rydberg electron transfer process, or the nature of the coupling between the dipole and valence states. The effect of coupling between the valence and dipole states is clearly observed in the RET spectra, yet is not fully understood or modeled theoretically. The wide profile of the observed RET spectra for these molecules rendered them unsuitable for application of the curve crossing model. The large binding energy of these dipole states (*EA* >20 meV) required too large an electric field to observe electric field detachment of these anions in the system employed, thus determination of the electron affinity was limited to use of Eq. [1]. The determined *EA*s have a significant uncertainty associated with them, specifically due to the observed ℓ dependence. For instance, the *EA* of the dipole bound anion of nitroethane was determined as 28.47 and 25.28 meV, for the n_s and n_d profiles, respectively. The *EA* for nitromethane was determined to be similar (~25 meV±5meV), somewhat higher than that previously published[53] due to its inclusion of the n_f series presenting a higher n^*_{max} and thus a lower *EA* as determined by Eq. [1]. The possibility of this coupling leading to dipole states acting as "doorway" states towards valence anion formation may have significant repercussions in understanding charge transfer in large biological molecules. Furthermore, the RET of the nitromethane dimer shows a small increase of the ion signal in an n* range commensurate with n^*_{max} for formation of the dipole bound anion of the monomer. This is interesting as the nitromethane dimer is expected to have a near zero dipole moment. This raises the possibility of an electron binding to a local dipole field, possibly facilitated by coupling to a valence state, or even binding to the quadrupole moment of this molecule. Binding of electrons to the quadrupole moment of a molecule

has been observed[55], though comprehensive modeling of these systems is limited by the difficulties in their unambiguous observation. Further study of molecules with large quadrupole but low dipole moment, both bound valence and dipole states, as well as molecules with low dipole moments but large local dipole moments, are vital to understanding these effects. Furthermore, observation of ℓ dependant RET formation of dipole bound anions should be sought out in an effort to better understand the fundamental reasons for this dependence, and allow for its theoretical consideration to improve current models. This experiment highlights just a few of the many questions surrounding dipole bound anion formation, and raises several intriguing possibilities about the impact these exotic negative ion states may have in other fields.

Rotational effects on detachment of dipole bound anions

As discussed above, dipole bound anions are very weakly bound anionic states in which the electron resides in a very diffuse orbital bound to the positive pole of the molecules dipole moment. This weak binding and extended structure raises questions as to the applicability of the Born-Oppenheimer, which requires the motion of the electron to be significantly faster than the nuclear motion. Therefore rotations of the molecule are an important consideration, as suggested early on by Garret and Crawford[30,31,32]. Observation of above threshold rotational resonances in photodetachment of valence bound anions with bound dipole states by Brauman[30] and Lineberger[39], suggest unbound rotationally excited dipole states, which may autodetach with some finite lifetime. Clary[56] and Simons[57] have explicitly considered these effects theoretically with Simons

making modifications to the original rotationally adiabatic model of Clary to calculate the rotational autodetachment lifetimes for the CH_2CN^- anion for J= 31 to 39. Rotational autodetachment of a dipole bound anion has not been observed experimentally, however detachment of these states in a penning trap as a result of black body photodetachment has been reported by Seuss et al. [58, 59]. A 300 K blackbody spectrum peaks at a photon energy of ~120 meV well above the photodetachment threshold for all known dipole-bound anions. Calculated lifetimes by Chernov et. al.[60] based upon direct photodetachment, are in agreement with the measured lifetimes. The calculated lifetimes are primarily a function of the dipole moment of the molecule and its electron affinity, however, experiments to be discussed below show that rotational characteristics of the molecule have a significant impact on the observed detachment of dipole bound anions.

Electron detachment from dipole bound anions studied is observed by detection of neutral molecules resulting from detachment of the dipole bound electron while the molecule is traveling down the flight tube of the mass spectrometer. The ability to make this observation is due to the sensitivity of the "Z-stack" micro channel plate assembly and the configuration of the TOF-MS discussed previously, which provides a deceleration to ions just prior to detection allowing for the neutral to arrive at a slightly smaller time of flight (Fig. 2.7). Verification of the neutral peaks came from the application of both magnetic and electric fields. A movable permanent magnet (~300 Gauss) was placed perpendicular to the path of the ions and neutrals down the flight tube. The ion signal is deflected by this magnetic field and disappears completely while the

neutral signal remains. The magnitude of the neutral signal varied dependent upon the placement of the magnetic field down the flight tube giving some indication as to where the detachment was taking place. Additionally, electrodes between the flight tube and detector were held at varying voltages (for normal operation these potentials were identical to the flight tube voltage), having a pronounced effect upon the time-of-flight of the ion signal but not the neutral signal.

The optimized geometry and pertinent molecular characteristics (dipole moment, electron affinity, and moment of inertia) of the polar molecules studied in this experiment are as shown in Fig 2.12. In light of the significant role of blackbody photodetachment in the detachment of dipole bound anions[58,59] the molecules were chosen in such a way as to allow focus on the rotational effects on the observed detachment. The lifetime of these molecules towards electron detachment due to blackbody photodetachment is primarily a function of the molecules dipole moment and electron affinity[60]. Thus molecules chosen for this study represent pairs of molecules [acetonitrile (CH_3CN) and trimethyl-acetonitrile ((CH3)3CCN), as well as acetone ($OC(CH_3)_2$) and cyclobutanone ($OC(CH_2)_3$)] with similar dipole moment and electron affinity, while varying in moment of inertia. The moments of inertia, primarily those orthogonal to the dipole moment, are expected to play an important role due to the extended nature of the diffuse electron orbital in which the dipole bound electron resides. By choosing pairs of molecules with similar dipole moments and electron affinities, and thus expected lifetime towards blackbody photodetachment, relative differences in observed detachment of these

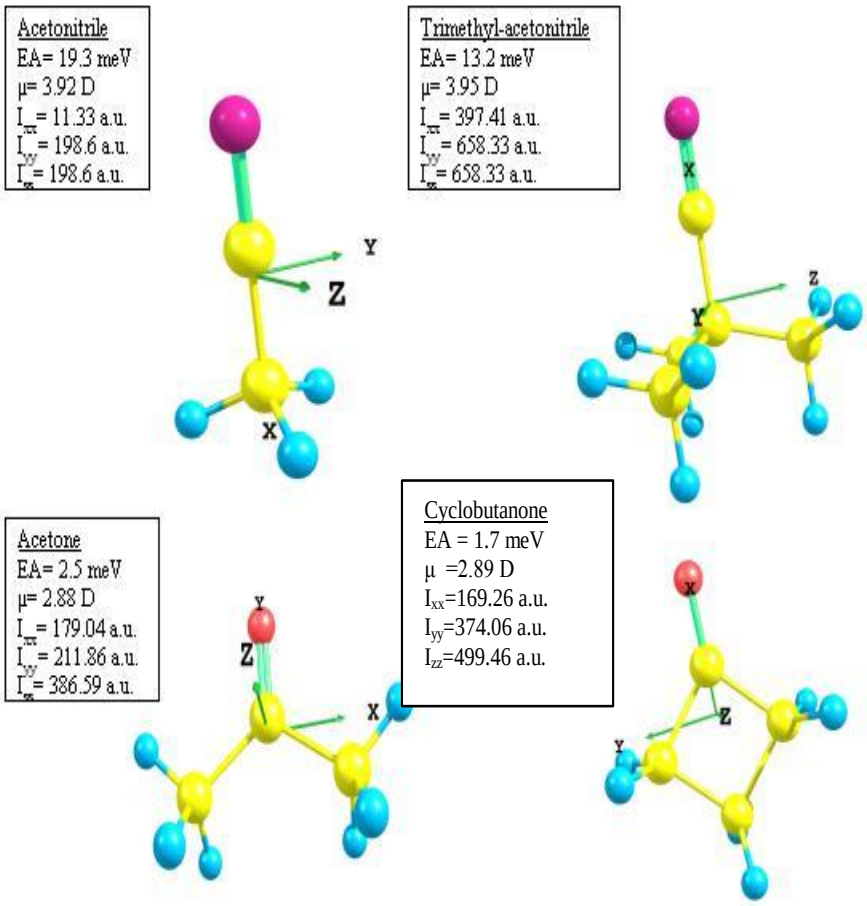

Figure 2.12. Structures of the polar molecules examined in this study along with their relevant physical properties.

molecules can be used to address the effect of rotations on the detachment of dipole bound anions.

The production of neutrals observed in this system can originate from many sources, such as autodetachment of a rotationally excited state, blackbody photodetachment, or collisional detachment. As such, production of the neutral signals observed in this study was highly dependent upon experimental conditions, primarily the background pressure inside the interaction region. This background pressure is greatly affected by the amount of gas pulsed in as well as the rate of pumping taking place in the interaction region. The pulsed nozzle-jet was directed downward into 500 l/sec turbo-molecular pump and the interaction region pressure varied from ~10^{-6} to ~10^{-5} torr, dependent upon the rate at which sample is pulsed into the region and the pumping rate. The pressure in this interaction region is significant as it will have an effect on the RET formation rate, as well influence the rate of collision induced processes such as collisional dissociation or collision induced rotational excitation. To account for varying ion signal, the relative neutral signal was taken as the ratio of neutral to ion signal. This relative signal was then studied for different interaction region pressures and pulsed valve conditions (i.e. amount of seeding to promote ro-vibrational cooling) for acetone (Fig 2.13) and acetonitrile (Fig. 2.14) as they produced large enough signal for quantitative analysis. The three data sets corresponds to an increasing amount of argon seeded into the pulsed valve expansion of the molecule of interest promoting vibrational and

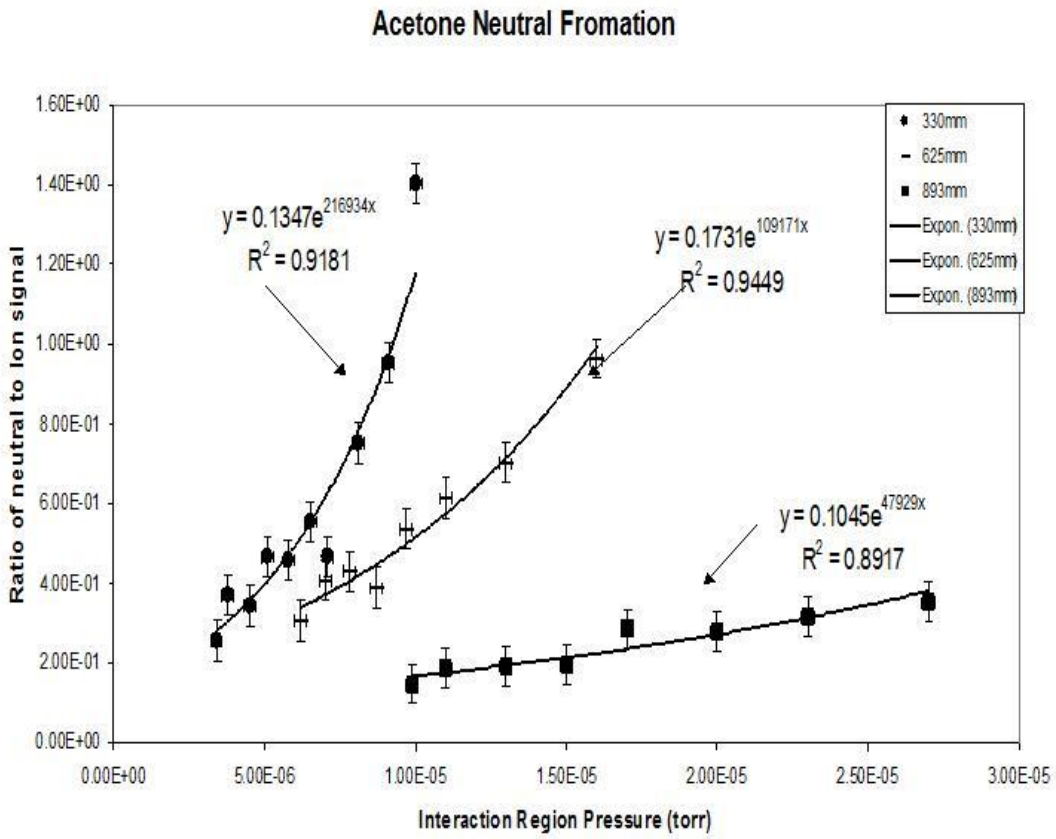

Figure 2.13. Relative neutral formation from dipole bound anions of acetone for varying interaction region pressures. Each data set corresponds to a increasing amount of seeded argon as measured by the backing pressure of the pulsed valve (330 mmHg triangles, 625 mmHg dashes, and 893 mmHg squares).

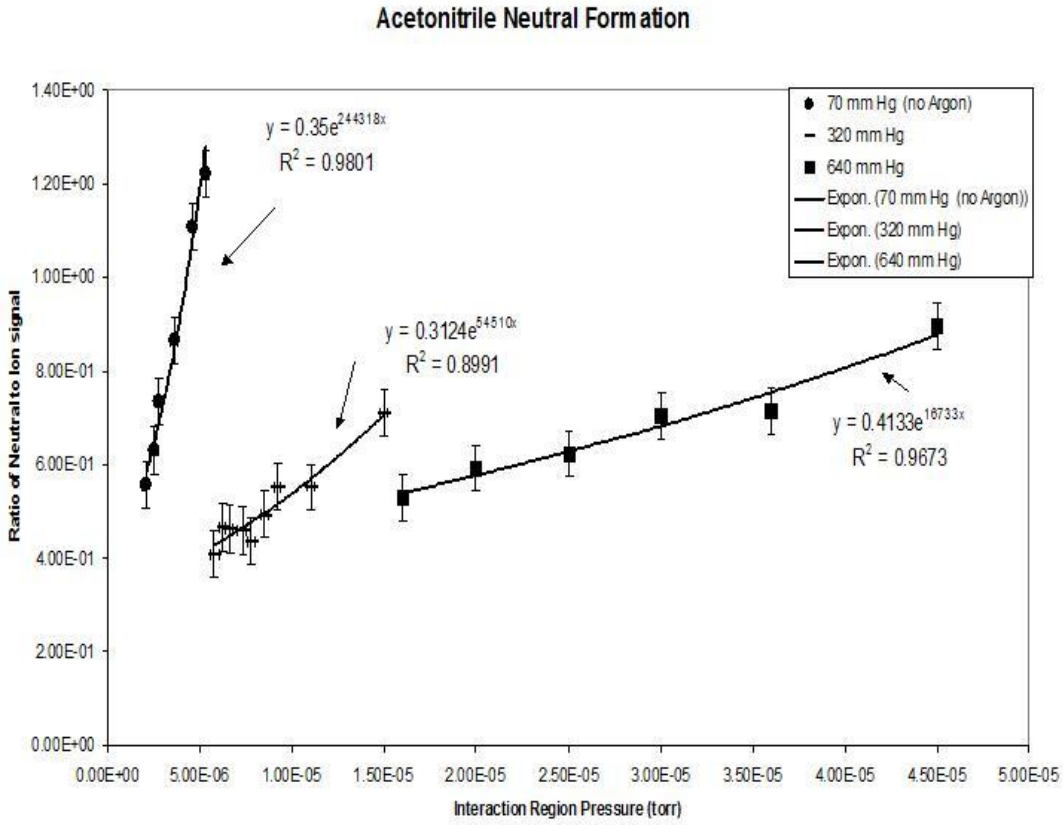

Figure 2.14. Relative neutral formation from dipole bound anions of acetonitrile for varying interaction region pressures. Each data set corresponds to a differing amount of seeded argon as measured by the backing pressure of the pulsed valve (70 mmHg (no argon) circles, 320 mmHg dashes, and 540 mmHg squares).

rotational cooling. As the density of the polar molecule is lowered by the argon seeding, larger amounts of seeded sample pulsed into the interaction region was required to produce ion signal. The pressure dependence on the neutral formation was then determined empirically by limiting the rate of pumping on the interaction region raising the background pressure. The neutral-to-ion ratio seemingly increases exponentially with increased pressure, as seen by the included fits to the data. Importantly, the data suggests a measurable amount of neutral present at the lowest pressures available, though it should be noted that the interaction pressure is measured by an ionization gauge (Varian 564) attached to the interaction region, thus only indicative of relative changes in pressure and not absolute measurements of pressure in the ion formation region. This would signify that neutral production is not solely due to a collisional process, either collisional dissociation or rotational excitation prompted by collisions. This may be indicative of rotational autodetachment of a dipole bound anion formed in a short lived rotationally excited state, however, it may also be accounted for by blackbody photodetachment, as their calculated lifetimes (70 to 100 μsec) suggest measurable neutral formation on our experimental time scale (20 to 60 μsec). Complete theoretical modeling of this pressure dependence is not possible, as in addition to the experimental uncertainties involved, many competing effects complicate the matter greatly. There is likely a substantial pressure dependence on dipole anion formation due to the density of the target molecule in the interaction region, as well as a pressure dependent effect on the relative collisional velocity of the molecule with the rydberg atom, known to influence RET rate[45]. Additionally there are the various collisional processes with undetermined pressure

dependencies, not all of which are observable in this experiment. Only neutrals resulting from rotational excitation from collisions, photodetatchment from background blackbody radiation, or rotational autodetachment from unbound rotationally excited states are expected to detach during the time of flight, and thus be observable in our system. Neutrals resulting from collisional detachment in the source will not be observable, however, as they are created before the molecule is fully accelerated down the flight tube, resulting in a significantly lower resolution of the neutral peak than the ion peak, which was not observed. Given the pressures inherent to the system (~10^6 to ~10^5 Torr) it is likely that collisions will continue as the ions travel down the flight tube, though the extent of which is undetermined. Qualitatively, though, there are important observations to be made about the relative pressure dependencies. The increase in relative neutral signal with increasing pressure indicates rotational excitation of these molecules prompted by collisions, as had been previously postulated[58,59] but not verified experimentally. Furthermore, the decreasing amount of relative neutral signal from "cooler" samples (i.e. samples pulsed with larger amounts of argon seed gas resulting in a lower distribution of ro-vibrational states of the polar molecule and thus the formed dipole bound anion) as well as the smaller rate of pressure dependence observed for these samples indicate the internal energy distribution of the dipole bound anion plays a major role in collisional excitation and detachment of these anions.

In light of the difficulties in quantifying the pressure dependence of the observed detachment, as well as the difficulty in exactly recreating experimental conditions, the

dipole bound anion pairs of commensurate dipole moment and electron affinity were studied simultaneously. This was possible due to each pair of molecules having similar RET spectra (i.e. signal versus n*), due to their similar electron affinities. The ion and neutral signals from production of dipole bound anions of acetone and cyclobutanone (Fig. 2.15), as well as acetonitrile and trimethyl-acetonitrile (Fig. 2.16), for various pressures in the interaction region are as shown. The previously mentioned pressure dependence is clearly evident. As the pressure in the interaction region is increased, we see an increase in the amount of neutrals detected with minimal impact on the ion signal. Acetonitrile and acetone consistently produce more neutral relative to ion signal than for the case of trimethyl-acetonitrile and cyclobutanone, respectively, independent of the experimental conditions employed. This contradicts predictions based on blackbody photodetachment rates, which would suggest equivalent or slightly higher rates of neutral formation for trimethyl acetonitrile and cyclobutanone due to their lower *EA*. We attribute the larger autodetachment to the effects of the moments of inertia of the two molecules. The moment of inertia for trimethyl acetonitrile and cyclobutanone are much larger than that of acetonitrile and acetone respectively, primarily along the principal axes perpendicular to the dipole moment (Fig 2.12). Thus the rotational energy spacing will be smaller for these molecules, influencing their internal energy distribution as well as their respective cross sections towards collision induced rotational excitation. The inability to probe direct collisional detachment of the molecules limits definitive analysis, as we are unable to distinguish whether the molecules with smaller moment of inertia truly exhibit increased detachment, or whether a larger portion simply detach on a longer

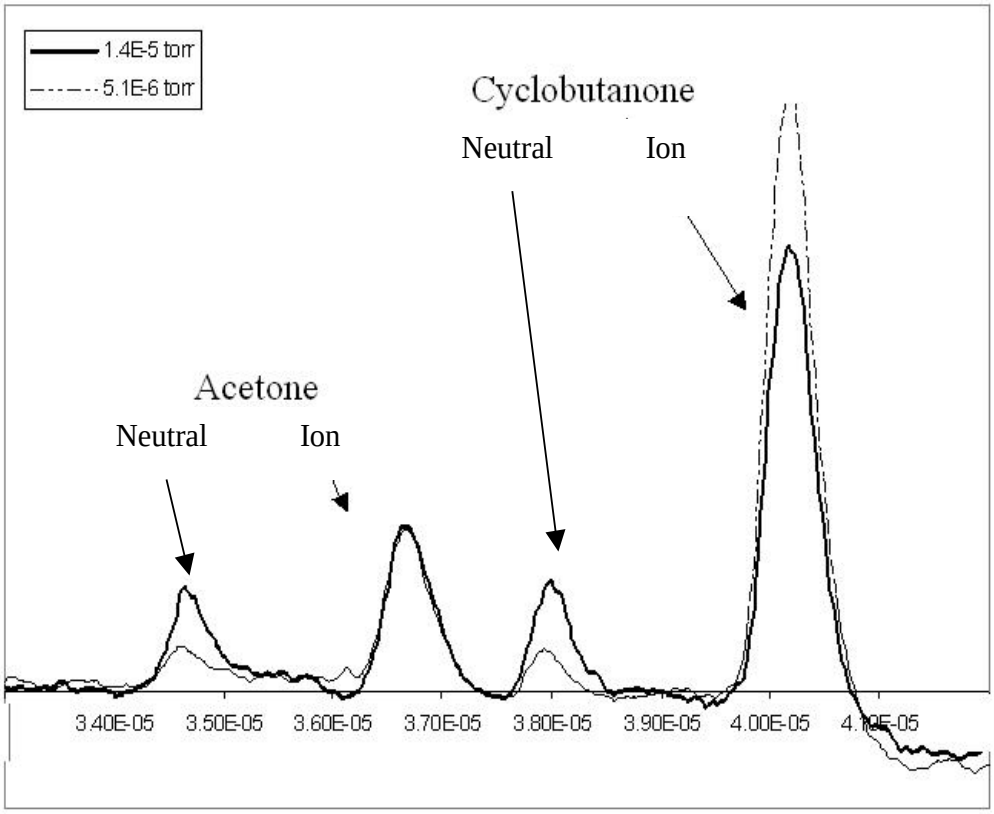

Figure 2.15. Time-of flight spectra showing dipole bound anions of acetone and cyclobutanone. The corresponding peaks of slightly shorter time are the neutral signals formed from detachment of the ions while in the flight tube. The overlying spectra represent varying pressures in the interaction region during the RET process.

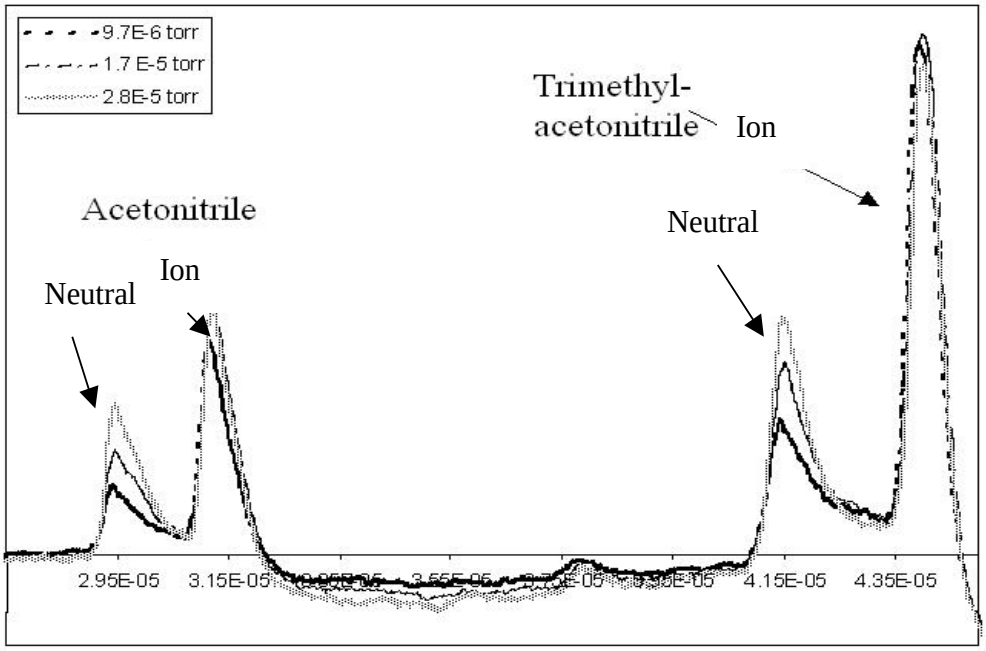

Figure 2.16, Time-of Flight spectra showing dipole bound anions of acetonitrile and trimethylacetonitrile. The corresponding peaks of slightly shorter time are the neutral signals formed from detachment of the ions while in the flight tube. The overlying spectra represent varying pressures in the interaction region during the RET process.

time scale (i.e. the molecules with larger moment of inertia may simply be more prone to direct collisional detachment in the interaction region resulting in a smaller relative signal of observable detachment in the flight tube).

In conclusion, these experiments highlight the importance that rotational characteristics of a molecule have on the stability of its dipole bound anion. Detachment of these ions on the time scale of 1 to 50 μsec is evident in the observation of neutral molecules resulting from detachment of dipole bound anions pulsed down the time-of-flight mass spectrometer. Predictions of blackbody photodetachment lifetimes for these molecules are fairly consistent with results, however, the significant dependence of the neutrals observed with the internal energy of the molecule, collisional cross section as determined by the background pressure in the interaction region, as well as the moment of inertia of the dipole bound anion imply that rotational characteristics of the molecule play an important role. Continued study of the lifetime of dipole bound anions, specifically with regard to their rotational characteristics, will greatly increase our ability to understand and model these systems.

Rotational States of Dipole Bound Hydrogen Cyanide

As a model molecular system there is great interest in the properties of the hydrogen cyanide molecule. HCN has been detected in the interstellar medium[61,62] as well as in some comets[63,64] using radio emissions and infrared absorption, respectively. Also, HCN is known to be involved in the synthesis of biologically significant molecules

such as amino acids[65]. As a polar closed shell molecule HCN does not support a valence bound negative ion. However, the μ=2.984 Debye dipole moment of *HCN*[66] is well above the critical moment of required for binding an excess electron to a polar molecule under real experimental conditions. HCN^- has long served as the simplest example of a dipole-bound anion[67] and a number of theoretical studies have predicted a weak binding energy of: 1.63 meV[68], 1.24 meV[69], and .87 meV[70] , all calculated within the Born Oppenheimer (BO) approximation. However, because the moment of inertia is small and the electron-dipolar binding is expected to be weak, it can be anticipated from earlier theoretical studies that non-Born-Oppenheimer effects, due to coupling of electron motion to rotational motion of the nuclei, will be of critical importance to the negative ion energy spectrum[71]. Theoretically predicted effects in their rotational spectra[71] have not previously been experimentally verified. The only spectroscopic signatures for such anions come from the experiments of Brauman[38] and Lineberger[39] in their previously discussed observation of rotational resonances in valence to dipole bound photoelectron spectra.

A polar molecule possessing a supercritical moment has an infinite spectrum of ground and excited anion states in the BO approximation, but the effects of rotational degrees of freedom are so important in the problem that inclusion of such effects reduces the expected spectrum to a finite number[71]. Indeed for small dipolar molecules (small moment of inertia) with supercritical moments near 2.5 Debye, such as HCN, the

predicted number of states reduces to very few – among the sparsest spectra of all real isolated quantum systems.

This experiment employs measurements of the RET spectra and field detachment rates of dipole bound HCN towards verification of the predicted rotational effects in this system. Theoretical collaborators L. Adamowitz and W. R. Garrett have provided theoretical predictions of the electron affinity and rotational spectra for this molecule with excellent agreement with observed results. This work represents an experimental observation of the breakdown in the Born Oppenheimer approximation, and signifies the importance of rotations in understanding dipole bound negative ion states.

The apparatus employed remains unchanged from previous description in this chapter. The HCN was produced by first placing 32 mg of NaCN in a sample holder at liquid nitrogen temperature. Then 2ml of H_2SO_4 was added and the sample holder was closed off and brought to room temperature, re-frozen, pumped, and thawed to produce clean HCN. The RET spectra observed differed drastically from the narrow peak in ion formation typical[45] of dipole states. The RET spectra was much wider than predicted by the curve crossing model of Desfrancois, and showed large variability in structure. The spectra were strongly influenced by ro-vibrational cooling factors (i.e. Ar seeding and pulsed valve conditions) as well as collisional factors (i.e. background pressure in the interaction region), being complicated by the fact that these factors are highly coupled, as cooling enhancement was accompanied by higher background pressure in the collision region. HCN beams seeded with 50% Ar yield a peaked profile [Fig 2.17, x], or a profile

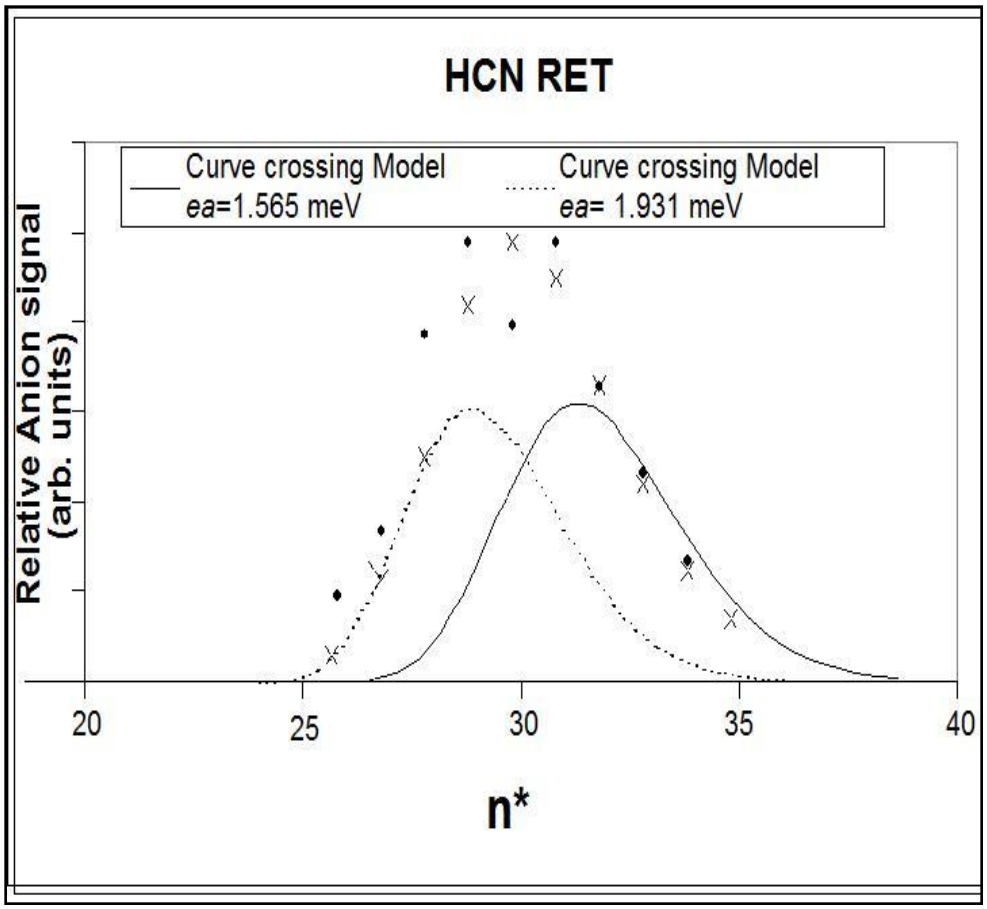

Figure2.17. Relative HCN- signal formed from Ar seeded (x) and unseeded(•) HCN, as well as unscaled theoretical fits for electron biding energies of 1.56 and 1.93 meV.

with a broader plateau. With neat HCN, broad profiles with two distinct peaks of variable intensity were produced [Fig. 2.17, •]. These results indicate Rydberg electron transfer corresponding to electron binding energies of 1.56 and 1.93 meV as indicated in Figure 2.17 as solid curves derived from the curve crossing model. The variable relative intensity of the two spectra resulting in the variability of observed RET spectra is due to the highly coupled influence of the collisional and cooling factors, which are impossible to decouple in the context of this experiment.

Further evidence of multiple negative ion states is found in the field detachment data for HCN^- formed from different n* levels of Rb. In previous studies, the field detachment profiles are smooth and modeled well bye Eq. [4]. The *Ea*s determined were consistent for ions formed from any of the n* levels in it's RET spectra, but for HCN [Fig 2.17] this is not the case. HCN^- formed at lower values of n* consistently showed the best agreement with theoretical expectations for a single state with $ea \approx 1.56$ meV, but those formed at higher n* values showed partial detachment at lower electric fields. The shape of the detachment curve for ions formed at larger n* can best be modeled with a convolution of two field detachment curves. Field detachment calculations using two electron affinities (1.2 and 1.56 meV) are shown in Fig. 2.18.

In order to understand these seemingly contrary observations, we must consider the predicted rotational spectrum for this anion. Calculations performed by Adamowitz, of the fixed dipole electron affinity within the BO approximation (Table 2.2) were

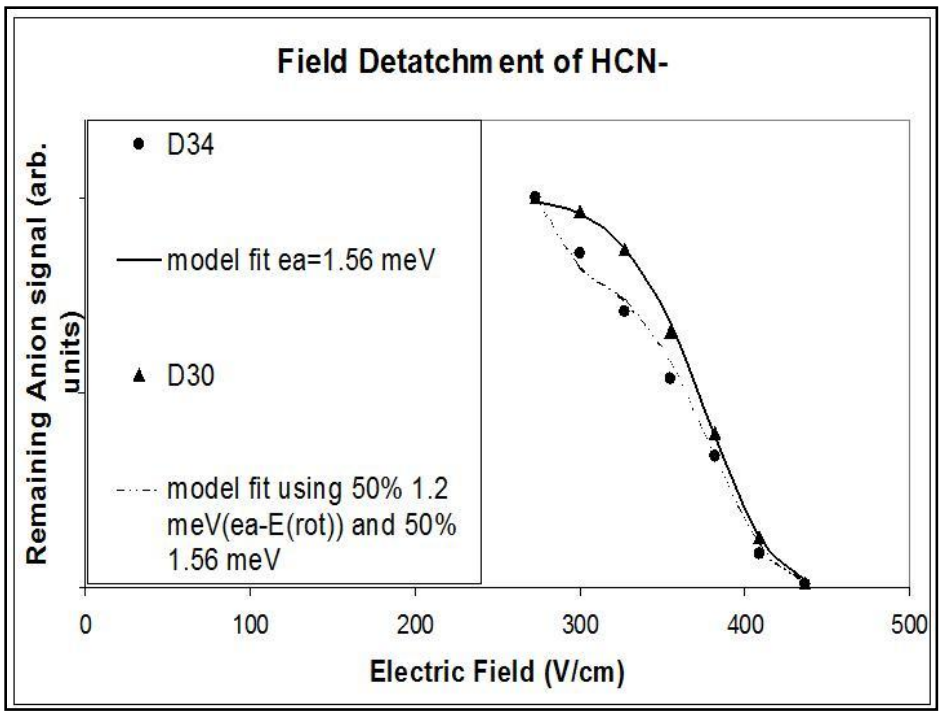

Figure 2.18. Experimental field detachment data from nd=34(•) and nd=30(▲) excited levels of Rb. Also shown are theoretical fits (Eq. 4) for an ea=1.56 meV and a convolution of ea=1.2meV and ea=1.56meV.

Table 2.2. Electron affinity of the HCN molecule calculated for the geometries fully optimized at the. MP2/aug-cc-pVTZ + level of theory.

Method/Basis Set	EA, meV
MP2/aug-cc-pVTZ +	1.842
MP2/aug-cc-pVQZ +	1.874
MP2/aug-cc-pV5Z +	1.896
MP2/aug-cc-pV6Z +	1.910
CCSD(T)/aug-cc-pVTZ +	1.548
CCSD(T)/aug-cc-pVQZ +	1.629
CCSD(T)/aug-cc-pV5Z +	1.646

calculated as the energy difference between neutral HCN and its anion at the MP2/aug-cc-pVxZ+ (x=T, Q, 5, 6) and CCSD(T)/aug-cc-pVxZ+ (x=T, Q, 5) levels with accounting for the zero-point energy correction. The singly occupied molecular orbital of the HCN anion (Fig 2.19) was also calculated showing the diffuse electron orbital associated with the positive pole of the HCN dipole moment. All calculations were performed using the Gaussian 03 program package[72]. For the theoretical ground state BO electron affinity, the lowest LUMO energy was produced when exponents for the (7s7p) shells were 0.064, 0.016, 0.004, 0.001, 0.000254, 0.0000625 and 0.000016 atomic units; the (3d) exponents were 0.016, 0.004 and 0.001 atomic units; the (1f) exponent was chosen to be 0.016 atomic units. Garrett continued the theoretical modeling of this ion by applying the dipole-rotor model, details of which are found in Ref[71]. By employing the calculated properties of the HCN molecule and the experimentally derived ground state electron affinity in the dipole-rotor model he was able to establish the rotational energy spectrum of the anion (Table 2.3 and Fig 2.20).

With reference to Fig. 2.20, all of the data can be reconciled as RET and FD measurements resolving a system possessing only three bound states. The RET and FD profiles are consistent with two states of the dipole bound anion, bound by 1.56 and 1.2 meV. The data implies that anions are formed from both the ground state and the first rotationally excited state of the neutral [Fig 2.19]. For HCN, the electron and nuclear motions are strongly coupled, thus in the RET process the rotationally excited neutral can form a ground state anion as well as its rotationally excited analog. This would imply an

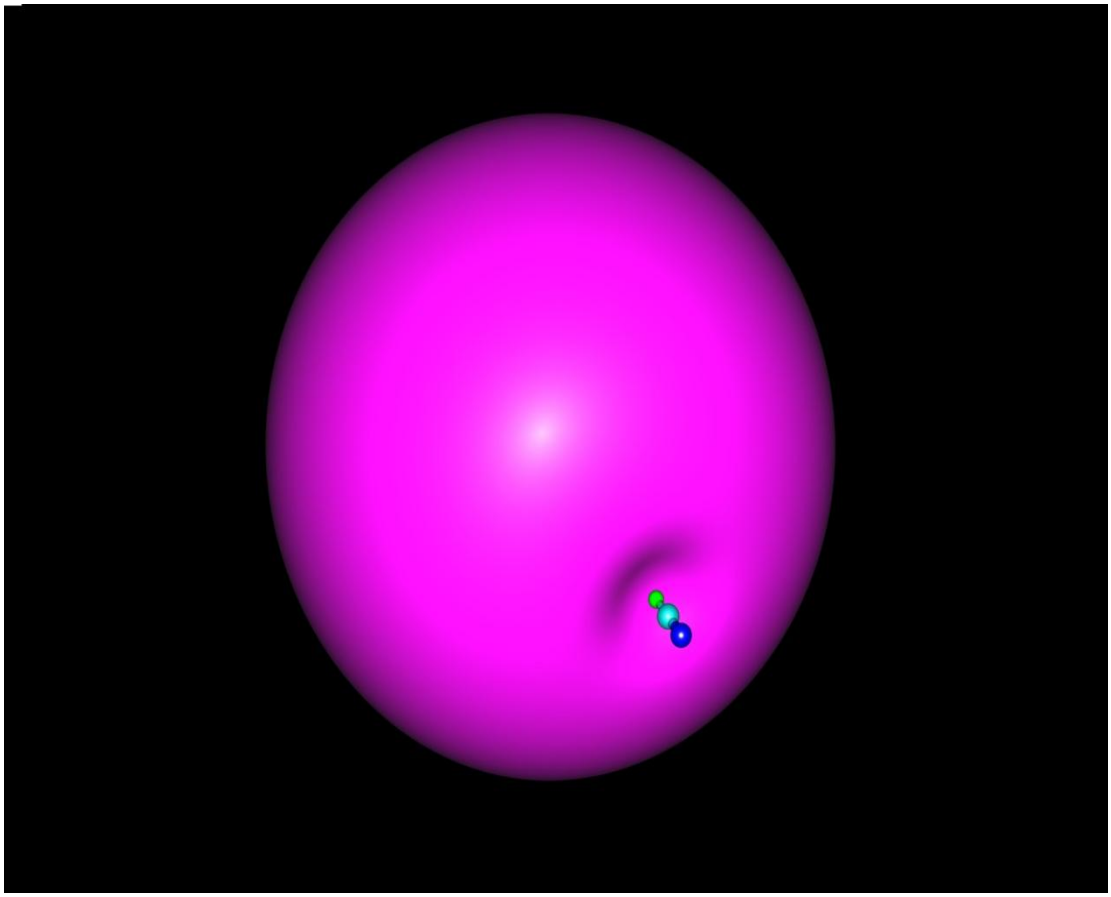

Figure 2.19. 3D plot of the singly occupied MO of the HCN anion. The contour value is 0.0015 a.u. and 97% of the total electron density is within this contour.

Table 2.3. *HCN*- energies in rotational states *J*=0,1,2,3 with infinite and proper HCN moments of inertia. Pseudopotential Parameters:V_0=2.0, R_m=4.4, Rc=3.05, α_0 =15.27, α_2=2.08, Q_{zz} =3.28, μ=1.170, S=2.04. (Atomic units)

Angular Momentum	Binding Energy (eV) Infinite Inertial Moment	Binding Energy (eV) HCN Inertial Moment
J=0	-.0016636	-.0015646
J=1	-.0016650	-.0011910
J=2	-.0016641	-.0004491
J=3	-.0016163	E >0.0

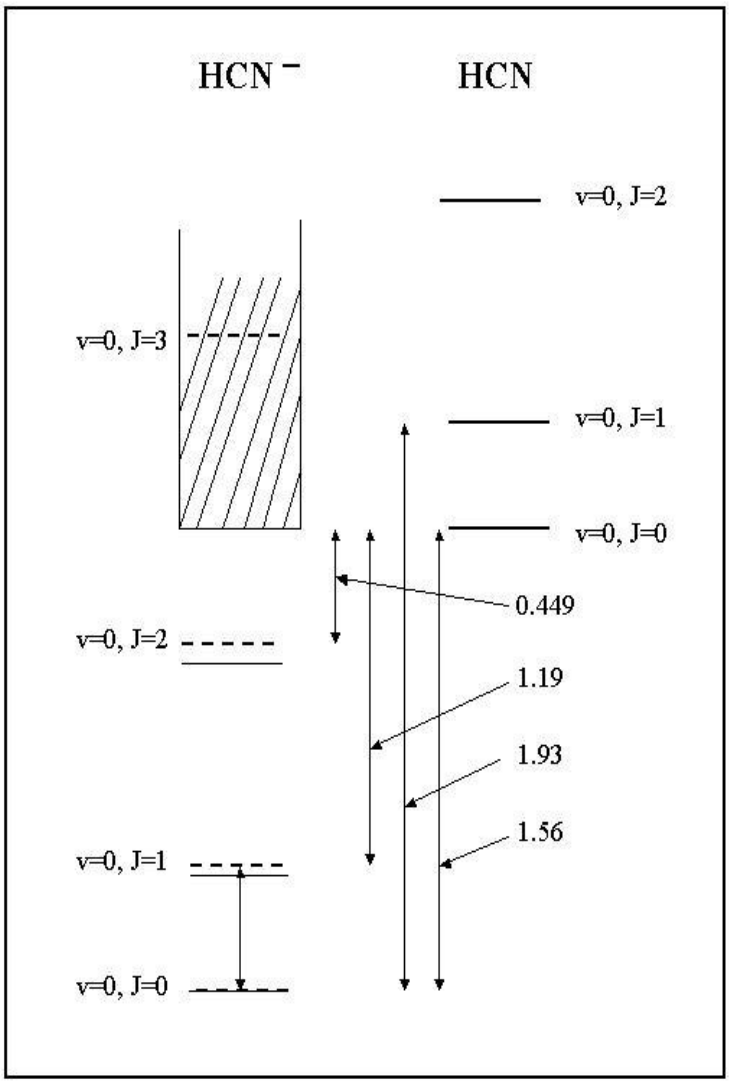

Figure 2.20. Energy levels for HCN and its dipole bound anion. Broken lines show close coupling levels. Solid lines are results in fixed nuclei approximation.

RET profile for the (*ea)* as well as for ($ea + E_{Rot}$). The varying RET profiles are then comprised of different convolutions of these two profiles. Therefore, the RET taking place at lower n*, and thus higher energy defect, is from *J=1* of the neutral to *J=0* of the anion. The RET at higher n* is from *J=1* to *J=1* as well as *J=0* to *J=0* (the true electron affinity). The field detachment data shows excellent agreement with an electron affinity of ~1.56 meV for anions formed from smaller n* values. But as the values of n* increases the data indicate detachment from a lesser-bound state. Therefore field detachment of anions formed from lower values of n* involve anions with *J=0* only, thus indicative of the true electron affinity, (found here experimentally to be 1.56(5) meV). Anions produced by RET from larger values of n* will include both the *J=0* and *J=1* states, as the RET from these n* states include both the *J=1* to *J=1* and *J=0* to *J=0* electron attachment. Field detachment of these anions will then include a *J=1* component that detaches at lower electric field. A convolution of detachment from *ea*=1.56 and ea-E_{Rot}=1.2 meV fits the data and the predicted values very well. From the theory we expect that the higher *J=2* level has an electron affinity sufficiently small to cause detachment to occur at fields too low for this state to be observed in this system (i.e. the anion is fully detached for fields greater than ~90 V/cm) while the J=3 state is in the continuum.

In light of these observations of the highly truncated nature of the rotational spectra for dipole bound anions as predicted, it is important to consider why this had not yet been observed given the extensive use of the techniques employed. The reasons lay in particular qualities of the molecular system examined. The HCN molecule has ideal

characteristics for the detection of multiple RET profiles and their subsequent field detachment. The most important feature is the low binding energy of the HCN dipole bound anion. This was important for several reasons. The low *EA* of this state required RET from n* states very near the ionization limit of the Rydberg atom, and thus very close energetically. This energetic difference essentially determines the "spectral resolution" of the observed Rydberg electron transfer. Furthermore, the low electron affinity of dipole bound HCN^- leads to very few of the rotational states being bound. The truncated nature of the observed rotational spectrum is vital in allowing us to unambiguously assign rotational transitions in the RET (i.e. *J=0* to *J=0* or *J=1* to *J=0*). If more bound rotational states were available, the inclusions of multiple rotational transitions would make analysis difficult or impossible. Equally important for observation of the rotational spectra is the low moment of inertia of the HCN molecule. This allows for adequate spacing in the rotational energy levels to be observed through RET as well as limiting the number of bound rotational states. The vast majority of dipole bound anions thus far studied have all displayed either too large an *EA* or to large a moment of inertia for the subtle effects of the truncated rotational spectra to be unambiguously observed, as it has been for HCN.

In conclusion, the small moment of inertia and *EA* of HCN allow for the application of RET and FD techniques to resolve rotational effects in a dipole bound anion for the first time. Predicted binding energies are observed for the *J*=0 (1.56 meV) and J=1 (1.2 meV) states, whereas *J*=2 is too fragile for observation and J=3 is unbound. The highly

truncated nature of this quantum rotor and the extreme importance of the non-Born Oppenheimer aspect of this problem is illustrated in that all rotational states of this anion with $J \geq 3$ are unbound. In a classical sense, the diffuse electron cloud shown in Figure 2.18 cannot "keep up" with the rotational motion of the dipole, and thus for $J \geq 3$ is effectively "sloughed off". Future experiments to further elucidate these rotational effects, with proper consideration of the necessary characteristics of the molecule and its dipole bound anion, will not only further our understanding of these exotic negative ion states but offer important insight into the application of the Born Oppenheimer approximation, thus impacting both physics and chemistry in a fundamental manner.

Chapter 3

Collision Induced Dissociation of Multiply Charged Anions (MCAs)

Introduction

While the bulk of experimental and theoretical research of negative ions has focused on singly charged species, experimental advances have allowed attention to turn to studies of gas phase Multiply Charged Anions (MCAs). Commonly observed in the solid and liquid phase, observations of small gas phase MCAs remain rare. Formation of gas phase MCAs is inhibited by the Coulombic repulsion between the excess charges, whereas in solids and solutions this repulsion is mitigated by background electrostatic fields. With the absence of these background fields in the gas phase, the Coulombic repulsion is seen to dominate at large distances. At very small distances the polarizability of the molecule leads to an attraction which may overcome this Coulombic repulsion. The superposition of this Coulombic repulsion and polarizability attraction leads to a potential barrier towards both the formation and dissociation of the MCA referred to as the Repulsive Coulomb Barrier (RCB). The RCB has been observed to add to the stability of MCAs, and even render unstable species metastable and long-lived (Fig 3.1). The lifetimes of these metastable anions can be very large as a result of the height and particularly the shape (width) of this barrier, analogous to metastable α- particle decay from a radioactive nucleus. It is

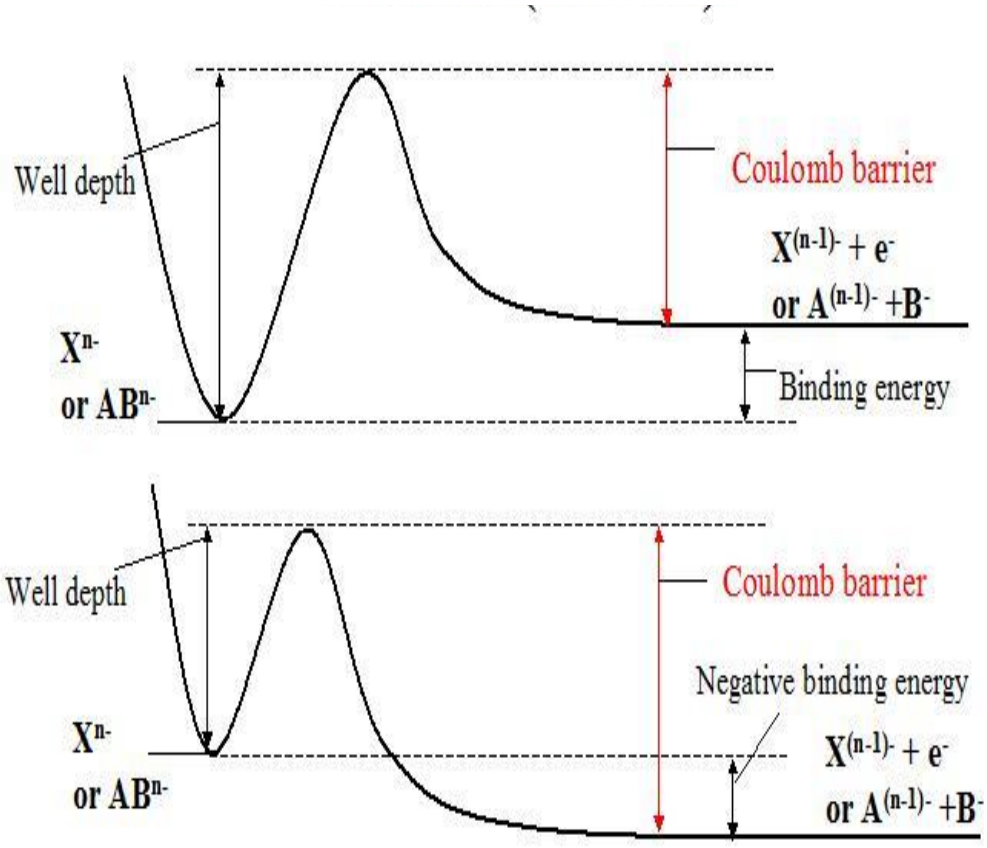

Figure 3.1. Idealized potential energy surface towards electron or charged fragment loss for an MCA, showing the relationship between the Coulomb barrier, binding energy and well depth for both stable and unstable species.

therefore imperative to consider the nature of this Coulomb barrier when seeking to understand the electronic and thermodynamic stability of gas phase MCAs.

While many studies have probed the existence of this Coulomb barrier[73,74,75,76,77], Wang et. al. have provided the bulk of initial experimental studies of RCB towards electron detachment[78]. Using Photoelectron Spectroscopy (PES) of selected dianions, this group was able to directly observe several prominent features of the Coulomb barrier. Initial experimental validation of the Coulomb barrier was through PES of the citrate dianion (CA^{2-}) at 3 photon energies[79]. The spectrum taken at 266nm (4.661 eV) showed electron detachment into two electronic states of the monoanion; the ground state, with a binding energy of 1.0 eV, and the first excited state estimated to be .6 eV higher. PES taken at 355 nm (3.496 eV) showed only detachment to the ground state monoanion even though the photon energy was higher than the binding energy for both electronic states (Fig 3.2). PES at 532 nm (2.331 eV) showed no photoelectrons observed even though the photon energy was again greater than the binding energies to either state. This clearly indicates the existence of a potential barrier towards the loss of an electron as illustrated if Fig 3.2. Further work by Wang's group illustrated the metastability conferred to an electronically unstable dianion by the RCB through observation of a negative electron binding energy for $[CuPc(SO_3)_4]^{4-}$, as well as electron tunneling through the Coulomb barrier[78, 80].

One of the most interesting aspects of this group's work was their estimation of the magnitude of this barrier towards electron detachment for a series of linear

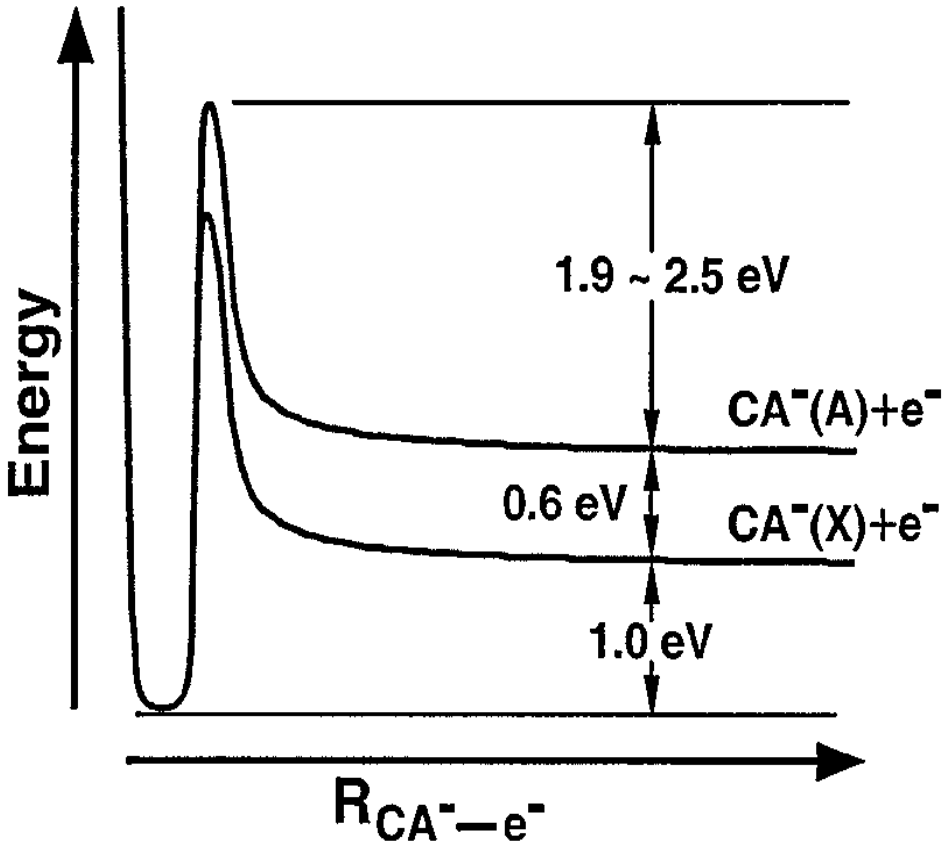

Figure 3.2. Schematic potential energy curves showing the adiabatic binding energies and the repulsive Coulomb barrier for detachment of CA^{2-}, leading to the *X* and *A* states of CA^{-}. Note that the barrier heights relative to the *X* and *A* states are assumed to be the same.[79]

dicarboxylate dianions[81], which served as the motivation for work to be discussed in this chapter. Using three different photon energies to perform the PES of these molecules, they were able to estimate the depth of the potential well inhibiting the detachment of the excess electron. Combined with experimentally measured second electron affinities for these molecules (binding energy of the highest energy electron in the dianion) they were able to estimate the magnitude of the RCB. The linear dicarboxylates, -O2C-(CH2)n-CO2-, with n indicative of the chain length, provided a systematic way to study the effect of charge separation on the magnitude of this barrier. The two excess charges of these dianions reside primarily on the outlying CO2 moieties, allowing for the average distance between the distant oxygens to be used as an estimate for the charge separation. They found that the electron binding energy as well as the magnitude of the RCB scale linearly with the inverse of this charge separation (Fig. 3.3). The extrapolated fit for the magnitude of the RCB, (RCB(eV)=.00(5)+16.8(3)/rn(Å)), fits very well qualitatively with a simple electrostatic model from Coulomb's law of $e2/4\pi\varepsilon or$ for repulsion between similarly charged point charges. For a vacuum ($\varepsilon o=1$) the expected slope is 14.4, slightly lower than found. This is attributed to a slight overestimation of the charge separation, as calculations of the highest occupied molecular orbitals for these dianions show the electron to be slightly delocalized across the CO2 units, supporting this contention. Thus it seems the RCB for electron detachment can accurately be estimated simply using Coulombs law for systems with highly localized excess electrons.

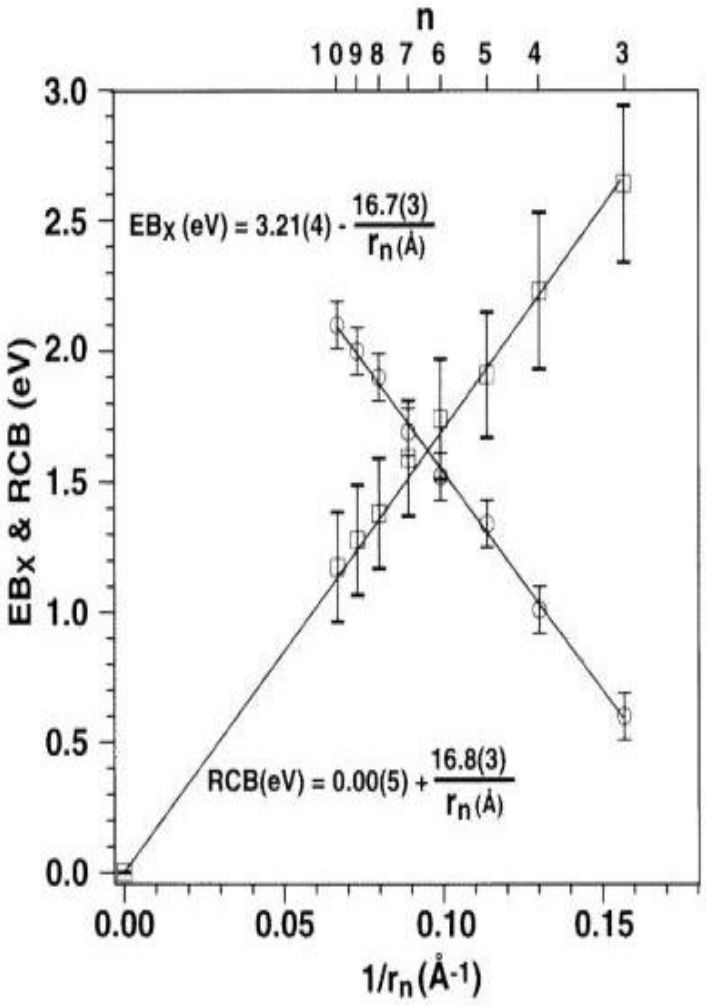

Figure 3.3. Measured adiabatic electron binding energies (EBx) and the estimated repulsive Coulomb barrier (RCB) heights for -O2C-(CH2)n-CO2- (DC2-) dianions (n = 3-10) as a function of 1/rn, where rn is the average equilibrium distance (Å) between the two charge centers in DC2-, assumed to be localized on the O atoms of the carboxylate groups. Key: circles, EBx; squares, RCB; lines, least-squares fits[81].

A vast majority of the research concerning the RCB and its affect on the stability of MCAs has been focused on electronic stability, i.e. stability towards electron loss. However, to be thermodynamically stable MCAs must also be stable towards dissociation into charged fragments. . Friedrich et. al.[82] have studied the Coulomb barrier towards ionic fragmentation using electronic photodissociation spectroscopy and kinetic energy release (KER) data to estimate the well depth and magnitude of the RCB towards ionic fragmentation for $IrBr_6^{2-}$ as 1.6±.2 eV and 2.2±.2 eV respectively. This implies the dianion is unstable with respect to ionic fragmentation, though rendered long-lived and metastable by the RCB. Interestingly, no evidence of electron detachment was observed, suggesting ionic fragmentation to be the dominant dissociation pathway for this molecule. Dessent et al.[83] have studied the relative well depths for electron detachment and ionic fragmentation using a quadruple ion trap to isolate specific dianions. They then applied a resonance excitation technique, (multiple low energy collisions with a background buffer gas of helium which acts similar to thermal excitation) such that the dianions will dissociate via the lowest energy pathway. It was demonstrated that ionic fragmentation is the dominant dissociation pathway for dianions that can fragment to produce two stable singly charged anions, such as many transition metal complexes, as well inorganic dianions $PtCN_6^{2-}$, $PtCN_4^{2-}$, $S_2O_8^{2-}$ and $H_3P_3O_{10}^{2-}$. Due to the importance of ionic fragmentation in understanding the total stability of gas phase MCAs, it is important to understand the role of the RCB in this dissociation and thus is a focus of the research herein.

A further complication involving interpretation of the RCB is the question of the role that delocalization of the excess charges may have. Do MCAs with highly delocalized excess electrons experience an increase or decrease in this Coulombic repulsion? There are only a few studies examining the subject of how the molecular structure and electronic properties of a dianion might affect its stability toward electron detachment. Skurski et al[84], experimentally and theoretically examined the electronic stability of two small dicarboxylate dianions having similar molecular size, geometry, and atomic structure: [$(O_2C{-}C \equiv C{-}CO_2)^{2-}$ (AD^{2-}) and $(O_2C{-}CH_2{-}CH_2{-}CO_2)^{2-}$ (SD^{2-})]. In this work electrospray mass spectrometry, photodetachment spectroscopy, and ab initio calculations were employed. They found that SD dianions were very difficult to produce whereas they reported large signals of AD dianions, even though their calculated electronic structure suggest they both have similar charge separations. Furthermore, their calculations showed that SD dianions are unstable toward electron detachment (negative adiabatic electron affinity) whereas AD dianions are stable with 0.418 eV adiabatic and 0.69 eV vertical electron binding energies. Their calculations also suggested that for AD dianions, the two excess charges are delocalized over the –CC- π-type orbitals while for SD dianions, charges are heavily localized on the CO_2^- groups. Their results indicated that even though the charge delocalization on AD dianions increases the Coulombic repulsion (as the charges are closer together), the D_{2d} structure of the AD dianions allows interaction between carboxylate group and the –CC- π-type orbitals, therefore increasing the stability of the AD dianions.

In 2003, Schwerdtfeger et al.[85] performed a theoretical study regarding the stability of a system of dianions with similar atomic structure, but slightly different electronic structure, i.e., $^{-}O\text{-}(CH_2)_n\text{-}O^{-}$, $^{-}O\text{-}(HC{=}CH)_n\text{-}O^{-}$, and $^{-}O\text{-}(C{\equiv}C)_nO^{-}$ where n is the number of carbon-carbon pairs (i.e., C-C, C=C, or C≡C). Their Density Functional Theory (DFT) calculations revealed that aliphatic dialkoxides, $^{-}O\text{-}(CH_2)_n\text{-}O^{-}$, are unstable toward electron detachment up to a chain length of n= 22 (charge separation of 30 Å) . While for $^{-}O\text{-}(HC{=}CH)_n\text{-}O^{-}$, and $^{-}O\text{-}(C{\equiv}C)_nO^{-}$ stable dianions exist for n≥10 and n≥6, respectively. In an effort to explain the necessary charge separation for these species to overcome the Coulombic repulsion of the excess electrons, Schwerdtfeger and his co-workers plotted the highest occupied molecular orbitals for stable $^{-}O\text{-}(C \equiv C)_6\text{-}O^{-}$ and $^{-}O\text{-}(HC{=}CH)_{10}\text{-}O^{-}$, and compared them to the unstable $^{-}O\text{-}(CH_2)_{22}\text{-}O^{-}$ dianion. Their results showed that increased delocalization of the charges over the carbon-carbon chain would reduce the necessary charge separation needed to stabilize these dianions from electron detachment. Delocalization of the excess charges in MCAs is an important consideration in determining the stability of these anions, as the simple model used to estimate the magnitude of the RCB is rendered moot by the inability to model the electrons as point charges. Furthermore, this delocalization of charges plays an important role in determining the likely dissociation pathway, as these studies imply an increased stability towards electron detachment, yet experiments to be presented herein seem to imply an increased propensity towards fragmentation and will be discussed in detail later in this thesis.

Experimental Setup

The anions studied were produced using an Electrospray Ionization (EI) source. Developed by Nobelist John Fenn et. al.[86], this ionization method has proved invaluable in advancing research in biology, chemistry and physics due to the capability of forming highly charged ions in the gas phase. This is of particular importance to those wishing to study large molecules, such as proteins, as the large charge conveyed to the molecule by this ionization process can lower the m/z ratio of the large molecule within the limits of the mass spectrometer employed. Additionally, this source is ideal for the formation of MCAs in the gas phase, which has allowed for the increased experimental attention towards understanding these anionic systems. In this context, the anion of interest is first formed in solution, where the background electrostatic field from counter-ions helps mitigate the Coulomb repulsion between the excess charges, thereby increasing the stability of many multiply charged anions (MCAs) while in solution. The solution is then passed through a small heated capillary, biased at several kilovolts (typically ~-3kV) relative to a skimmer cone at the entrance to the coupled mass spectrometer. The skimmer cone (typically biased between 0-100V) reduces the system pressure to the levels required for the mass spectrometer as well as guiding the ions into the system. The high electric field at the capillary tip facilitates the formation of small highly charged droplets (Fig.3.4). The solvent evaporates from the droplets as it travels from the capillary to the skimmer cone, often facilitated by a sheath flow nebulizing gas or a slightly heated desolvation gas. As the solvent evaporates from the highly charged droplet, the charge on the surface of these droplets grows until it reaches a critical

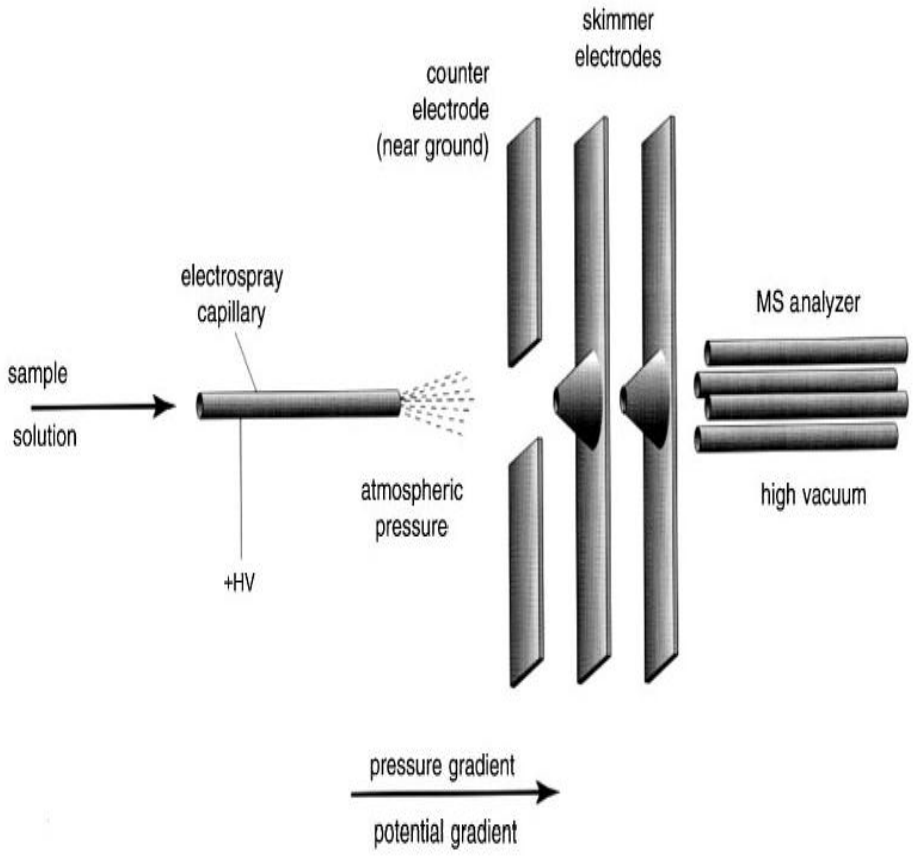

Figure 3.4 Schematic representation of an Electrospray ionization source[87]

point, called the Rayleigh limit, when it can no longer support the excessive charge. Fragmentation of the droplet, or Coulomb explosion, then occurs leaving a plethora of previously unattainable MCAs available for study in the gas phase.

The anions studied were then probed through collisional activation, or Collision Induced Dissociation (CID), using a commercial triple quadrupole tandem mass spectrometer (MicroMass Quattro II) (Fig. 3.5). Once created with the EI source, the ions are accelerated into a quadrupole mass spectrometer. Here a mass spectra is recorded and the ion of interest can be accentuated by adjusting such parameters as the solution flow rate, capillary or cone voltages, and flow rate of the nebulizing or desolvation gasses. The ion is then mass selected and directed into a hexapole collision cell filled with argon gas operating under approximately single collision conditions. In this cell a DC voltage is employed to provide variable collision energy, with a hexapole ion guide used to limit off-axial losses of ions thus maximizing collection efficiency of the collision products. Following the collision, the products are then analyzed using a second quadrupole mass spectrometer. An energy retardation technique is employed to calibrate the energy scale of the system as contact potentials, surface charge effects, and other possible voltage reading offsets in the apparatus may have a significant impact on observed collisional energies. An intense ion signal of Br- (formed from a solution of ammonium bromide (NH_4Br) with 5 μM concentration in a mixed solvent of CH_3OH: H_2O = 10000:1 introduced to the electrospray ionization

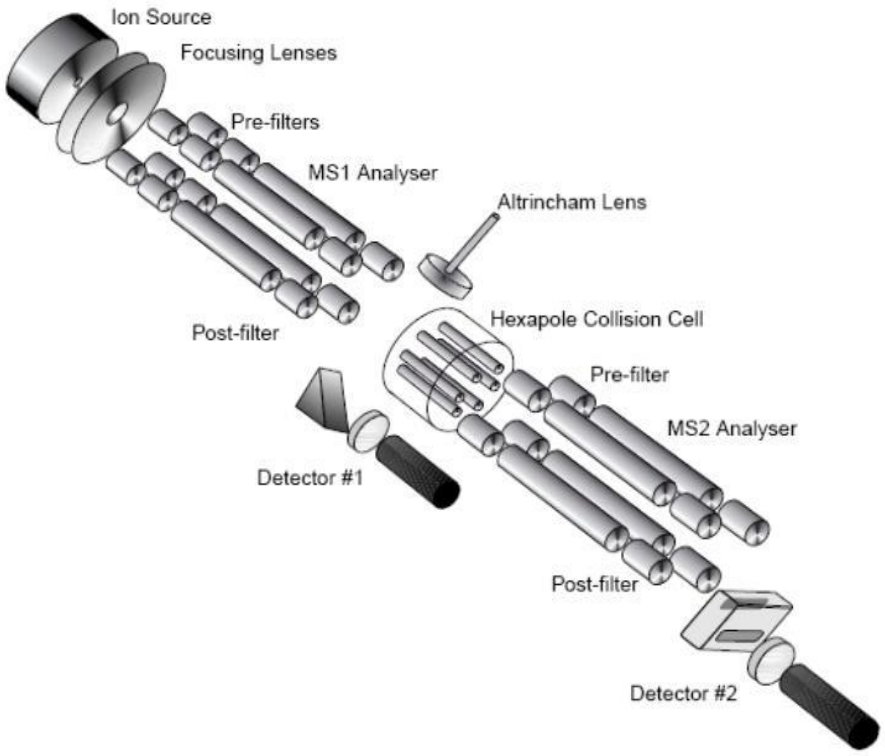

Figure 3.5. MicroMass triple quadrupole tandem mass spectrometer.

source) is accelerated through the collision cell without gas, at energies near and below zero (Fig.3.6). As the ion energy is retarded to zero energy, the ion signal disappears. The derivative of this curve (Fig.3.7) supplies us with the energy distribution of the ion beam studied. The peak of this derivative is interpreted as the calibrated zero of the system. The results indicate a calibrated zero of .44 eV and a full width half max of the ion beam kinetic energy of ~.5 eV for this apparatus.

CID of Sodium Chloride Cluster Dianions

Initial experiments employing this apparatus to study CID of gas phase MCAs focused on sodium chloride clusters of the form $Na_xCl_{x+2}^{2-}$(x=7,15). 40mM solutions of sodium chloride in D_2O were introduced into the ESI source at a flow rate of 10 μl/min. The ESI capillary voltage was set to -2.5 kV. The cone voltage was varied from 0 to +80 V. The optimum cone voltage in which doubly charged ions were observed was +40 V. The source block temperature was set to 48 °C and the desolvation temperature was 120 °C. The nebulizing and desolvation gases were nitrogen with flow rates of 40 and 300 liters/hour, respectively.

The pre-collision mass spectrum of ions produced by electrospray of this sample is shown in Fig. 3.8. In general the mass spectra is very similar to that previously reported by Friedrich et al.[88]. The singly charged ions observed are all of the form $Na_xCl_{x+1}^-$, while the doubly charged ions were of the form $Na_xCl_{x+2}^{2-}$ from x=6-27 with decreasing intensity for larger ions. The stoichiometry of the ions was

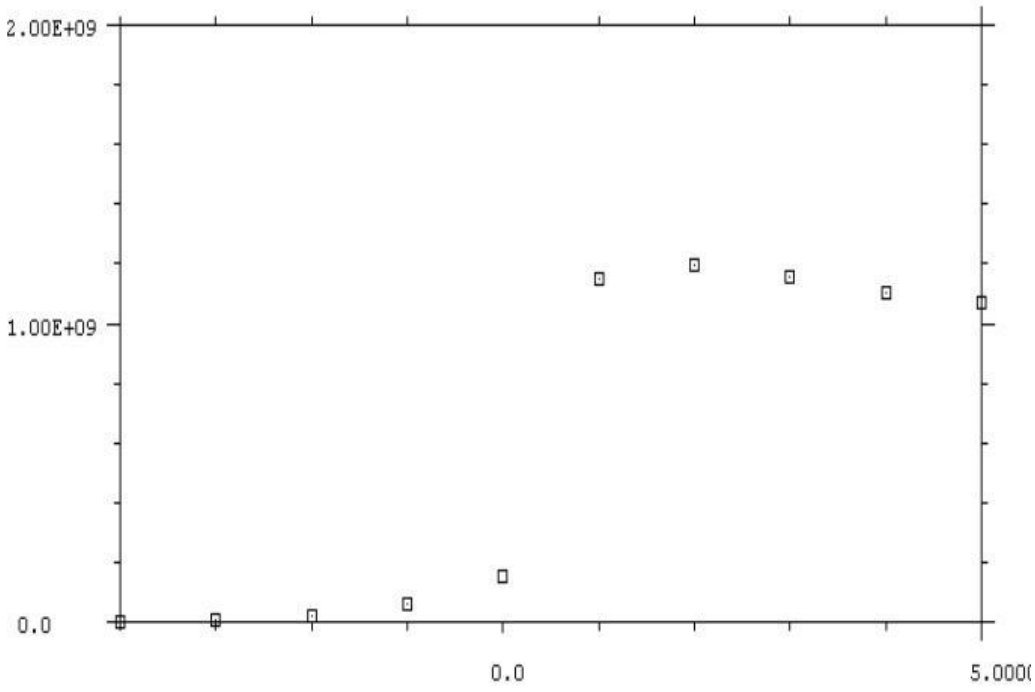

Figure 3.6. Signal from Br- with no collision gas. By taking the derivative of this signal retardation curve we can establish the full width half maximum of the ion energy. distribution (~0.5 eV). The peak of the derivative is taken true zero of the system for calibration purposes (see Fig 3.7).

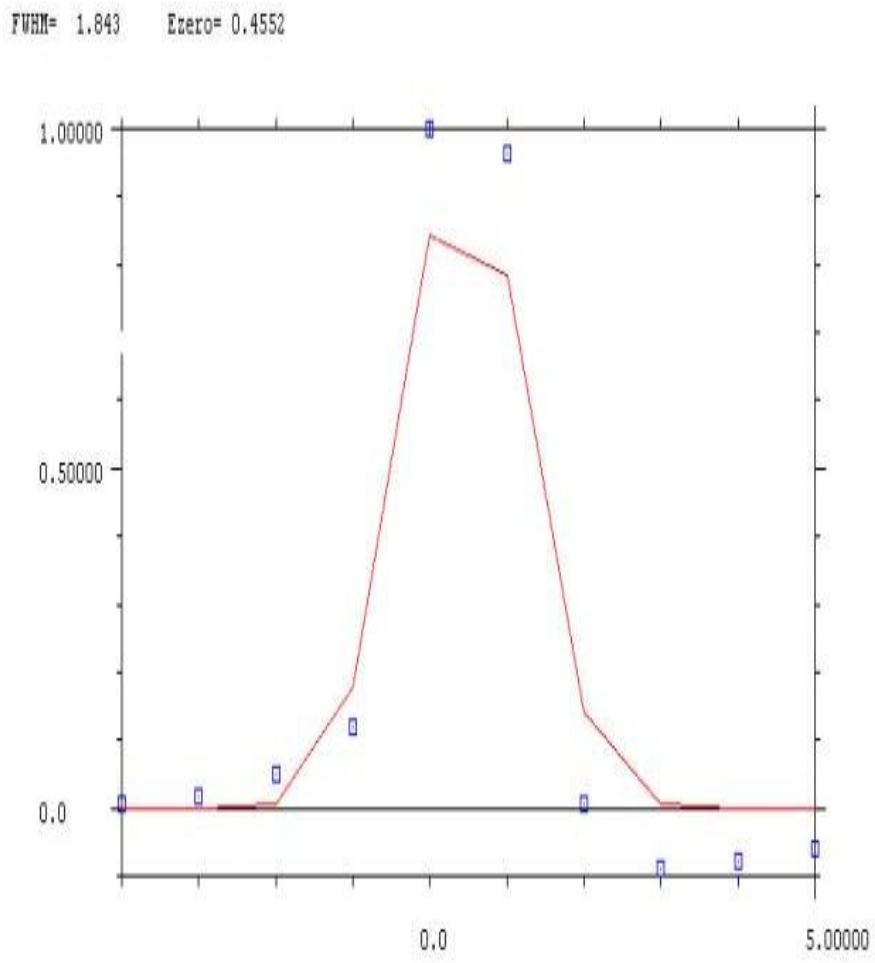

Figure 3.7. Derivative of curve from Figure 4 from which we find the estimated zero and energy distribution of the ion beam in the laboratory system.

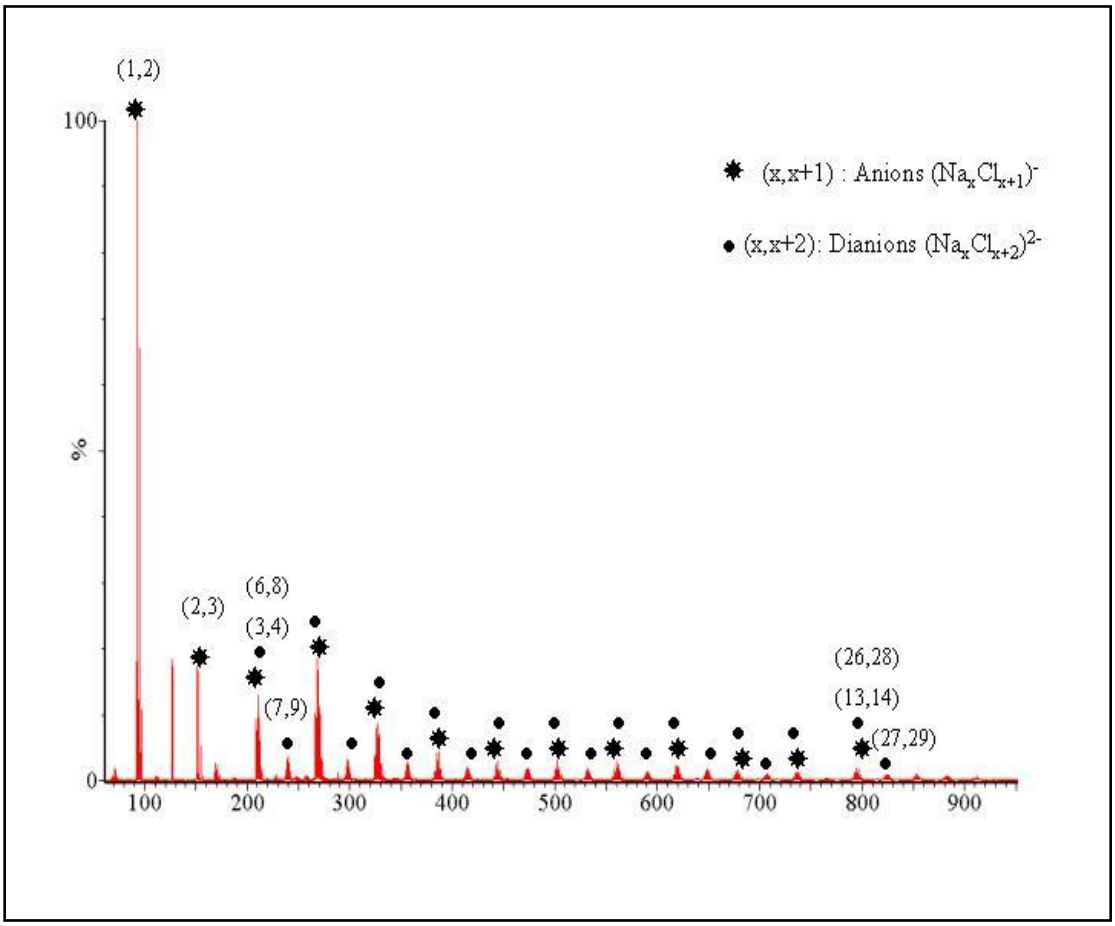

Figure 3.8. Pre collision mass spectrum of ions formed from electrospray ionization of the prepared NaCl solution. The dianions are presented as filled stars and monoanions are denoted as filled circles.

easily identified by the mass to charge ratio measured as well as their respective isotopic ratios as highlighted in Fig. 3.9. The doubly charged ions were identified as such by their respective half mass separation in their isotopic distribution resulting from being doubly charged as highlighted in Fig. 3.10. The smallest dianion observed was that of $Na_6Cl_8^{2-}$ or $(6,8)^{2-}$ for brevity, which overlapped with the (3,4) anion, common of all dianions with an even number of Na and Cl atoms. Therefore, the dianions chosen for study we composed of odd numbers of atomic constituents, with the (7,9) dianion having the lowest mass and largest signal. The study was limited to two representative dianions as severe signal degradation resulted over time from accumulation of salt coatings on the electrodes of the apparatus.

Results of the CID of the $Na_xCl_{x+2}^{2-}$ (x=7,15) dianion are shown in Figures 3.11-3.14. The CID of the dianions show fragmentation into conjugate pairs of the form $NaCl_2^-(NaCl)_n + NaCl_2^-(NaCl)_{5-n}$ for n=0,1,2 and $NaCl_2^-(NaCl)_n + NaCl_2^-(NaCl)_{13-n}$ for n=0,1,2,3,4,5,6 for the (7,9) and (15,17) dianions, respectively. Evidence of collisional electron loss, leaving $Na_7Cl_9^{1-}$ and $Na_{15}Cl_{17}^{1-}$ at 480 and 947 amu respectively, is not observed for collision energies up to 400 eV in the lab frame. It should be noted that these ions are not observed in the pre-collision mass spectra for any of the settings employed implying that they may not be stable and thus evidence of electron loss may be unobservable in this system. The ratios of conjugate ions is not one to one as expected, possibly due to the further dissociation of the $Na_7Cl_9^{1-}$ and $Na_{15}Cl_{17}^{1-}$ anions through neutral fragmentation altering these ratios, or due to differential collection efficiencies of the conjugate ions. Also of note is the observation of $Na_7Cl_8^{1-}$ and

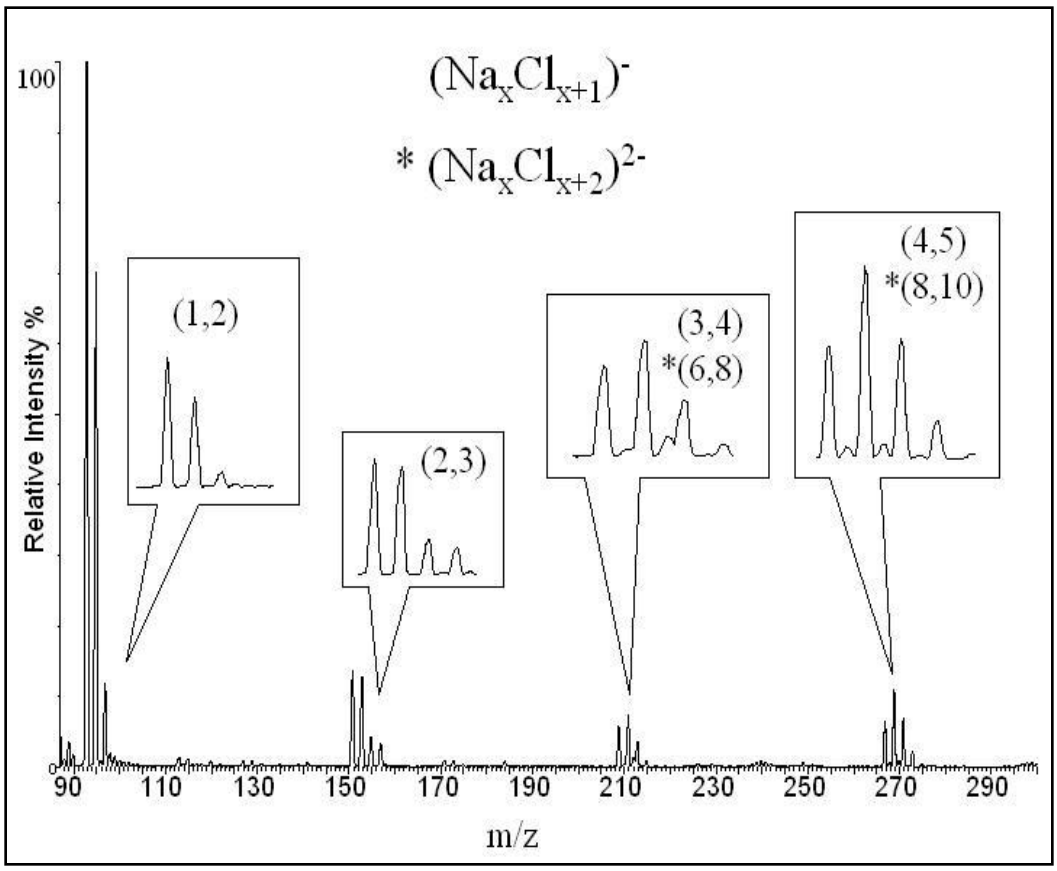

Figure 3.9. Selected pre-collision mass spectrum emphasizing the isotopic distribution of monoanions and even numbered dianions (*) which overlap. Peaks from Na6Cl82- are odd mass peaks between the peaks from Na3Cl4-, and peaks from Na8Cl102- are odd mass peaks between the peaks from Na4Cl5- monoanion.

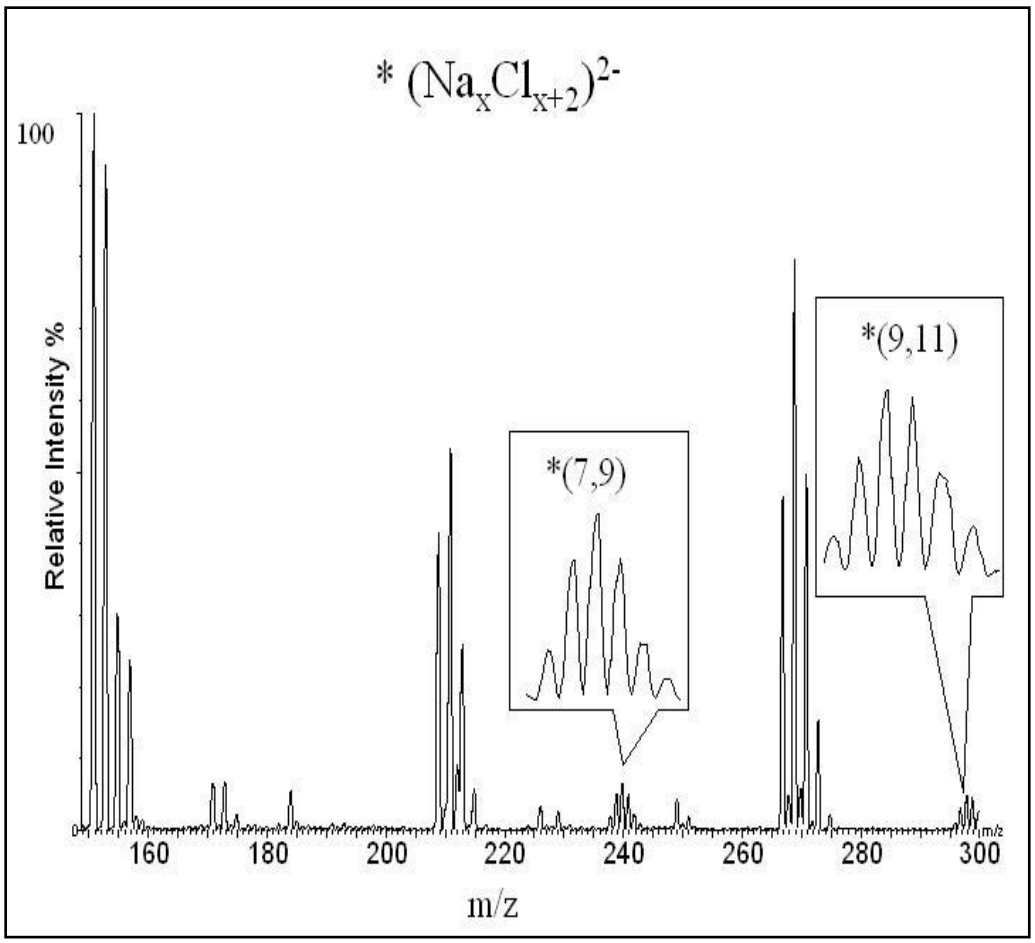

Figure 3.10. Pre collision mass spectrum highlighting the isotopic distribution and half mass separation of the (7,9) and (9,11) dianions.

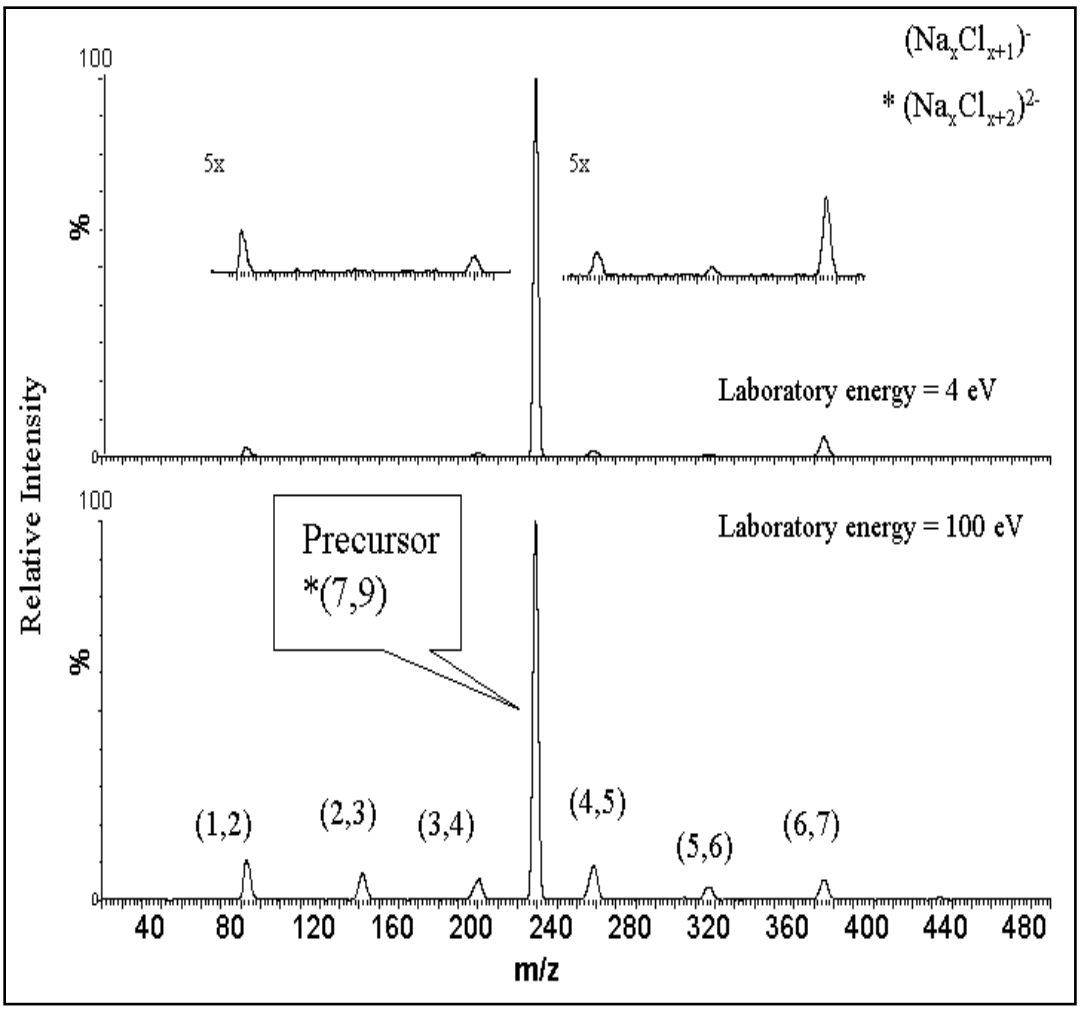

Figure 3.11. Collision- induced dissociation of Na7Cl92- (240 amu) at laboratory energies of 4 and 100 eV.

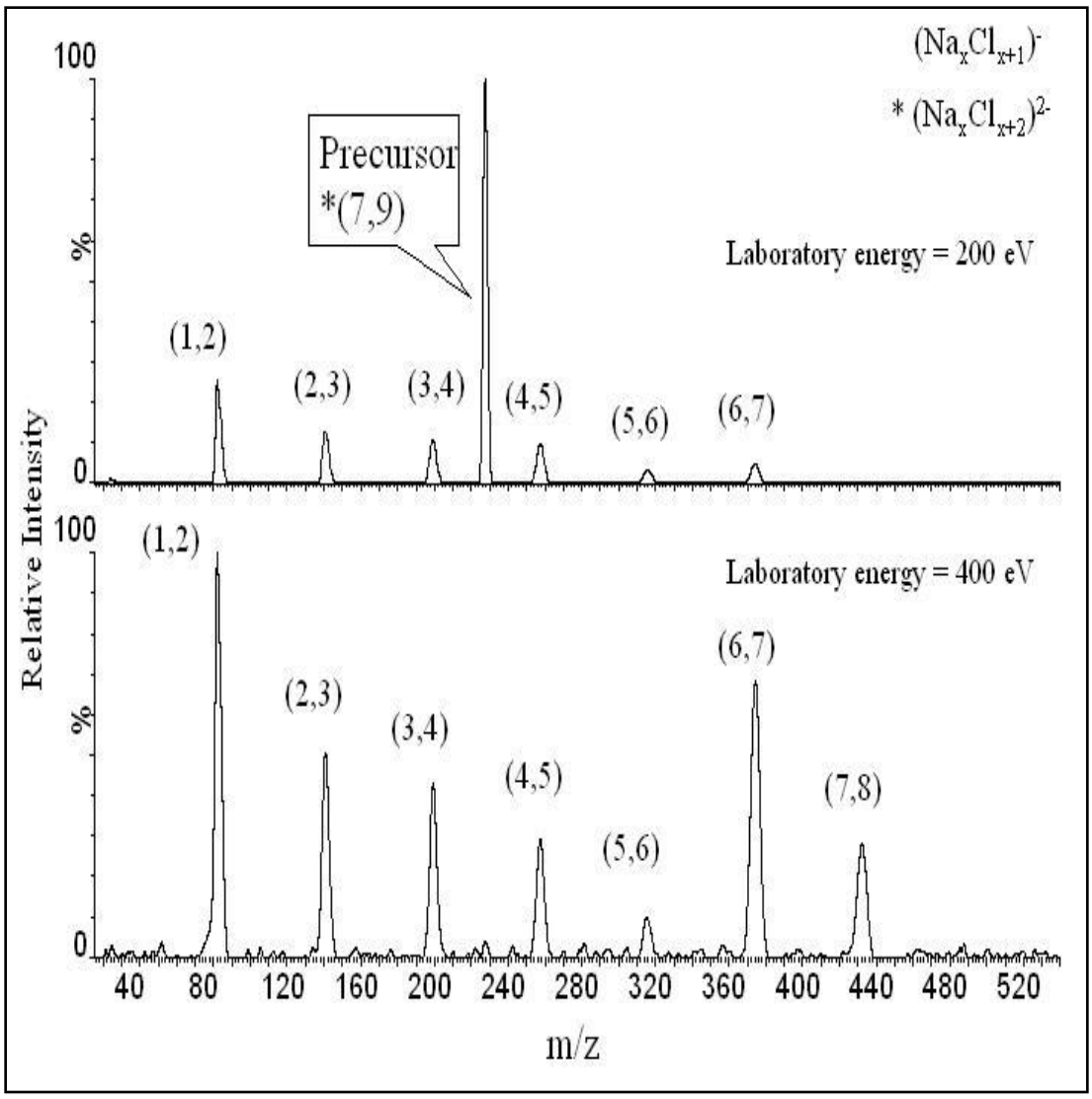

Figure 3.12. Collision induced dissociation of Na7Cl92- (240 amu) dianions at laboratory energies of 200 and 400 eV.

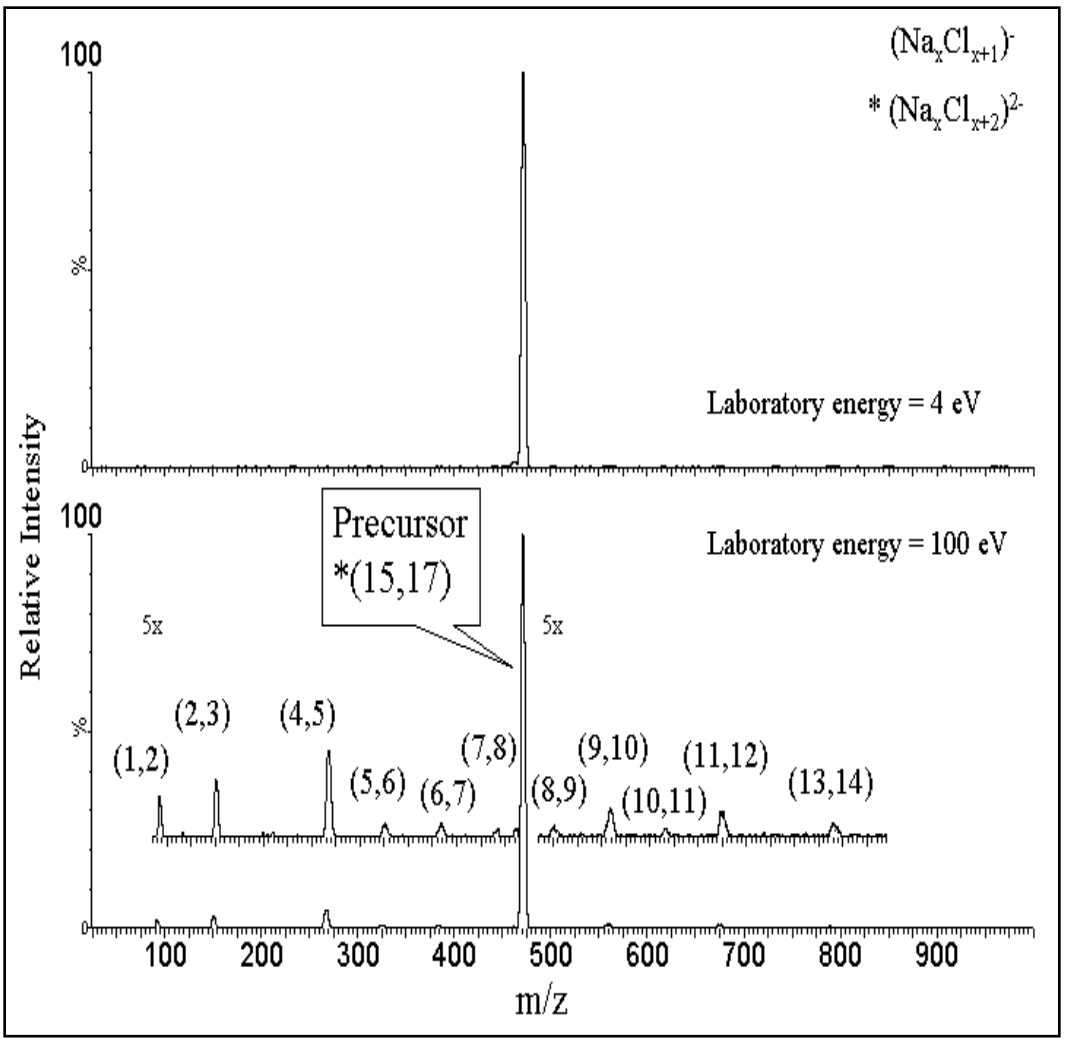

Figure 3.13. Collision induced dissociation of Na15Cl172- (474 amu) dianions at laboratory energies of 4 and 100 eV.

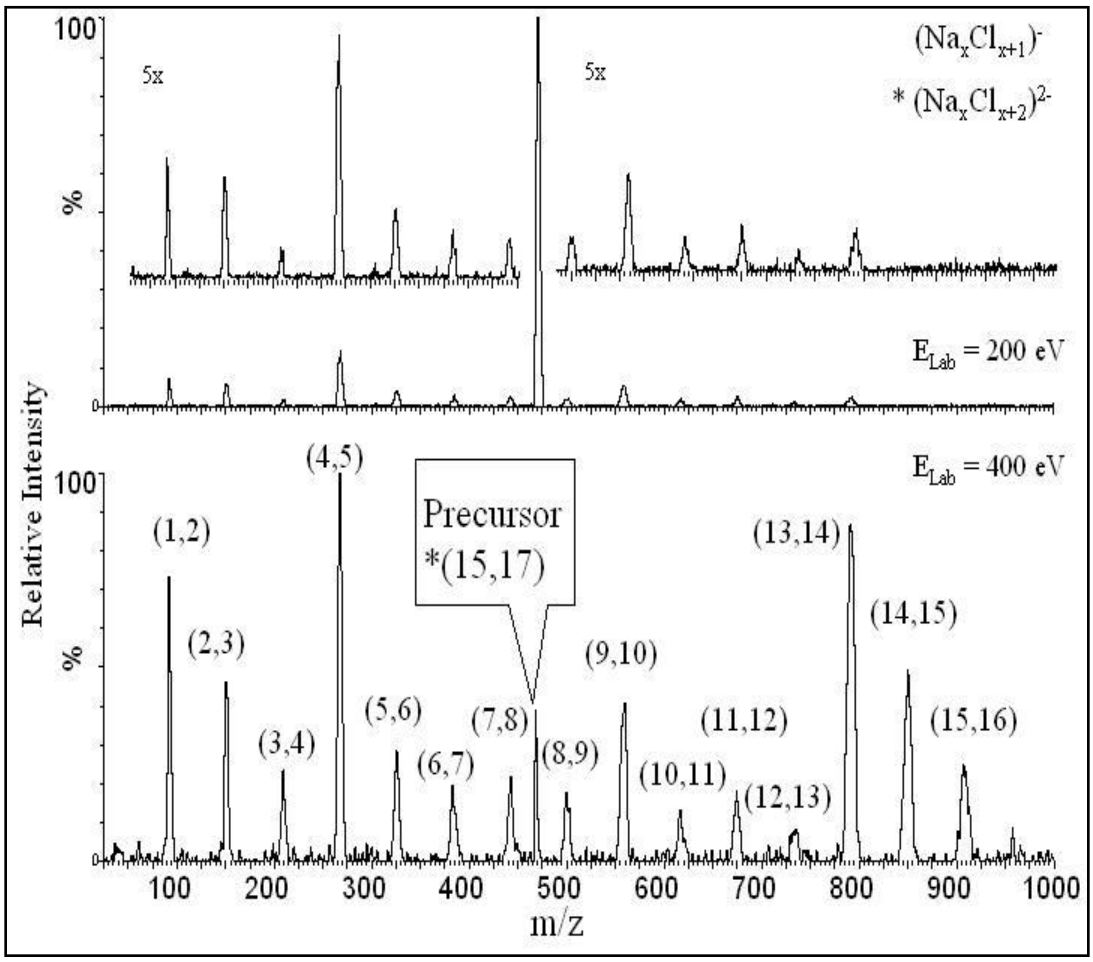

Figure 3.14. Collision induced dissociation of Na15Cl172- (474 amu) at laboratory energies of 200 and 400 eV.

$Na_{15}Cl_{16}^{1-}$ at very high collision energies without the conjugate Cl^- signal. This may be indicative of electron loss followed by neutral fragmentation as well. Thus unobservable dissociation channels cannot be ruled out for these dianions.

The energy dependence of this fragmentation for the (7,9) dianion was then probed by considering the relative cross sections of these channels with respect to the collision energy in the center-of-mass reference frame. The ratio of fragment signal to that of the parent dianion signal was used to model these cross sections, as near threshold these ratios are directly proportional to the actual cross section. Furthermore, employing these ratios allowed us to account for the variable intensity of ion signal resulting from the electrospray ionization source. The energy dependence of these relative cross sections is shown in Figure 3.15. We see that each of these fragmentation pathways are observed at very low energies with apparent thresholds near or below zero energy. To further understand the stability of this dianion towards fragmentation, calculations of dissociation energy for several of the fragment ions[88] was considered, and the effect of the RCB was considered by calculating the well depth, or inner barrier towards dissociation for loss of Cl^- and $NaCl^-$ by our theoretical collaborators Patrick Weis and Manfred Kappes. Dr.s Weis and Kappes performed their calculations using the TURBOMOLE calculation package, details of which are found in (Ref 88). The results are shown in Table 3.1 and Figures 3.16 and 3.17. This dianion is calculated to be unstable towards all fragmentation channels except dissociation into $NaCl_2^-$ and its conjugate pair, yet ample dianion signal is observed in our system, implying

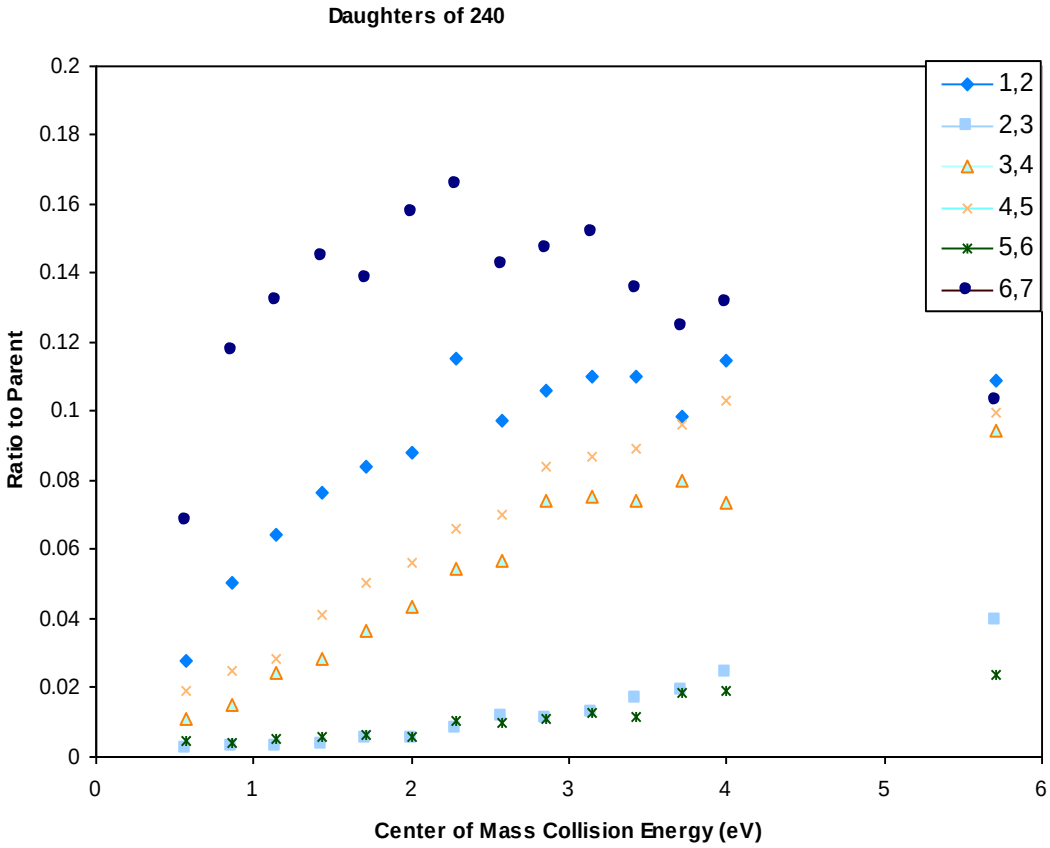

Figure 3.15. Relative cross-sections for formation of fragments products from collision-induced dissociation of $Na_7Cl_9^{2-}$ (240 amu) in center of mass frame.

Table 3.1. Calculated dissociation energies for $Na_7Cl_9^{2-}$ toward loss of Cl^-, $NaCl_2^-$, $Na_2Cl_3^-$, and $Na_3Cl_4^-$ and calculated well depths towards Cl^- and $NaCl_2^-$ fragmentation.

	Cl^- -loss	$NaCl_2^-$ - loss	$Na_2Cl_3^-$ - loss	$Na_3Cl_4^-$ - loss	Units
$Na_7Cl_9^{2-}$	-7.3[81]	1.5[81]	-13.7[81]	-62.1[81]	KJ/mol
	-0.076	0.016	-0.14	-0.64	EV
Well Depth	95	76	----------	----------	KJ/mol
	0.99	0.79	----------	----------	EV

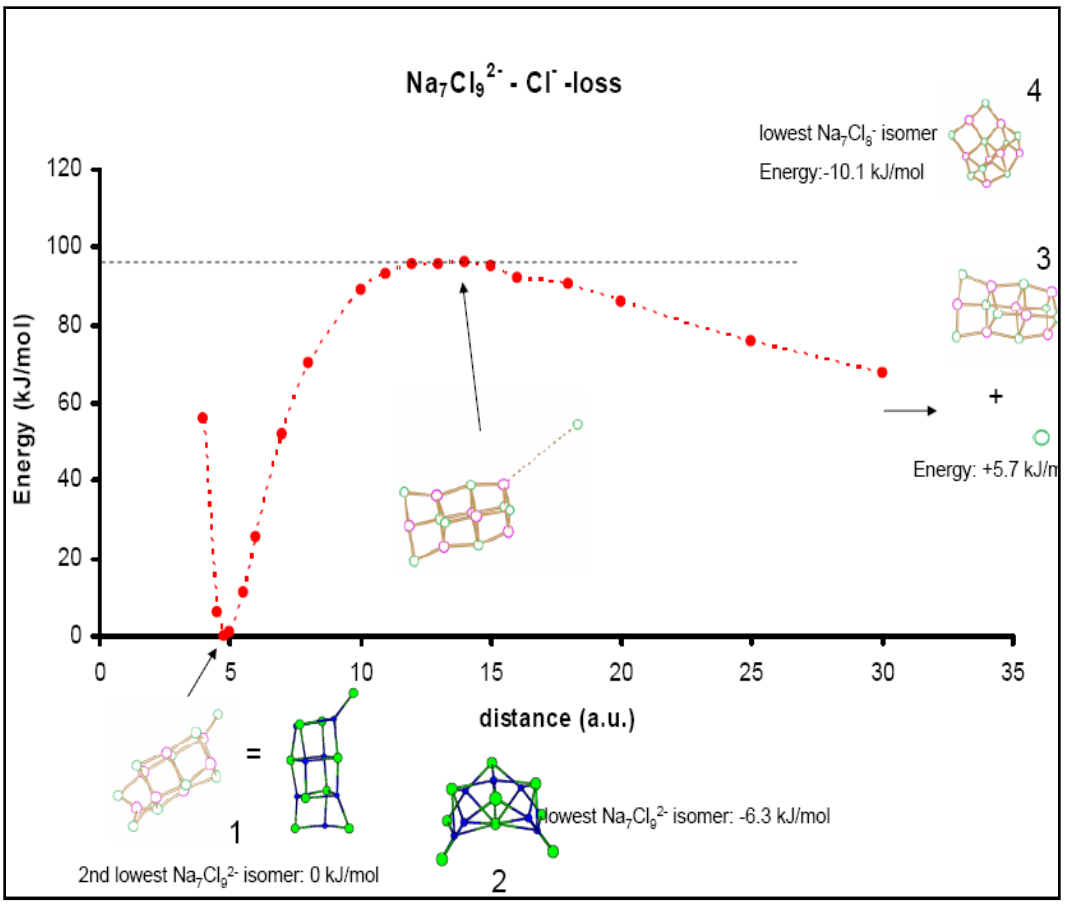

Figure 3.16. Well depth calculation for dissociation of $Na_7Cl_9^{2-}$ into $Na_7Cl_8^-$ and Cl^-. The inner barrier height for the loss of Cl^- is about 95 KJ/mol (0.99 eV).

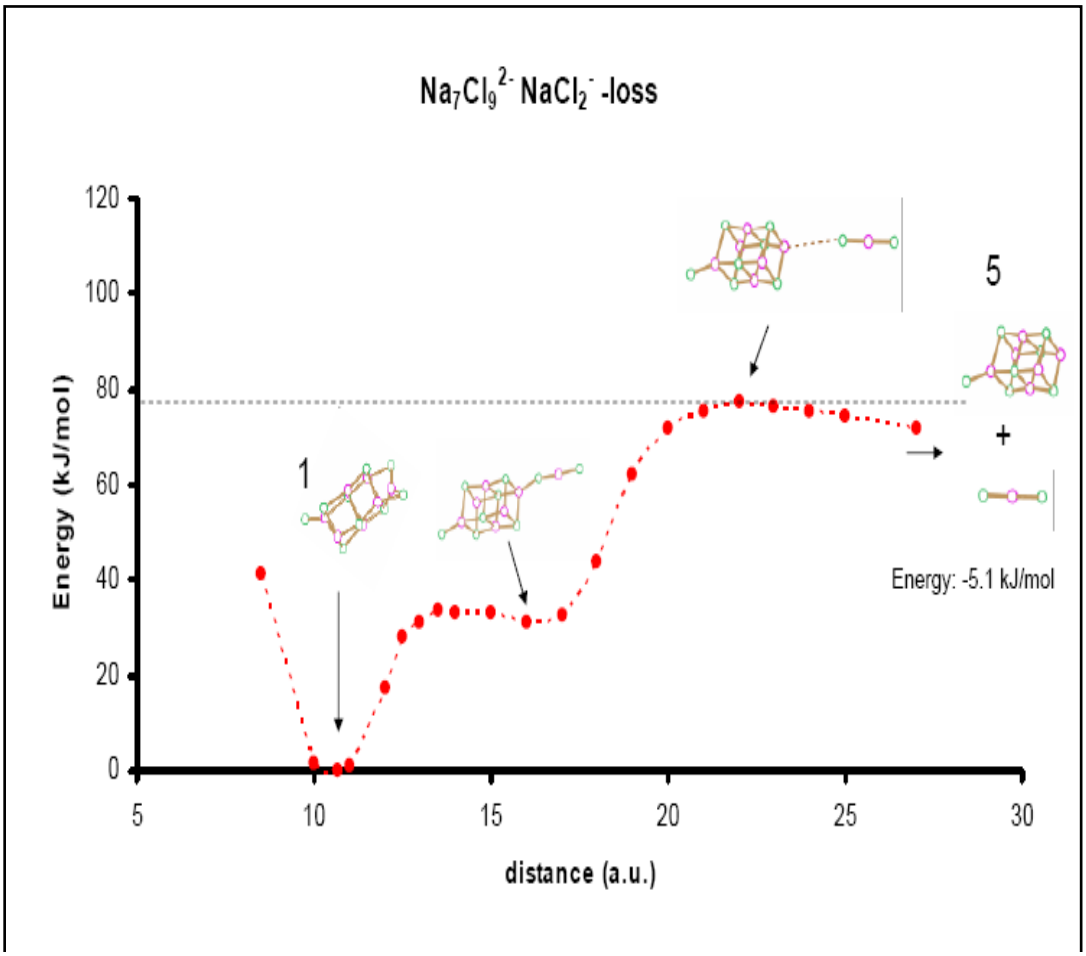

Figure 3.17. Well depth calculation for dissociation of Na7Cl92- into Na6Cl7- and NaCl2-. The inner barrier height is calculated to be about 76 KJ/mol (0.79 eV)

metastability. The relative cross sections agree with the metastability of these dianions toward these fragmentation pathways as the thresholds appear near or below zero. the RCB renders these unstable dianions to be long-lived and thus observable in our system. Figures 3.16 and 3.17 highlight the RCB that is rendering these dianions metastable, as it is estimated to provide an additional 0.99 and 0.79 eV of stability towards fragmentation of Cl^- and $NaCl_2^-$, respectively. It should be noted that these barrier calculations show Cl^- loss to be unstable with a barrier of only 1 eV to overcome, yet is not observed except for possibly at significantly higher energies. This discrepancy with experimental observation signifies the difficulties in these types of calculations and is indicative of a complicated system in which many aspects are likely to be involved as the RCB is a type of transition state, which remain notoriously difficult to model with any certainty.

In conclusion, this work has shown the ability of the apparatus employed to produce MCAs for collisional dissociation. Furthermore, the observation of dianions calculated to be unstable emphasizes the added stability rendered to MCAs by the RCB. This highlights the impressive ability of the electrospray ionization source to form unstable negative ions for study in the gas phase. This particular molecular system is not well suited to significantly probe effects of the RCB due to the metastability of the dianions studied, as well as the multiple fragmentation pathways, and the likelihood of unobservable dissociation pathways. These difficulties are important, however, in that

they lead us to focus on molecular systems where these effects can be minimized, thus allowing features of the RCB to explored in greater detail.

CID of Sulfonic and Carboxylic Containing Dianions

As shown in the previous experiment, our ability to probe the RCB towards ionic fragmentation is largely a function of the molecule studied. In this regard we turned our attention to a series of ringed dianions containing ligands of SO_3, or CO_2 in various conformations. These molecules formed ample dianion signal using the aforementioned electrospray ionization source and provide the opportunity to probe several interesting questions about the RCB based on their respective electronic properties. The dianions containing ligands of SO_3 provide a system in which to probe the RCB towards ionic fragmentation and the relationship with charge separation, similar to the work preformed by Wang et. al.[81] for electron detachment. The CID of these molecules results in the fragmentation of the dianion into SO_3^- and it resultant conjugate pair. This ionic fragmentation appeared with a clear threshold, allowing us to estimate the magnitude of the RCB towards this fragmentation when we include calculated dissociation energies for these dissociation pathways. The samples containing ligands of CO_2 allow for consideration of the effect delocalization of the excess charges may have on the dissociation pathway. Calculations of the highest occupied molecular orbitals for these dianions show the excess charges to be delocalized across the benzene or naphthalene like ring as well as the CO_2 ligands. This

important characteristic of the molecule has significant impact on the lowest energy dissociation pathway and will be discussed in detail.

The dianions studied were formed from 20 μg/ml solutions of benzene-1,2-disulfonic acid dipotassium salt [$C_6H_4(SO_3)_2K_2$], benzene-1,3-disulfonic acid disodium salt $C_6H_4(SO_3)_2Na_2$, 2,6-naphthalenedisulfonic acid disodium salt [$C_{10}H_6(SO_3)_2Na_2$], 1,5-Naphthalenedisulfonic acid disodium salt hydrate $C_{10}H_6(SO_3)_2Na_2 \cdot xH_2O$, terephthalic acid disodium salt [$C_6H_4(CO_2)_2Na_2$], 2,6-naphthalenedicarboxylic acid dipotassium salt [$C_{10}H_6(CO_2)_2K_2$], and 4-sulfobenzoic acid potassium salt [$C_6H_4(SO_3)_1(CO_2)_1KH$] (Figure 1) in 50/50 water and methanol mixture and were introduced to the ESI at a rate of 5 μl/min. Salt samples were purchased from Sigma-Aldrich (USA) and used with no further purification. Specifics of the CID remain unchanged from those discussed earlier in this chapter. Geometrical optimization of the dianions, as well as calculation of the relative stabilities of the dianion towards electron detachment and fragmentation were performed using the Gaussian 03 program suite[72]. Calculations were performed at the level of Density Functional Theory (B3LYP) using the 6-311++G** basis set. Binding energies were determined as the difference in optimized energies for the dianion and monoanion or resultant fragments.

The disulfonic dianions studied are shown in Fig. 3.18. These molecules provide a system of atomically similar dianions in which the primary variable is the separation of the SO_3 units. SO_3 is itself a very stable gas phase anion, with an

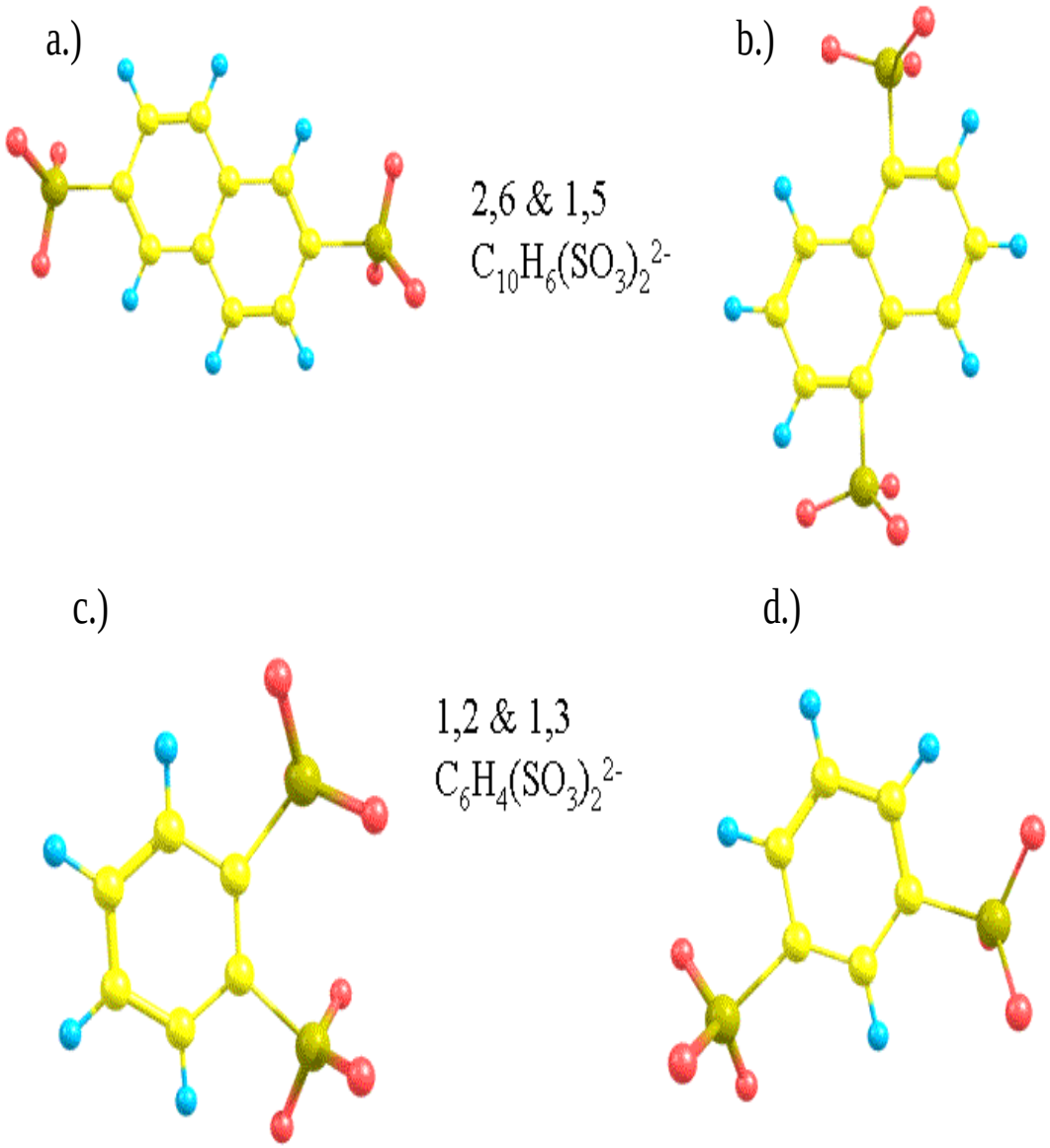

Figure 3.18. 2,6 (a.) and 1,5 (b.) C10H6(SO3)22- as well as 1,2 (c.) and 1,3 (d.) C6H4(SO3)22- geometrically optimized at the B3LYP level.

experimentally derived electron affinity of 1.9 eV found from photoelectron spectroscopy[89]. Thus one would expect the excess charges of these disulfonic dianions to reside primarily on these SO_3 units, which calculations of the highest occupied molecular orbital for the 1,2 disulfonate dianion (Fig 3.19) and the 2,6-naphthalenedisulfonic dianion (Fig. 3.20) clearly support. The highly localized nature of this charge distribution allows for an estimation of the charge separation as the average distance between the outlying oxygens, and thus the ability to probe the relationship between this charge separation and the magnitude of the RCB towards ionic fragmentation.

The results of the CID for the disulfonic dianions studied are shown in Fig. 3.21 for a collision energy of 60 eV in the lab frame. The only dissociation channel observed is the ionic fragmentation into SO_3^- and its conjugate pair. Electron detachment resulting in singly charged anions of the parent is not observed. These monoanions are not observed in the pre-collision mass spectra under any of the experimental conditions employed. Additionally, calculations show that monoanions of the parent are expected to be very unstable, and thus likely unobservable in this system. Calculations also show the binding energy of an SO_3^- to be less than that of an electron for each of these molecules. Thus fragmentation will be the dominant dissociation pathway for this system if the RCB affects ionic fragmentation in a manner similar to that found for electron detachment, which is one goal of this study to examine.

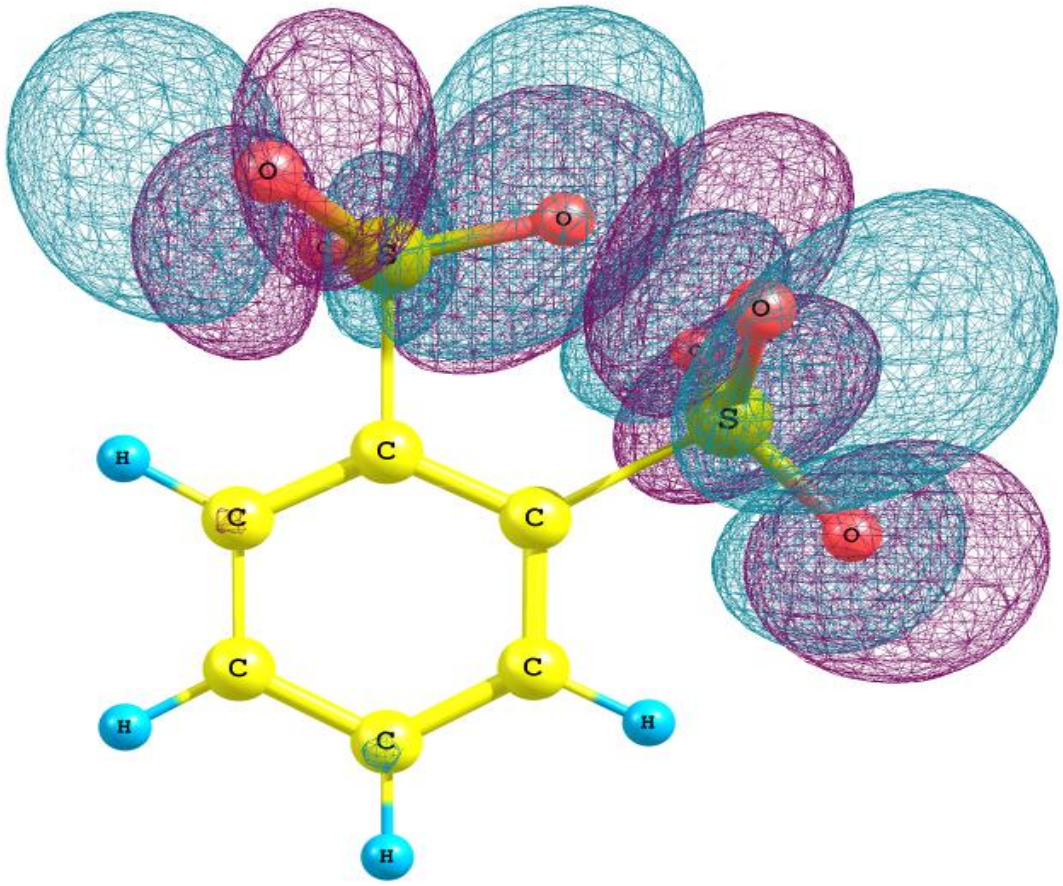

Figure 3.19. Highest occupied molecular orbital visualization for 1,2- disulfonate dianion using Density Functional theory (B3LYP) and 6-311++G basis set.**

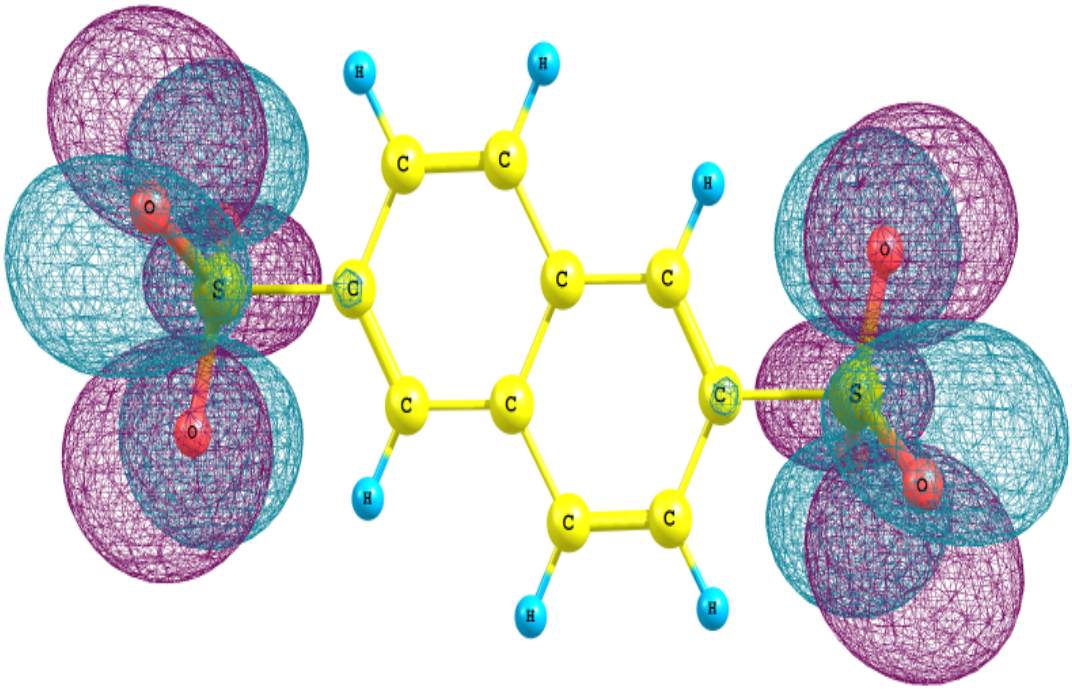

Figure 3.20. Highest occupied molecular orbital visualization for 2,6-naphthalenedisulfonic dianion using Density Functional theory (B3LYP) and 6-311++G basis set.**

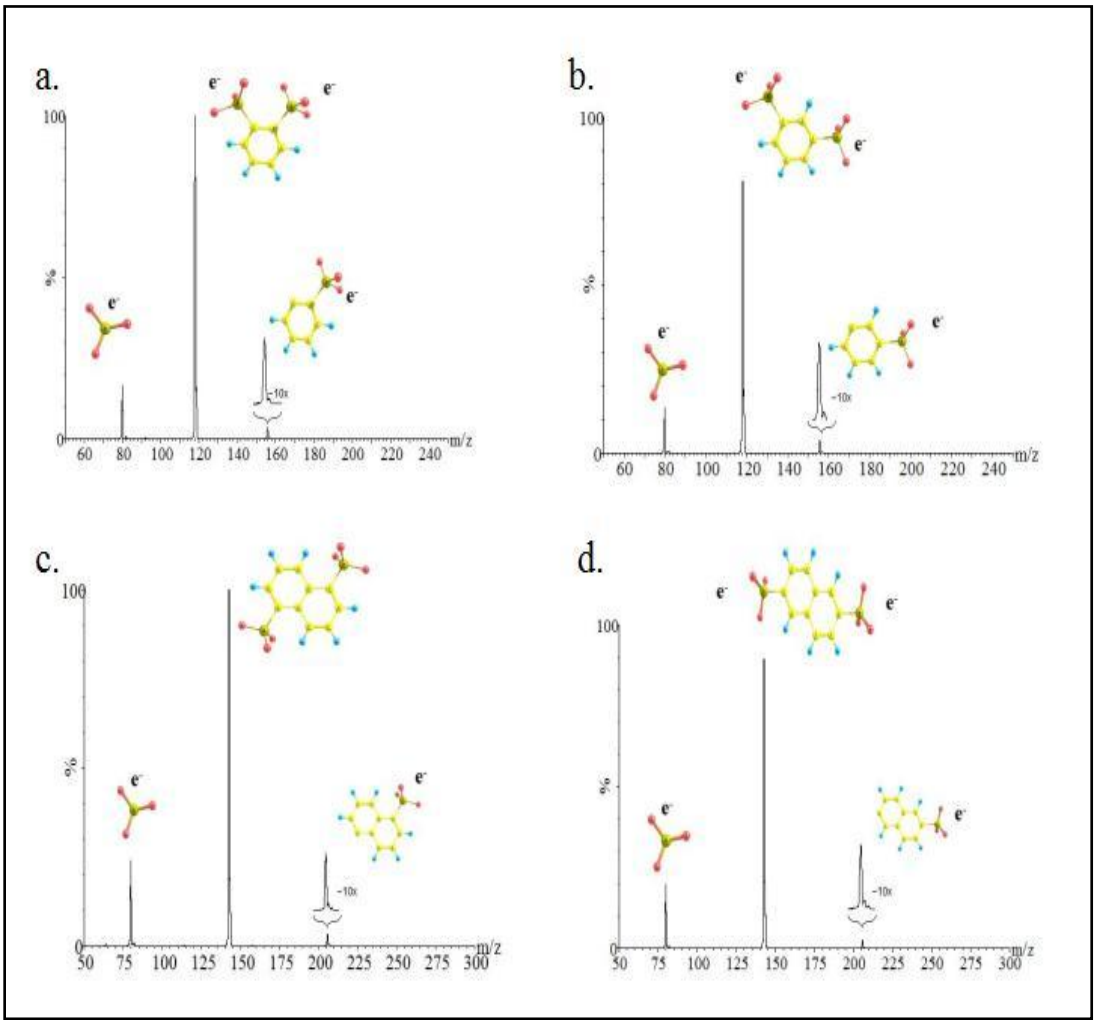

Figure 3.21. Mass spectrum of secondary ions produced by collisions of the benzene-1,2-disulfonate (a), benzene-1,3-disulfonate (b), 1,5-naphthalenedisulfonate (c), and 2,6-naphthalenedisulfonate (d) parent dianions with a static argon background at a laboratory collision energy of 60 eV.

The relative cross sections towards dissociation into SO_3^- and its conjugate pair are shown in Fig. 3.22. As with the salt dianions previously discussed, these relative cross sections are determined from plotting the ratio of the fragment SO_3^- anion to that of the parent dianion, for each collision energy in the center of mass reference frame. Each of the disulfonic dianions studied clearly show a threshold above zero, allowing us to estimate the depth of the potential well inhibiting this dissociation as the determined threshold. The thresholds were determined in the fairly simple manner of taking a linear fit to the near threshold relative cross sections, and extrapolating the fit to zero. The threshold was determined for both the SO_3^- anion and its conjugate pair for each dianion with good agreement between the two. This simple method to determine the threshold does not take into account such variables as internal and kinetic energy of the reactant dianion (electronic, vibrational, and rotational), or broadening by the thermal motion of the collision gas (Doppler broadening). Attempts were made to employ the CRUNCH program designed by Armentrout et al.[90] to take these factors into account to no avail. The experimental apparatus employed is not well suited to model the full cross section, as at higher collision energies the dianion signal is not faithfully represented in detection by the second quadrupole mass spectrometer, thus the relative cross sections seemingly continue to increase with higher energy in contradiction to model predictions. This limits analysis to near threshold behavior where this differential efficiency in detecting the reactant dianion and product anions is minimal. The inability to model the threshold in detail, combined with the reliance on calculations for the dissociation energies, highlights the qualitative over quantitative

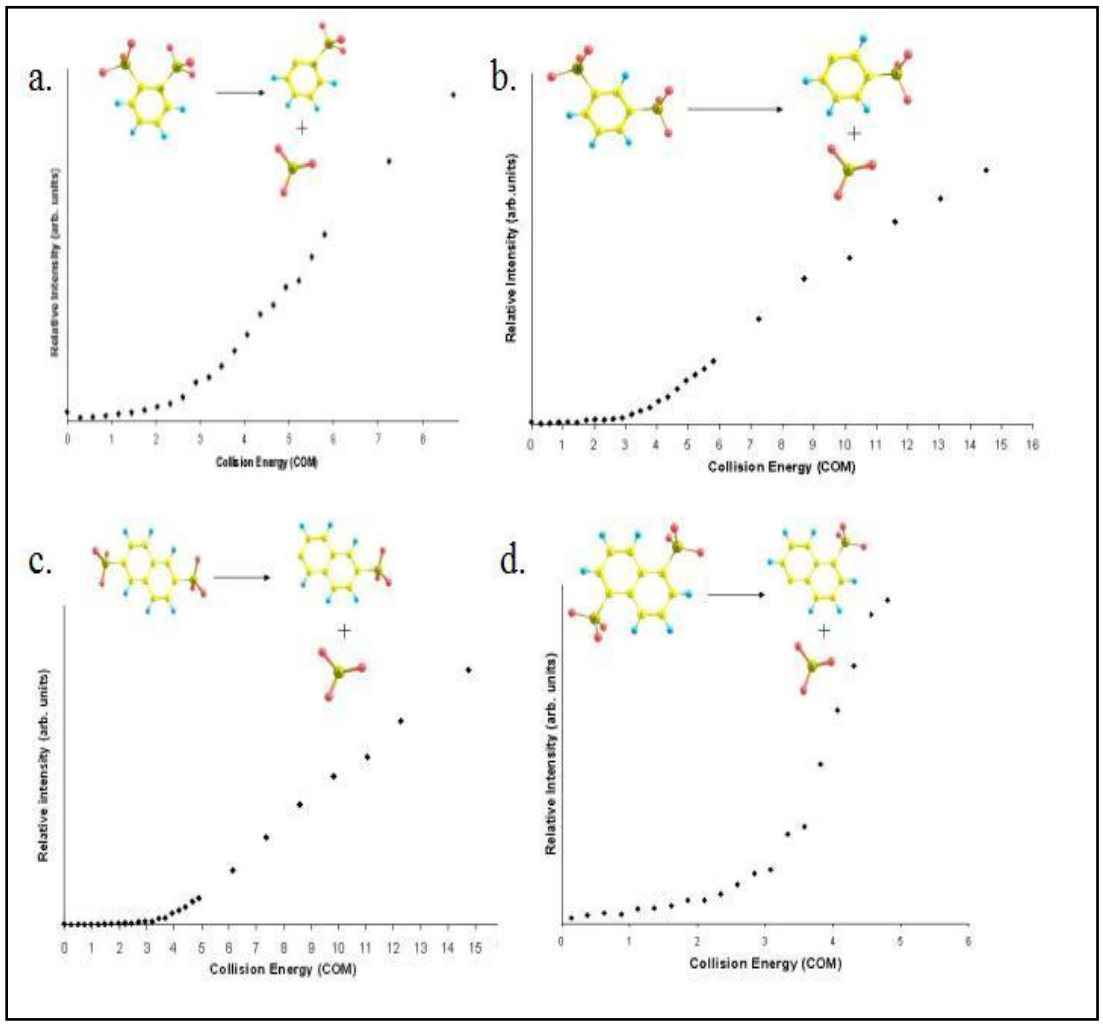

Figure 3.22. Collisional energy dependence for the formation of SO_3^- and its conjugate pair from CID of benzene-1,2-disulfonate (a), benzene-1,3-disulfonate (b), 1,5-naphthalenedisulfonate (c), and 2,6-naphthalenedisulfonate (d) parent dianions in the center-of-mass frame.

aspects of this work. Relative values attained for each dianion studied is therefore the focus, as this will allow us to consider the relationship between charge separation and the effect of the RCB in an empirical manner.

The determined thresholds and the calculated dissociation energies for the loss of an SO_3^- from the each of the parent dianions are shown in Table 3.2. The magnitude of the RCB towards this dissociation is then determined as the difference in the observed threshold to ionic fragmentation and the calculated dissociation energy (Fig. 3.1). Interestingly the 1,2 disulfonate dianion is calculated to be unstable with respect SO_3^- loss, yet is observed in our system, again emphasizing the metastability conferred by the RCB. The magnitude of the RCB observed by each of these dianions is then plotted against the inverse of the average separation between outlying oxygen units, taken as an average charge separation (Fig. 3.23) and compared to the results of Wang et al.[81] for electron detachment. We see that there is excellent agreement between the two. Thus the magnitude of the RCB towards electron detachment and ionic fragmentation are essentially the same. The 1,2 disulfonate dianion does diverge slightly from the linear relationship, yet the uncertainties in the experiment and analysis are too significant to state this definitively. Certainly for very small charge separations the treatment of the excess electrons as point charges is expected to break down. The polarizability of the fragment anions may need to be taken into account to properly understand the RCB in systems of this size, and is worthy of continued experimental and theoretical interest.

Table 3.2. Threshold to dissociation and calculated dissociation energies for 1,2-disulfonate,1,3-disulfonate, 2,6-naphthalenedisulfonic, and 1,5-naphthalenedisulfonic dianions are presented. The difference of which supply an estimate of the magnitude of the RCB. All values are in units of eV.

	Threshold to dissociation	Calculated dissociation energy	|RCB|
1,2-disulfonate dianion	2.3	-0.39	2.7
1,3-disulfonate dianion	3.0	0.69	2.3
2,6-naphthalenedisulfonic dianion	3.5	1.67	1.8
1,5-naphthalenedisulfonic dianion	3.0	.92	2.1

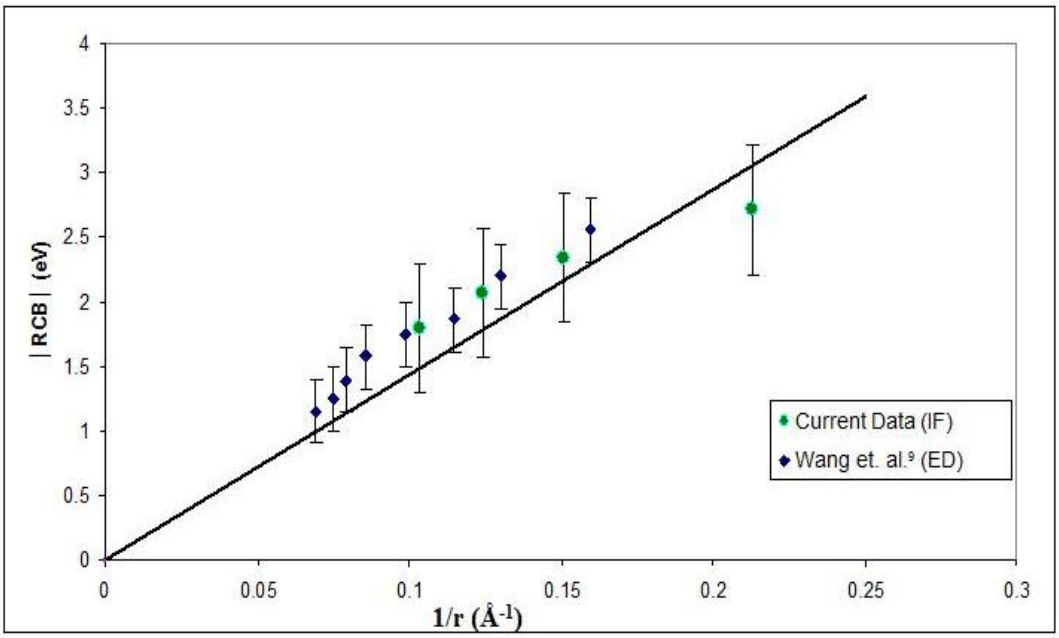

Figure 3.23. Magnitude of the RCB towards Ionic Fragmentation (IF) and Electron Detachment (ED) (Wang et. al.[81]) plotted versus the inverse of the average charge separation. The plotted line shows the value of e2/r= 14.4 (eV*Å)/r (Å).

With reasonable confidence in the relationship between the magnitude of the RCB towards ionic fragmentation and the distance separating the excess charges, we turn our attention to a system where this charge separation is not so easy to discern. Dianions containing two carboxyl, as opposed to sulfonic, ligands; ($C_6H_4(CO_2)_2^{2-}$ and $C_{10}H_6(CO_2)_2^{2-}$, or teraphthalic and 2,6-naphthalenedicarboxylate dianions respectively), as well as a dianion containing both an SO_3 and a CO_2 ligand;($C_6H_4(CO_2)(SO_3)^{2-}$ or 4-sulfobenzoic dianion), offer systems in which the excess electrons are considerably more delocalized than the disulfonic systems. Calculations of the highest occupied molecular orbitals for these dianions (Figs. 3.24-3.26) show a large portion of the electron density to be on the benzene or naphthalene ring in addition to the ligands. One might expect the RCB corresponding to a charge separation of the outermost oxygens to serve as a lower limit to the RCB observed in this system, as the electrons are actually "closer" than this upper limit of charge separation. Previously discussed work by Skurski et al.[84] and Schwerdtfeger et al.[85] suggest this delocalization will increase the stability of these dianions, at least towards electron detachment. The question yet remains as to how this delocalization will affect fragmentation of these dianions.

The results of the CID for these molecules are shown in Fig 3.27 for a collision energy of 60 eV in the lab frame. The dianions with two carboxyl ligands showed fragments resulting from the loss of one or both CO_2 ligands and a free electron (Fig 3.27a, b). The CID of the 4-sulfobenzoic dianion (Fig 3.27c) containing both a CO_2

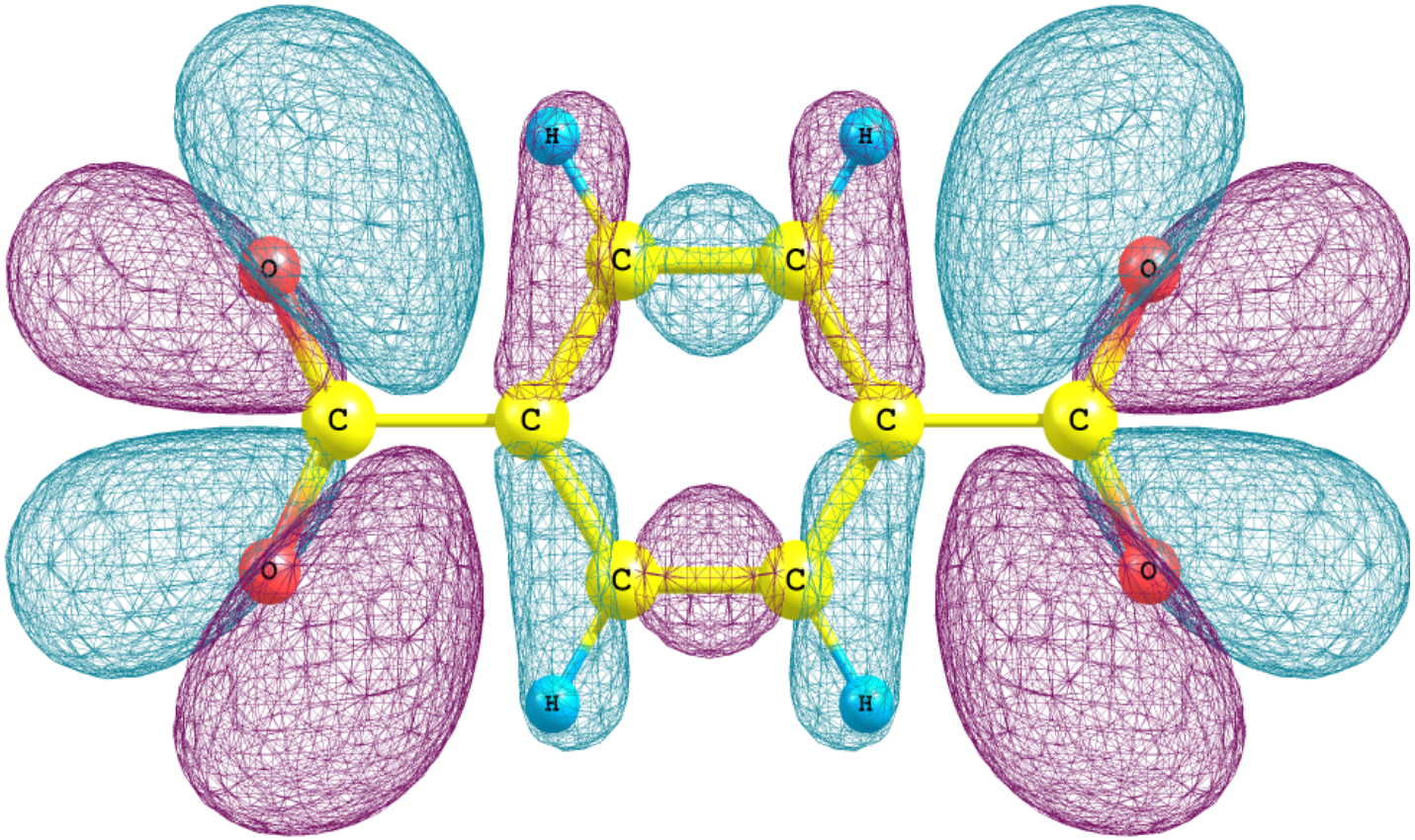

Figure 3.24. Highest occupied molecular orbital visualization for teraphthalic dianion using Density Functional theory (B3LYP) and 6-311++G basis set.**

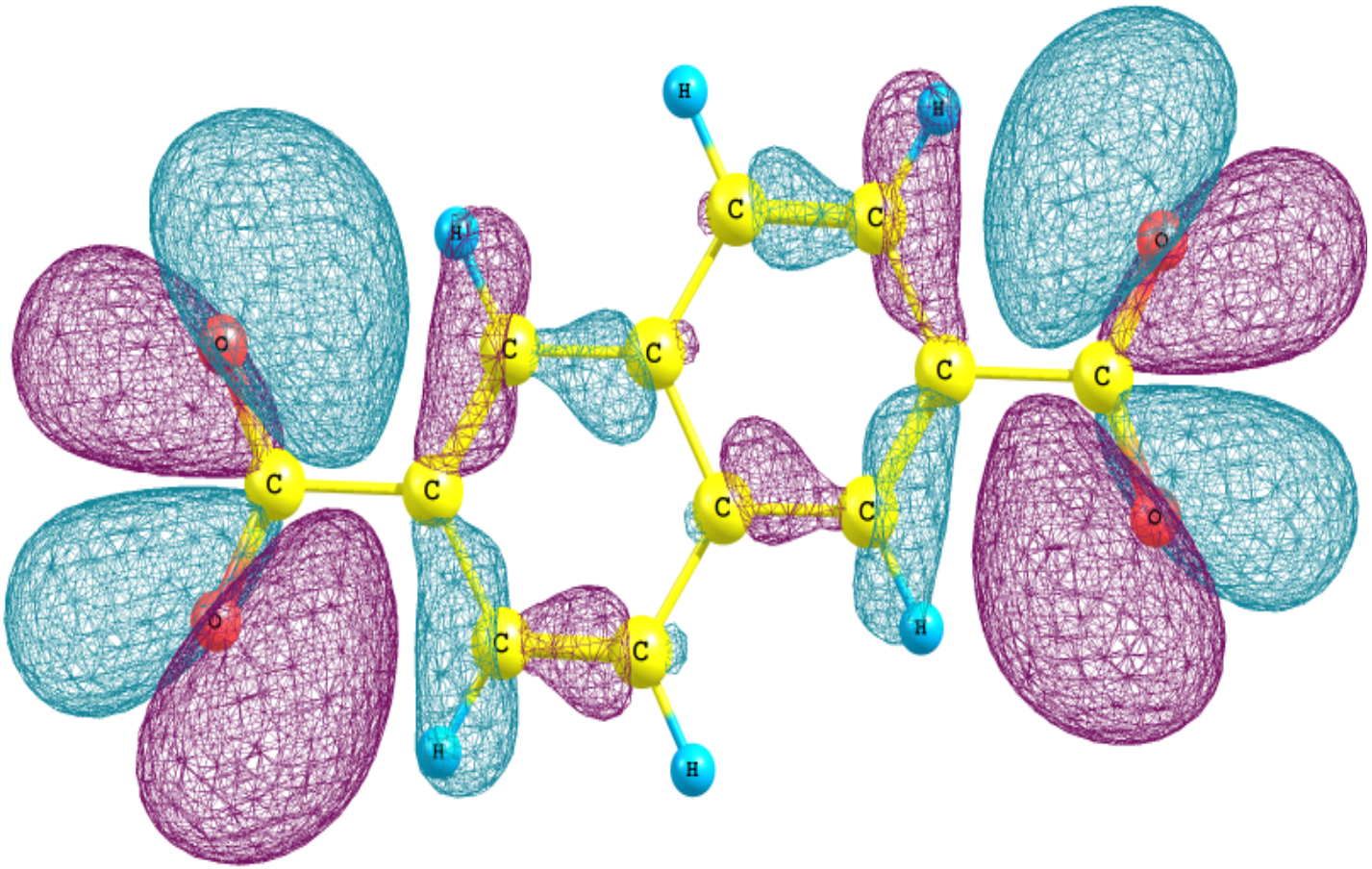

Figure 3.25. Highest occupied molecular orbital visualization for 2,6-naphthalenedicarboxylate dianion using Density Functional theory (B3LYP) and 6-311++G basis set.**

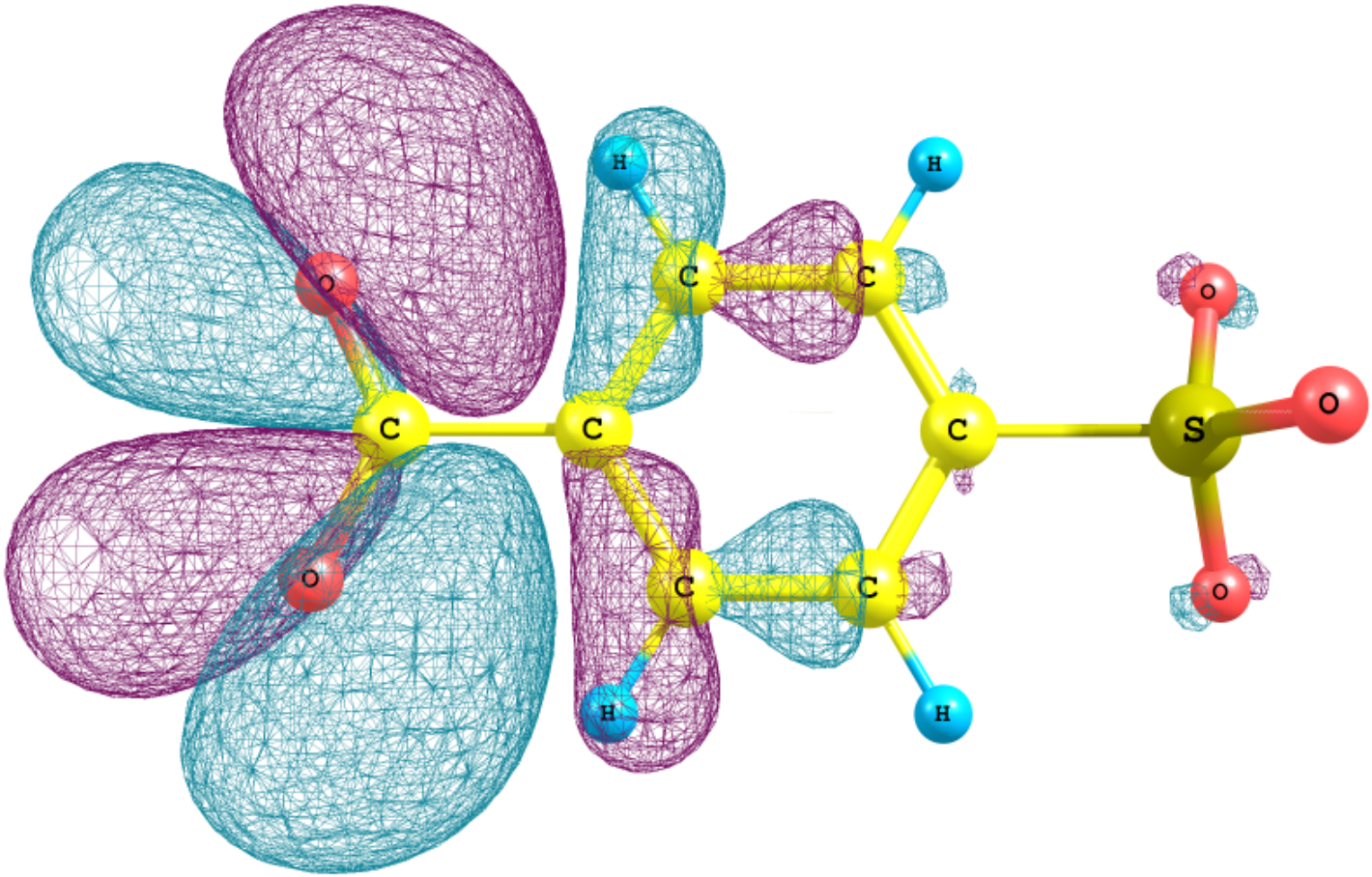

Figure 3.26. Highest occupied molecular orbital visualization for 4-sulfobenzoic dianion using Density Functional theory (B3LYP) and 6-311++G basis set.**

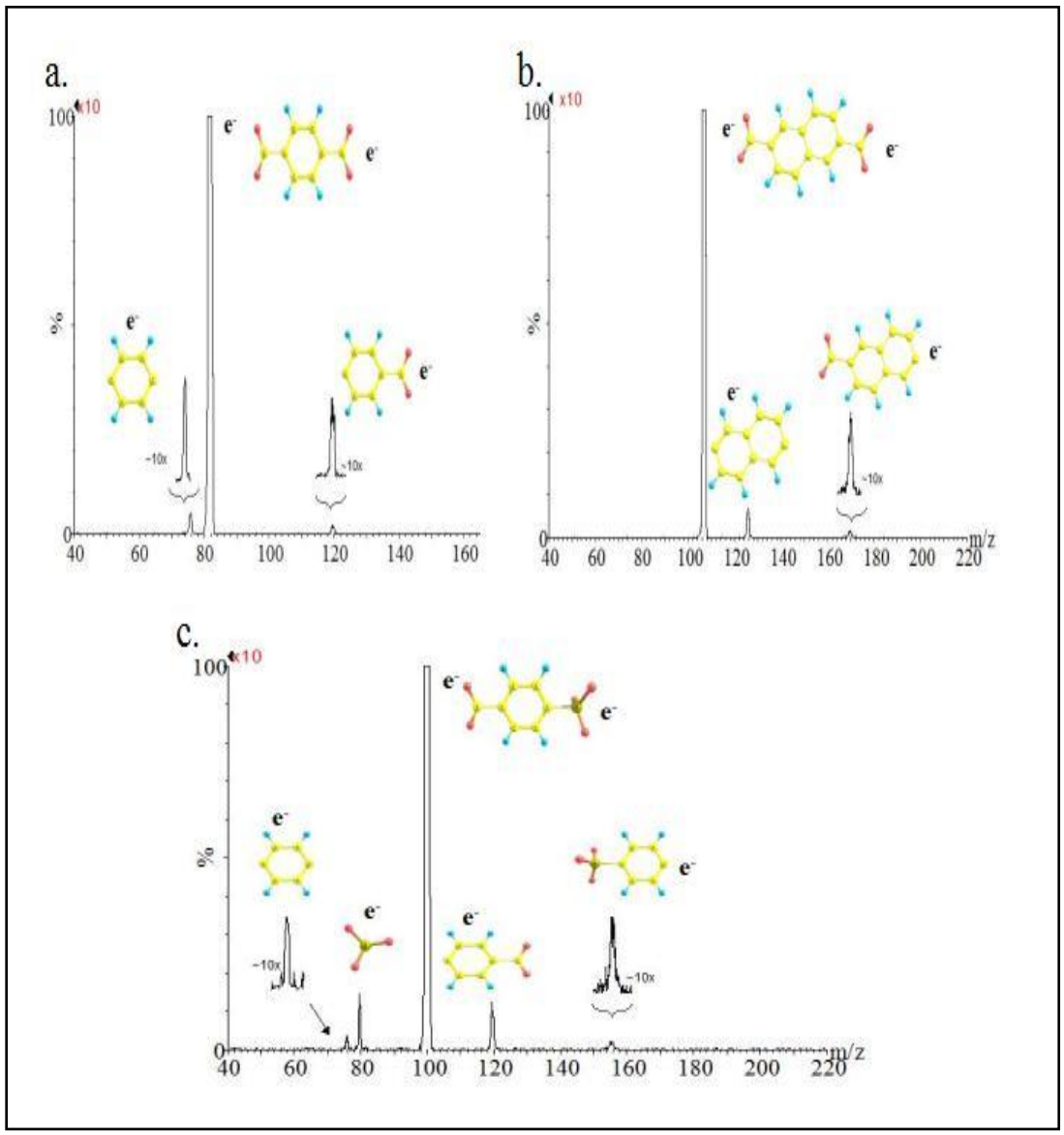

Figure 3.27. Mass spectrum of secondary ions produced by collisions of the terephthalate (a), 2,6-naphthalenedicarboxylate (b), and 4-sulfobenzoate (c) parent dianions with a static argon background at a laboratory collision energy of 60 eV.

and an SO_3 ligand, showed loss of the CO_2 ligand and a free electron, as well as fragmentation of SO_3^- at higher collision energies. Interestingly, no corresponding signal for CO_2^- was observed for any of these dianions. Initially this was attributed to the well established metastability of CO_2^- towards autodetachment, with a lifetime varying between 20-90 μseconds depending upon the internal ro-vibrational energy present in the CO_2^- ion[91]. It was believed that the experimental time frame (~1ms) was simply too long to allow observation of this ion. In direct contradiction to this, CID experiments performed on the linear 1,11-undecanedicarboxylic dianion (Fig 3.28) did show evidence of CO_2^- fragmentation in both the detection of CO_2^- and its conjugate pair, though the CO_2^- is likely greatly diminished due to the aforementioned instability. As opposed to the ringed carboxyl containing dianions, the excess electrons of this molecule are quite localized on the CO_2 end moieties, similar to the molecules studied by Wang et. al.[81]. The observation of CO_2^- from CID of this dianion does establish the ability of this apparatus to detect this metastable anion and highlights the absence of observed CO_2^- from CID of the other carboxyl containing dianions. Another interesting aspect of the fragmentation of these dianions is the observation of a benzene or naphthalene like ringed anion resulting from the loss of both carboxyl ligands and a free electron from the dicarboxylate dianions, or both the carboxyl and sulfonic ligands as well as a free electron from the 4-sulfobenzoic dianion. These anions were not observed in CID of the disulfonic dianions at any collision energy, indicative of the strong association the excess electrons of these dianions have with the SO_3 ligands.

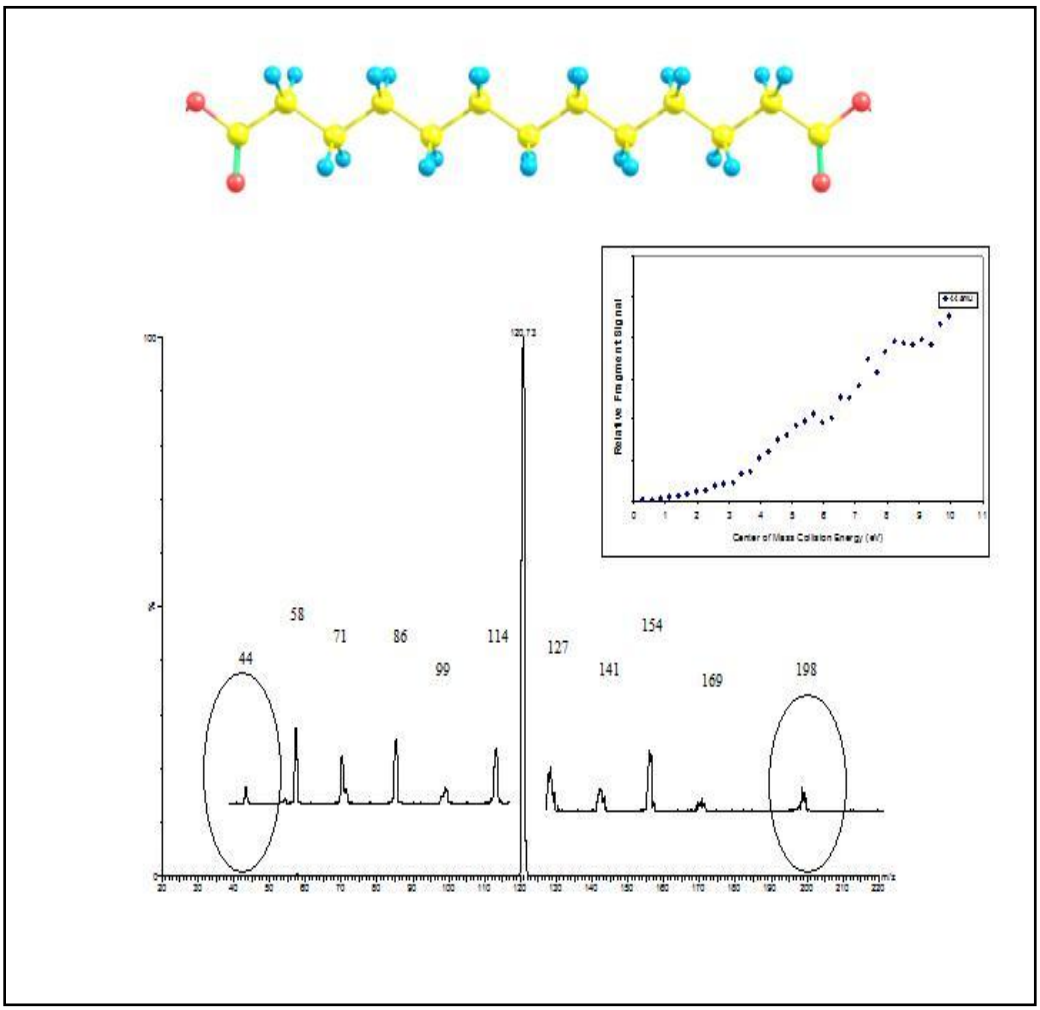

Figure 3.28. Secondary mass spectra of anions formed from CID of the 1,11-undecanedicarboxylic dianion at a collision energy of 60 eV in the lab frame. The inset shows the relative cross section for the fragmentation of CO_2^-.

The relative cross sections for the various fragmentation channels was also studied (Fig. 3.29) with interesting results. The loss of 1 or both CO_2 ligands and an electron was observed with no clear threshold for the dicarboxylic dianions (Fig 3.29a, b), as was the loss of the CO_2 ligand and an electron from the 4-sulfobenzoic dianion (Fig 3.29c). Signal resulting from loss of both CO_2 ligands experienced an increase in intensity corresponding with a decrease in observation of the loss of a single CO_2 ligand, implying a sequential dissociation. The 4-sulfobenzoic dianion displayed observation of SO_3^- with a threshold in agreement with the observation of the ringed anion stripped of both ligands, again implying CID of anions remaining from a metastable decay, as the likelihood of multiple collisions is quite small. CID of the terapthalic dianion with no collision gas (Fig. 3.30) further supports the contention that these dianions are metastable towards the loss of CO_2 and an electron, as this dissociation is observed with out being initiated by collision. The loss of CO_2^- from the linear 1,11-undecanedicarboxylic dianion showed a clear threshold (Fig. 3.28 inset) indicative of inhibition by the RCB for this dissociation pathway caused in part by the localization of the excess charges on the CO_2 end moieties.

In an attempt to help clarify these results, dissociation of the 4-sulfobenzoic dianion and 2,6-naphthalenedicarboxylate dianions (the teraphthalic dianion was not observed using this system) using Infrared multiple-photon dissociation and detachment (IRMPD) experiments performed by our collaborator and former member of the Dept. of Chemistry, Dr. Jeff Steill at the FELIX free-electron laser facility at

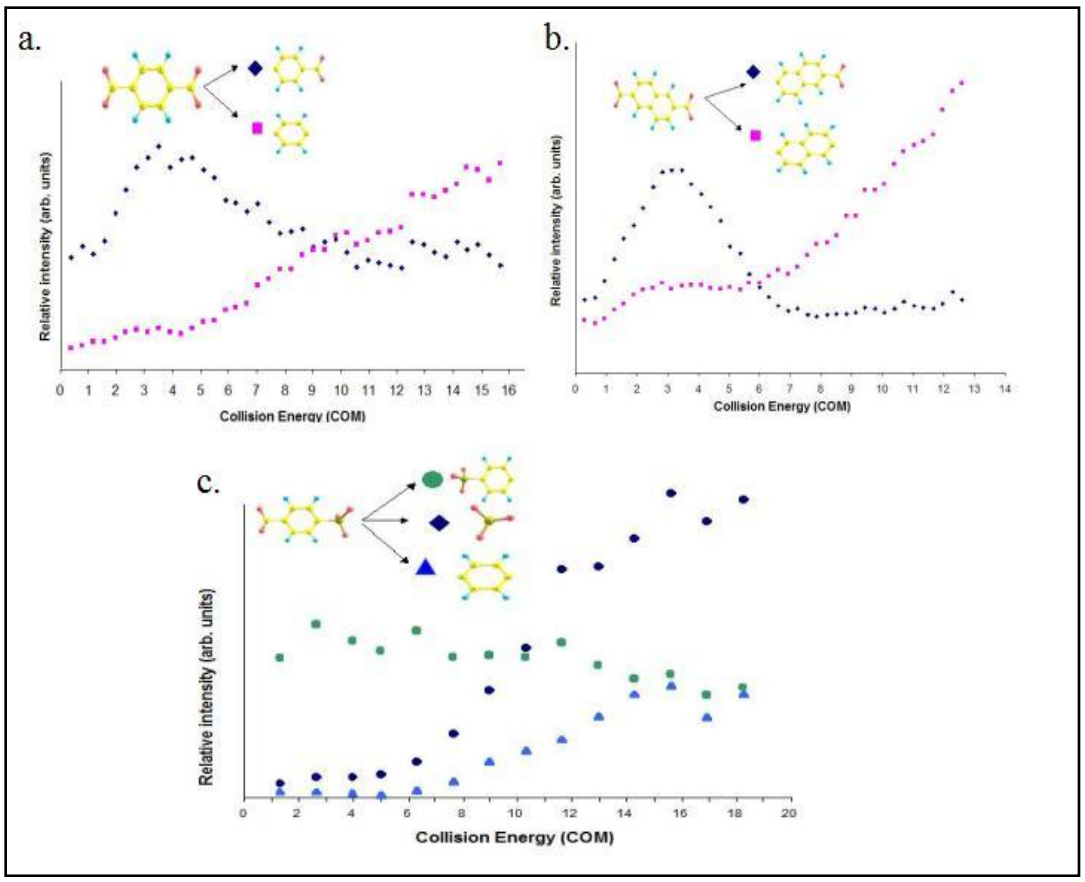

Figure 4.29. Collisional energy dependence for the various dissociation pathways observed for terephthalate (a), 2,6-naphthalenedicarboxylate (b), and 4-sulfobenzoate (c) parent dianions in the center-of-mass frame.

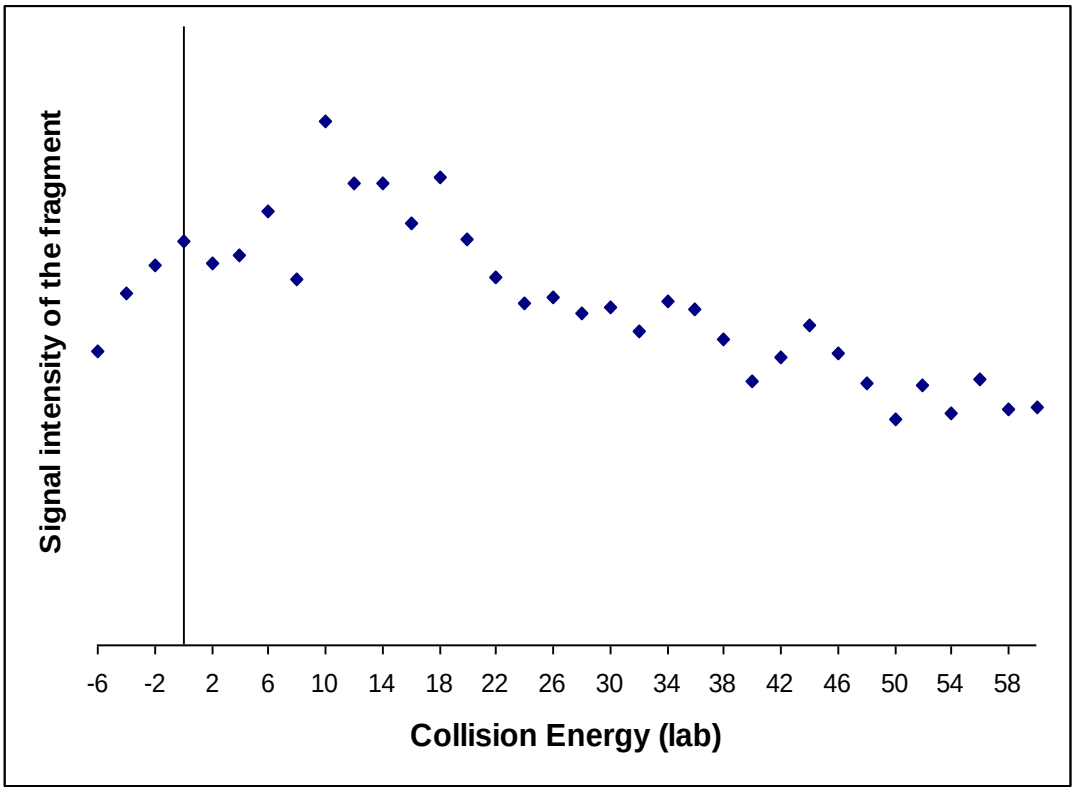

Figure 3.30. Signal intensity of the singly charged remnant resulting from metastable loss of a CO2 ligand and a free electron from the teraphthalic dianion in experiments with no collision gas.

Rijnhuizen. Ions were generated with ESI from 2mM salt solutions made in 50/50 water and methanol mixture. Ions were isolated, stored, and irradiated in a Fourier-transform ion cyclotron resonance mass spectrometer (FTICR-MS). On-resonance irradiation of the *p*-sulfono benzoate dianion (Fig 3.31) led primarily to production of the $C_6H_5SO_3$ anion radical, involving loss of CO_2 plus an electron. The production of free electrons was observed indirectly by using SF_6 as an electron scavenger[92] in the ICR cell, which attaches low energy free electrons to form SF_6^-. An ensemble of ions is detected after seconds of irradiation, so it is not possible to determine if the SF_6^- signal is due to electrons produced by direct electron detachment of the parent dianion or delayed autodetachment of metastable CO_2^-. Some SO_3^- ion production is observed at certain wavelengths, but this is determined to be due to sequential dissociation of the $C_6H_5SO_3^-$ anion fragment. Thus, the primary fragmentation pathway observed from IRMPD involves CO_2 plus an electron loss. The results from 2,6-naphthalenedicarboxylate dianions are commensurate, as the primary fragmentation pathway observed involves CO_2 plus an electron loss. Included in Fig. 3.31 are calculated IR active frequencies, with scaled DFT harmonic vibrational frequency calculations in reasonable agreement with the overall spectrum. Importantly, no metastable dissociation or detachment is observed for these dianions, contrary to our CID work. It should be noted the IRMPD experiments employed a time delay and collisional cooling of the ions prior to isolation in the ICR cell, likely limiting the ability to make this observation. Calculations of the parent dianions and the possible daughter fragments show these molecules to be stable towards electron

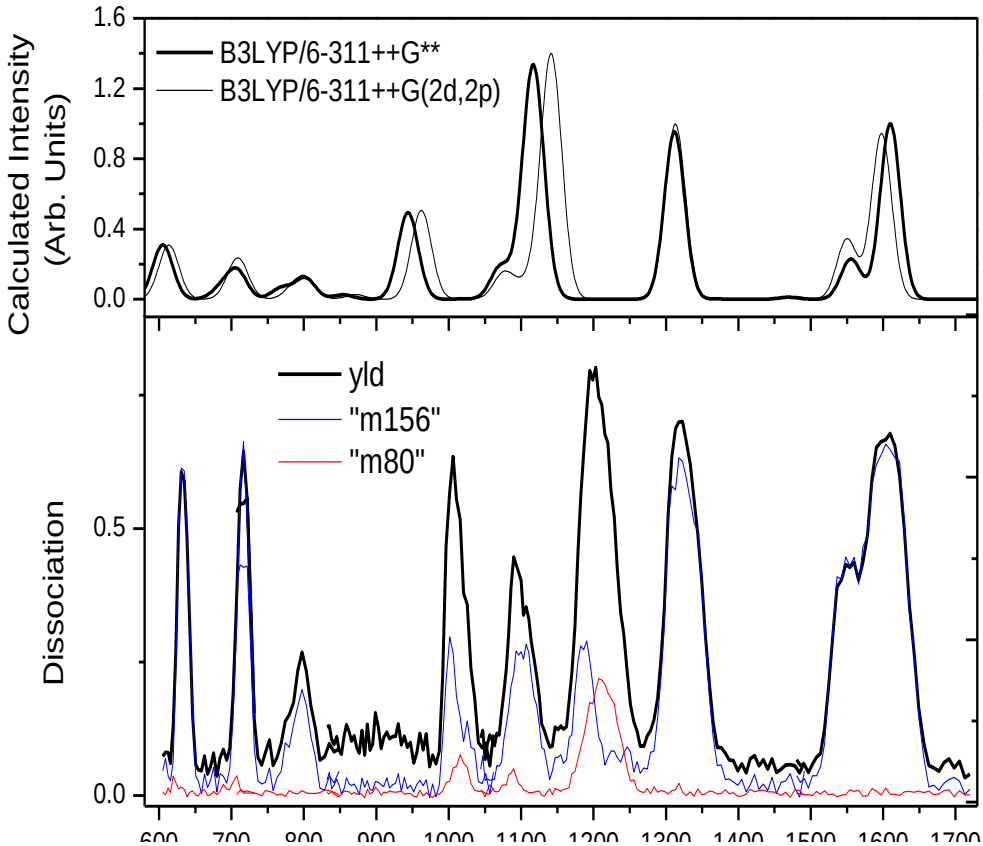

Figure 3.31. IRMPD spectrum of p-sulfonobenzoate dianion showing loss of CO2 and an electron through observations of the remaining anion at 156 amu as well as observation of SO3- from further dissociation of this anion. Frequency calculation employing Density functional theory (B3LYPP) and two different basis set are shown above.

detachment as well as towards fragmentation leading to CO_2 or CO_2^-, respectively (Table 3.3). When one considers the influence of the RCB towards the detachment of CO_2^- it seems that the likely dissociation pathway is that of neutral CO_2, followed by rapid autodetachment of the resultant dianion, which would be highly unstable (Table 3.3). This contention is supported by other experiments[93, 94] that represent dicarboxylate dianions decaying with loss of a neutral molecule (CO_2), e.g. ^-O_2C - $(CH_2)_nCO_2^- \rightarrow {}^-O_2C$ - $(CH_2)_n^- + CO_2$. This dissociation channel is only available due to the delocalization of the excess electrons across the molecule. This is supported the observation of the "ring anions" resulting from the loss of both ligands for the carboxyl containing dianions. These "ring anions" were not observed in the disulfonic dianions due to the considerable localization of the charges on the SO_3 units and thus no opportunity for neutral fragmentation leaving the electron behind. Furthermore, the observation of CO_2^- with a clear above-zero threshold from CID of the 1,11 undecanedicarboxylic dianion indicates the localization of the excess charges on the CO_2 moieties of this linear molecule limits dissociation of this molecule to the RCB inhibited ionic fragmentation. The delocalization of the charges essentially allow for a dissociation pathway "around" the RCB by allowing for neutral fragmentation unencumbered by this potential barrier.

The apparent metastability of the carboxyl containing dianions in this study remains somewhat perplexing. According to observations in the CID experiment, all of the carboxyl containing dianions appear to be metastable towards the observed loss of

Table 3.3 Calculated electron binding energies (second electron affinities) and dissociation energies of the carboxyl containing dianions using Density Functional Theory (B3LYP) with 6-311++G basis set. All values are in eV.**

	P^- AEA	$[P\text{-}CO_2]^{2-} + CO_2$	$[P\text{-}CO_2]^- + CO_2^-$	$[P\text{-}CO_2]^- + CO_2 + e^-$	$[P\text{-}CO_2]^-$ fragment EA
Terephthalate	0.50	3.00	1.36	0.99	-1.92
2,6-naphthalenedicarboxylate	0.98	2.71	1.83	1.46	-1.17
4-sulfonobenzoate	1.06	2.83	1.61	1.24	-1.50

a CO_2 ligand and a free electron; however the dianions studied with IRMPD (the teraphthalic dianion was not observed in this system) were stable with respect to detachment and dissociation. To investigate the influence of the internal energy on the stability of the dianions, Dr. Steen B. Nielsen from Aarhus University, Denmark, examined this question by measuring the lifetimes of the terephthalic and 2,6-naphthalenedicarboxylic dianions. Lifetime measurements were carried out using the Electrostatic Ion Storage Ring (ELISA) [95]. In this experimental setup, dianions are produced with an electrospray ionization source and then transported to an ion trap filled with helium buffer gas for nearly 0.1 second for accumulation and cooling before they are injected into the storage ring. Metastable decay as well as collisions with residual background gas leads to the production of neutral fragments, which are counted by a micro-channel plate detector. The lifetime of the 2,6-napthalenedicarboxylate dianion was measured to be about 1.5 seconds (Figure 3.32). This represents the limit of the storage capability of this apparatus, thus the ions are considered to be essentially stable. The teraphthalic dianion was not observed in this system. Either the lifetime of the terephthalic dianion was too short to survive transport to the storage ring, or it was not produced in the source. It takes about 100 microseconds for the dianion to travel from the source to the storage ring, meaning that although the teraphthalic dianions were collisionally cooled with helium gas, their lifetimes were still shorter than 100 microseconds. This could indicate that teraphthalic dianions are thermodynamically metastable as observed in the CID experiment. The apparent metastability of the other carboxyl containing dianions studied by CID is

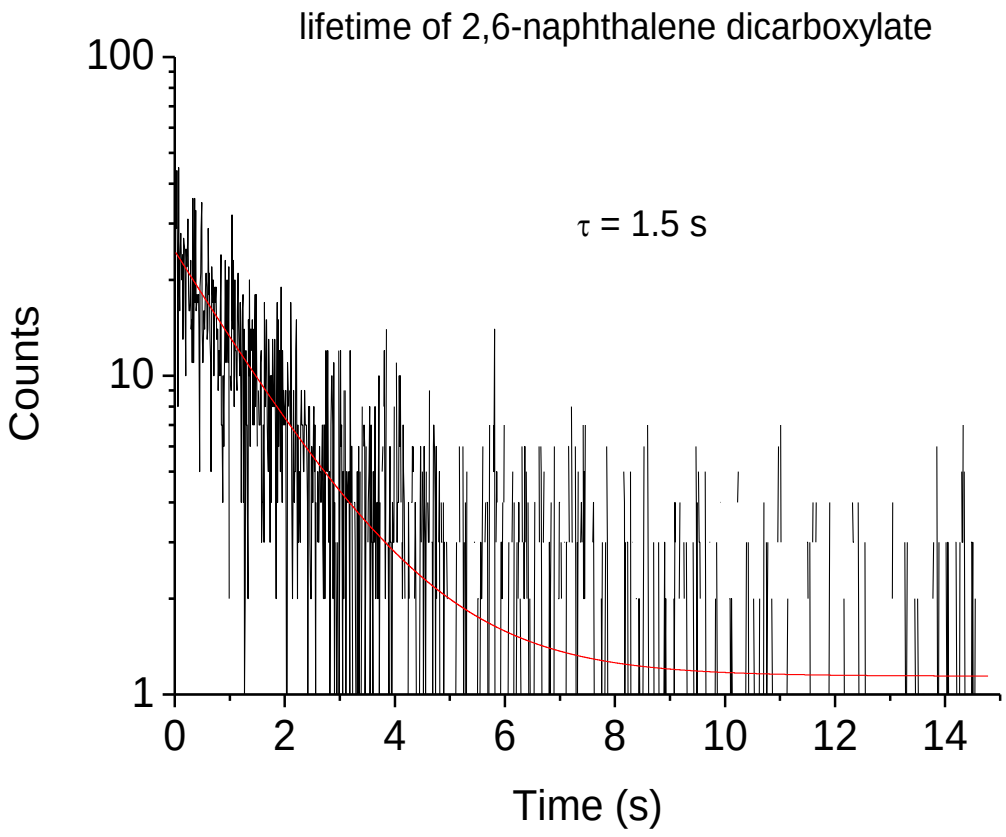

Figure 3.32. Lifetime measurements of 2,6-naphthalenedicarbxylate dianion measured by Dr. Steen B. Nielsen employing the ELISA apparatus.

likely due, in part, to the lack of collisional cooling or any other cooling mechanism. The anions formed from electrospray ionization are vibrationally "hot", with a significant population above the ground ro-vibrational state. However, this does not fully explain the observed metastable dissociation. Dissociation via neutral CO_2 fragmentation is unencumbered by a barrier towards dissociation, thus no mechanism remains for imparting metastability. Molecules of sufficient internal energy would simply dissociate immediately upon creation. If the dianion dissociates via CO_2^- loss and its internal energy was greater than the necessary dissociation energy, it may be expected to tunnel through RCB with some finite lifetime. However, since we are talking about a fairly massive fragment, as opposed to a light electron, we would not expect the tunneling dissociation rate to be very large, much less significant enough to account for the abundant metastable decay observed. We suggest that the delocalization of the excess electrons in this system may provide the answer. Just as the electron probability distribution is spread across the ring structure as well as the CO_2 ligand, the potential surface towards dissociation could be considered a superposition of the barrier-less dissociation via CO_2 neutral, corresponding to the electron probability on the ring, and the RCB affected dissociation via CO_2^- obviously corresponding to the electron probability on the CO_2 ligand (Fig 3.33). Thus a molecule with enough internal energy to dissociate via neutral CO_2 loss would seem metastable so long as the electron remained associated with the CO_2 ligand.

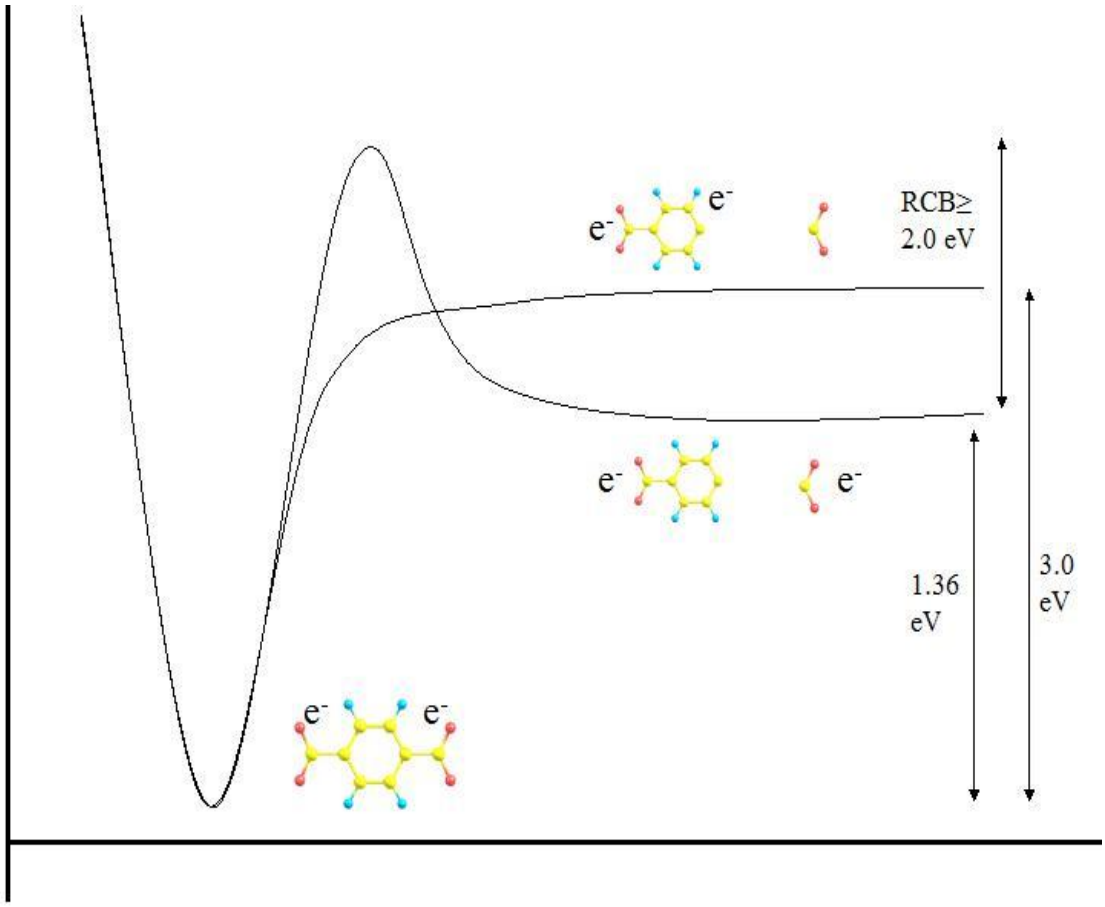

Figure 3.33. Idealized potential energy surface encountered by the teraphthalic dianion as it dissociates via barrier less CO2 loss, or RCB affected CO2- loss.

In conclusion, the stability of multiply charged anions is intimately connected with the Repulsive Coulomb Barrier as well as the manner in which the excess charges are distributed over the anion. For systems with highly localized excess electrons the RCB can be effectively modeled using Coulomb's Law, adding extra stability towards electron detachment or ionic fragmentation of $e^2/4\pi\varepsilon_o r$, with r representing the charge separation of the excess charges. This model likely begins to fail for very small MCAs, as the ability to model the excess electrons as point charges breaks down. Future studies of these small MCAs will help shape theoretical models as to how the polarizability of the resultant fragment anions may affect the observed stability. Furthermore, MCAs with delocalized charges may allow for neutral fragmentation to be the dominant dissociation pathway, due to the lack of an RCB inhibiting this process. A complete understanding of the RCB and its affect on the stability of MCAs remains difficult, as in addition to the experimental uncertainties intrinsic to their study the RCB remains a complicated transition state, difficult to model fully. Whereas we may be able to propose a possible interpretation of the magnitude of this barrier based on our measurements, the actual shape and possibly time evolving nature of this potential surface is complicated and not easily described. Further consideration of the RCB for a wide array of MCAs as well as experimental and theoretical advances may offer new insights into this interesting and fundamental aspect of physics.

References

[1] J. J. Thomson, Phil. Mag. **13** 561 (1907)
[2] T. Andersen, H. K. Haugen, H. Hotop, J. Phys. Chem. Ref. Data, **28** (1999)
[3] H. Haberland, T. Kolar, T. Reiners, Phys. Rev. Lett. **63**, 1219 (1989)
[4] H. S. W. Massey, Negative Ions (Cambridge Univ. Press, London, ed. 3, 1976).
[5] H. S. W. Massey, Adv. At. Mol. Opt. Phys. **15**,1 (1979).
[6] H. Hotop and W. C. Lineberger, J. Phys. Chem. Ref. Data **14**, 731 (1985).
[7] D. R. Bates, Adv. At. Mol. Opt. Phys. **27**, 1 (1990).
[8] D. J. Pegg, Rep. Prog. Phys., **67**, 857 (2004)
[9] M. K. Scheller, R. N. Compton, L. S. Cederbaum, Science, **270**, 1160 (1995)
[10] R. Wildt, Astrophys J.. **89** 295 (1939)
[11] Bates D R 1940 *Astrophys. J.* **91** 202
[12] Chandrasekhar S 1945 *Astrophys. J.* **102** 223
[13] Branscomb L M and Smith S J 1955 *Phys. Rev.* **98** 1028
[14] McCarthy, M. C., Gottlieb, C. A., Gupta, H. C., & Thaddeus, P. 2006, ApJ, 652, L141
[15] P. J. Sarre, Journal of Molecular Spectroscopy, **238**, 1 (2006)
[16] H. Amemiya, Y. Nakamura, J. Geomagnetism and Geoelectricity, **48**, 391 (1996)
[17] V. Shoshan-Barmatz, A. Israelson, D. Brdiczka, S.S. Sheu , Curr. Phar. Des., **12**, 2249 (2006)
[18] A. S. Verkman , L. J. Galietta,, Nat. Rev. Drug Discov., **8**, 153 (2009)
[19] N. Goel, G. R. Etwaroo, Psychol. Med., **36**, 1253 (2006)
[20] J. D. Jackson, Classical Electrodynamics (John Wiley & Sons Inc., New York, ed. 2, 1975)
[21] E. Fermi, E. Teller, Phys. Rev. **72,** 406 (1947)
[22] A. S. Wightmann, Phys. Rev. **77**, 521 (1949)
[23] J. E. Turner and K. Fox, Phys. Rev. Lett. **23**, 547 (1966).
[24] M. H. Mittleman and V. P. Meyerscough, Phys Lett. **23**, 545 (1966).
[25] J. M. Levy-Leblond, Phys. Rev. **153**, 1 (1967).
[26] W. B. Brown and R. E. Roberts, J. Chem. Phys. **46**, 2006 (1967).
[27] R. F. Wallis, R. Herman, H. W. Milnes, J. Mol. Spect., **4**, 51 (1960)
[28] J. E. Turner, V. E. Anderson, K. Fox, Phys. Rev. **174**, 81 (1968)
[29] W. R. Garrett, Mol. Phys., **24**, 465 (1972)
[30] O. H. Crawford, Mol. Phys. **20**, 585 (1971)
[31] W. R. Garrett, Phys. Rev. **3**, 961 (1971)
[32] O. H. Crawford, W.R. Garret, J. Chem Phys., **66**, 4968 (1977)
[33] J. A. Stockdale, F. J. Davis, R. N. Compton, C. E. Klotts, J. Chem. Phys., **60**, 4279 (1974)
[34] J. V. Coe, G. H. Lee, J. G. Eaton, S. T. Arnold, H. W. Sarkas, K. H. Bowen, C. Ludewigt, H. Haberland, D. R. Worsnop, J. Chem. Phys., **92**, 3980 (1990)
[35] J. H. Hendricks, S.A. Lyapustina, H.L. de Clerq, J.T. Snodgrass, K. H. Bowen, J. Chem. Phys. **104**, 7788 (1996)
[36] C. E. Dessent, C. G. Bailey, M. J. Johnson, Chem. Phys. **102**, 6335 (1995)
[37] R. Hashemi, E. Illenberger, J. Chem Phys., **95**, 6402 (1991)

[38] E.A. Brinkman, S. Berger, J. Marks, and J.I. Brauman, J. Chem. Phys. **99**, 7586(1993).
[39] A.S. Mullins, K.K. Murray, C.P. Schultz, W.C. Lineberger, J. Phys. Chem. **97**, 1028(1993).
[40] R.N. Compton and N.I. Hammer, in Advances in Gas Phase Ion Chemistry, edited by N. Adams and L. Babcock pp. 257-**259**, Vol. 4. (Elsiever, New York, 2001).
[41] C. Desfrancois, H. Abdoul-Carmine, J. P. Schermann, Int. Jounal of modern Physics, **10**, 1339 (1996)
[42] N.I. Hammer, F. Gao, R. M. Pagni, R. N. Compton, J. Chem. Phys. **117**, 4299 (2002)
[43] C. Desfrancois, Phys. Rev. A, **51**, 3667 (1995)
[44] C. Desfrançois, H. Abdoul-Carime, N. Khelifa, and J. P. Schermann, Phys. Rev. Lett. **73**, 2436 (1994).
[45] N. I. Hammer, K. Diri, K. D. Jordan, C. Desfrancois, R. N. Compton, Journ. Chem. Phys. **119**, 3650 (2003)
[46] C. Desfrancois, V. Pe´riquet, S. Carles, J. P. Schermann, D. M. A. Smith, L. Adamowicz, J. Chem. Phys. **110**, 4309 (1999).
[47] N. I. Hammer, R. J. Hinde, R.N. Compton, K. Diri, K. D. Jordan, D. Radisic, and K. H. Bowen, J. Chem. Phys. **120**, 685(2004).
[48] N. I. Hammer, L. Adamowicz, S.G. Stepanian, R.N. Compton, Phys. Rev. Lett., **94**, 153004 (2005)
[49] P. C. Engelking, Chemical Reviews, **91**, 399 (1991)
[50] D.A. Dahl and J.E. Delmore, SIMION version 4.0, Idaho National Engineering Laboratory, Idaho Falls, ID,1988.
[51] S. T. Stokes, K. H. Bowen, T. Sommerfeld, S. Ard, N. Mirsaleh-Kohan, J. D. Steill, R. N. Compton, J. Chem. Phys. **129**, 64308 (2008)
[52] C. Desfrancois, V. Periquet, S. A. Lypustina, T. P. Lippa, D. W. Robinson, K. H. Bowen, H. Nonaka, and R. N. Compton, J. Chem. Phys. **111**, 4567 (1999).
[53] R. N. Compton, H. S. Carman, C. Desfrancois, H. Abdoul-Carime, J. P. Schermann, J. H. Hendricks, S. A. Lyapustina, and K. H. Bowen, J. Chem. Phys. **105**, 3472 (1996).
[54] J. A. Stockdale, F. J. Davis, R. N. Compton, and C. E. Klots, J. Chem. Phys. **60**, 4279 (1974).
[55] C. Desfrançois, Y. Bouteiller, J.P. Schermann, D. Radisic, S.T. Stokes, K.H. Bowen, N.I. Hammer, R.N. Compton, Phys. Rev. Lett., **92**, 830003 (2004)
[56] D.C. Clary, J. Phys. Chem. **92**, 3171(1988).
[57] J. Simons, J. Phys. Chem. **91**, 6858(1989).
[58] L. Suess, Y. Liu, P. Parthasarathy and F.B. Dunning, J. Chem. Phys. **119**, 12890(2003).
[59] L. Suess, Y. Liu, P. Parthasarathy and F.B. Dunning, Chem. Phys. Lett. **376**, 376(2003).
[60] V.E. Chernov, A.V. Danilyan, A.V. Dolglikh, F.B. Dunning and B.A. Zon, Chem. Phy. Lett. **426**, 30(2006).
[61] L.E. Snyder, D. Buhl Astrophys. J. 163, L47–L52 (1971)
[62] A.M.S. Boonman, *et al*, Astrophys. J. **553**, L63–L67 (2001).
[63] K. Magee-Sauer, *et al*, Icarus **142**, 498–508 (1999)

[64] D. Bockelée-Morvan, et al., Astron. Astrophys. **353**, 1101–1114 (2000).
[65] J. Oro, T. Mills, A. Lazcano, Origins Life **21**, 267–277 (1992).
[66] C. Degli Esposti, *et al*, Infrared Physics, **28**, 21(1988).
[67] K.D. Jordan and F. Wang, Annu. Rev. Phys. Chem., **54**, 367-96 (2003).
[68] K.A. Peterson, M. Gutowski, J.Chem. Phys., **116**, 3297 (2002)
[69] P. Skurski, M. Gutowski, J. Simons, Chem. Phys., **114** 7442 (2001)
[70] M. Gutowski, K.D. Jordan, P. Skurski, J. Phys. Chem. A, **102**, 2624 (1998)
[71] W.R. Garrett, J. Chem. Phys. 77, 3666 (1982).
[72] Gaussian 03, Revision C.02, M. J. Frisch, G. W. Trucks, H. B. Schlegel, G. E. Scuseria, M. A. Robb, J. R. Cheeseman, J. A. Montgomery, Jr., T. Vreven, K. N. Kudin, J. C. Burant, J. M. Millam, S. S. Iyengar, J. Tomasi, V. Barone, B. Mennucci, M. Cossi, G. Scalmani, N. Rega, G. A. Petersson, H. Nakatsuji, M. Hada, M. Ehara, K. Toyota, R. Fukuda, J. Hasegawa, M. Ishida, T. Nakajima, Y. Honda, O. Kitao, H. Nakai, M. Klene, X. Li, J. E. Knox, H. P. Hratchian, J. B. Cross, V. Bakken, C. Adamo, J. Jaramillo, R. Gomperts, R. E. Stratmann, O. Yazyev, A. J. Austin, R. Cammi, C. Pomelli, J. W. Ochterski, P. Y. Ayala, K. Morokuma, G. A. Voth, P. Salvador, J. J. Dannenberg, V. G. Zakrzewski, S. Dapprich, A. D. Daniels, M. C. Strain, O. Farkas, D. K. Malick, A. D. Rabuck, K. Raghavachari, J. B. Foresman, J. V. Ortiz, Q. Cui, A. G. Baboul, S. Clifford, J. Cioslowski, B. B. Stefanov, G. Liu, A. Liashenko, P. Piskorz, I. Komaromi, R. L. Martin, D. J. Fox, T. Keith, M. A. Al-Laham, C. Y. Peng, A. Nanayakkara, M. Challacombe, P. M. W. Gill, B. Johnson, W. Chen, M. W. Wong, C. Gonzalez, and J. A. Pople, Gaussian, Inc., Wallingford CT, 2004.
[73] M. K. Scheller, R. N. Compton, and L.S. Cederbaum, Science 270, 1160(1995)
[74] C. Jin, R. L. Hettich, R. N. Compton, A. Tuinman, A. Derecsei-Kovacs, D.S. Marynick, and B.I. Dunlap, Phys. Rev. Lett. 73, 2821 (1994)
[75] R. L. Martin and J. P. Ritchie, Phys. Rev. B48, 4845 (1993).
[76] C. Yannouleas and U. Landmann, Chem. Phys. Lett. 217, 175(1994).
[77] R. N. Compton, A. A. Tuinman, C. E. Klots, M. R. Pederson, and D. C. Patton, Phys. Rev. Lett. 78, 4367 (1997).
[78] X. B. Wang, L. S. Wang, Nature (London) 400 (1999) 245.
[79] X. Wang, C. Ding, L. Wang, Phys. Rev. Lett, 81 (1998) 3351
[80] X. Wang, L. Wang, Phys. Rev. Lett. 83 (1999) 3402
[81] L. Wang, C. Ding, X. Wang, J. Nichols, Phys. Rev. Lett., 81 (1999) 2667
[82] J. Friedrich, S. Gilb, O. Ehrler, A. Behrendt, M. Kappes, Jour. Chem Phys., 117 (2002) 2635
[83] W. Boxford, J. Pierce, C. Dessent, Chem. Phys. Lett., 399 (2004) 465
[84] P. Skurski, J. Simons, X. B. Wang and L.S. Wang, J. Am. Chem. Soc. 122 (2000) 4499
[85] P. Schwerdtfeger, A. Hammerl, and R. Wesendrup, Int. J. Mass Spectrom. **228,** 341 (2003).
[86] J. B. Fenn, M. Mann, C. K. Meng, S. F. Wong, C. M. Whitehouse, Science 246, (1989) 64
[87] S. Gaskell, J. Mass Spectrometry, 32 (1997) 677.

[88] J. Friedrich, P. Weis, J. Kaller, R. L. Whetten, and M. M. Kappes. Eur. Phys. J. D, **9**, 269 (1999).
[89] S. Dobrin, B.H. Boo, L.S. Alconcel, R.E. Continetti, J. Phys. Chem. A, 104 (2000) 10695
[90] K. M. Ervin, S. K. Loh, N. Aristov, P. B. Armentrout, J. Phys. Chem. **87** (1983) 3593.
[91] C. D. Cooper, R. N. Compton. Chem. Phys. Lett. **14,** 29 (1972).
[92] Steill, Jeffrey D.; Oomens, Jos; Eyler, John R.; Compton, Robert N, Journal of Chemical Physics, **129** (2008) 244302
[93] K. W. M. Siu, G. J. Gardner, and S.S. Berman, Org. Mass Spectrom. **24**, 931 (1989).
[94] S. M. Bacharch, M. Hare, and S. R. Kass, J. Am. Chem. Soc. **120**, 12646 (1998).
[95] S. P. Møller, Nucl. Instrum. Meth. Phys. Research A **394**, 281 (1997).

Vita

Shaun Ard was born in Tampa, FL. He graduated from Gaither high School in 1996. He then attended the University of Florida, earning a Bachelors of Science in physics in May of 2000. He began his doctoral research at the University of Tennessee in the fall of 2004.